VIETNAM
JOURNAL OF HYDRO - METEOROLOGY

ISSN 2525 - 2208

VIETNAM METEOROLOGICAL AND HYDROLOGICAL ADMINISTRATION

No 8
8-2021

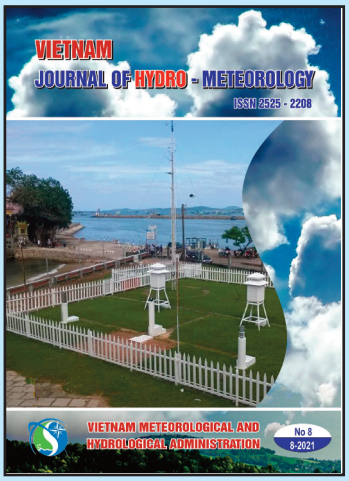

Publishing licence
No: 166/GP-BTTTT - Ministry of Information and Communication dated 17/04/2018

Editorial office
No 8 Phao Dai Lang, Dong Da, Ha Noi
Tel: 024.39364963
Email: tapchikttv@gmail.com

Engraving and printing
Vietnam Agriculture Investment Company Limited
Tel: 0243.5624399

VIETNAM JOURNAL OF HYDROMETEOROLOGY
Volume 08 - 8/2021

TABLE OF CONTENT

VIETNAM JOURNAL OF HYDROMETEOROLOGY

Research Article

Projection of abnormal cold surge in winter over the northern part of Viet Nam using RegCM model according to RCP4.5 and RCP8.5 scenarios for 2020–2100 period

Hoa Vo Van[1*]

[1] Northern Delta Regional Hydro–Meteorological Center; vovanhoa80@yahoo.com

*Correspondence: vovanhoa80@yahoo.com; Tel.: +84–912509932

Received: 08 April 2021; Accepted: 25 June 2021; Published: 25 August 2021

Abstract: This article presents the results of projection of abnormal cold surge in winter in the Northern region of Vietnam for the period 2020–2100 based on the regional climate model RegCM under different scenarios Climate change RCP4.5 and RCP8.5 are generated from five Atmospheric–Ocean Global Circulation Models (AOGCM) including CNRM–CM5, CSIRO, MPI–ESM, EC–Earth and GFDL–ESM. The magnitude and variability of abnormal cold surge vary considerably across scenarios and across different global inputs. The estimated results show a decreasing trend of abnormal cold surge in winter over the Northern region in the period 2020–2100 under both scenarios RCP4.5 and RCP8.5. The reduction under the RCP8.5 scenario is larger than that of the RCP4.5 scenario. The frequency of abnormal cold surge in the early 21st century is higher than in the middle and late 21st century.

Keywords: Abonormal cold surge; Winter; Northern region of Viet Nam; RegCM model; RCP scenarios.

1. Introduction

Due to the influence of climate change, the climate regime in most regions of Vietnam has changed significantly in recent years. The increasing occurrence of abnormal cold surge in winter in the Northern region is one of the typical examples for the above–mentioned change in climate. Specifically, cold surges tend to occur more often with stronger intensity and create many extreme weather events such as the air temperature in many places dropping below 0 degrees Celsius, snow occurring in some places where never occurred in the observed data series. The question is how under the impact of climate change, how often has the occurrence of abnormal cold surge in winter changed in recent years and how will it change in the future according to different climate change scenarios?.

According to the study [1], cold extreme events bring air masses from high latitudes into mid–latitudes and low–latitudes, causing many extreme weather phenomena and have negative impacts on socio–economic activities and people. There have been many studies on extreme cold phenomena in winter done around the world, especially for East Asia. In it, two concepts have been proposed including “cold day” and “cold surge”. The concept of a cold day was proposed in the study [2] which is defined as the day with the maximum anomaly of daily minimum/average temperature. Meanwhile, the cold surge was proposed in the study [3] which is based on the degree of sudden temperature drop over several consecutive days. In general, the concept of a cold day is usually associated with the average temperature value while a cold surge is associated with the variation of temperature

by day. Therefore, global warming may be correlated with the change in the number of cold days but not necessarily with the number of cold surges.

[2] showed that in the context of increasing global temperature, the warming trend in East Asia is very large. The average temperature tends to increase and the distribution function shifts towards the higher temperature range, leading to the low temperature extremes also increasing. This result leads to a decrease in the number of cold days as shown in the study [4]. The decrease in the number of cold days in East Asia was also shown in the studies. [8] showed that no clear trend was found in the variation of the number of cold extremes in Europe and the United States, although global temperatures are trending upward direction. To date, there have been many studies on the characteristics of extreme cold surge [9–10] and their relationship with large–scale circulation [9–11] in East Asia. However, there are very few studies on the trends of these phenomena as well as the effects of global warming on the trends of changes in these phenomena. extreme cold in the northern part of Viet Nam.

In this paper, we apply the RegCM regional climate model version 4.6.2 to estimate the change of abnormal cold surge over the Northern region in the period 2020–2100 based on the RCP4.5 and RCP8.5 scenarios are generated from 5 atmospheric–ocean global circulation models (AOGCM). Subsequent sections present detail the method for identifying abnormal cold surge, the data set used, and the expected results.

2. Dataset and Methodology

2.1. Definition of abnormal cold surge và model data process

The method to determine abnormal cold surge in winter in the Northern region is proposed based on the study [12]. If $T_{10pi,j,k}$ is called the 10th percentile of the average daily temperature value of the jth day in the kth month at the ith station, a day is defined as occurering abnormal cold surge event if the average temperature of given day is smaller than $T_{10pi,j,k.}$ The 10^{th} percentile value is calculated for each day of the winter months (November to March of the next year) based on the IPCC method which uses a dataset of 10–day time windows (where the given day in time window is 5 days).

For simulation and estimated data according to RCP scenarios from RegCM model (daily temperature data are provided on the model grid), theoretically it can be determined on grid space as in the study [13] or at the station point by interpolating values from the regional climate model grid. In order to minimize the effect of differences in the resolution of regional climate models used, the differences of the simulated and estimated datasets under the RCP scenarios, in this study we choose the method of determining the abnormal cold surge from the space–based RegCM climate model of 84 monitoring stations in the Northern region. With this option, the air temperature data simulated and estimated according to the RCP scenarios from the climate models will be interpolated to the station point. The interpolation method that will be used is the nearest point interpolation method. The temperature data after being interpolated will be corrected to limit the influence of errors. The bias correction method is used according to the study [14].

2.2. Regional climate model configuration

In order to enhance the ability to capture the weather patterns that govern the abnormal cold surge in winter in the northern region, the integral region of the RegCM model extends to the north. Specifically, the integral domain center is selected at 20°N and 110°E with the 138 grid points along to latitude and longitude direction corresponding to a resolution of 32 km in each direction. Figure 1 illustrates the integral domain for the RegCM model and the study area (northern part of Viet Nam).

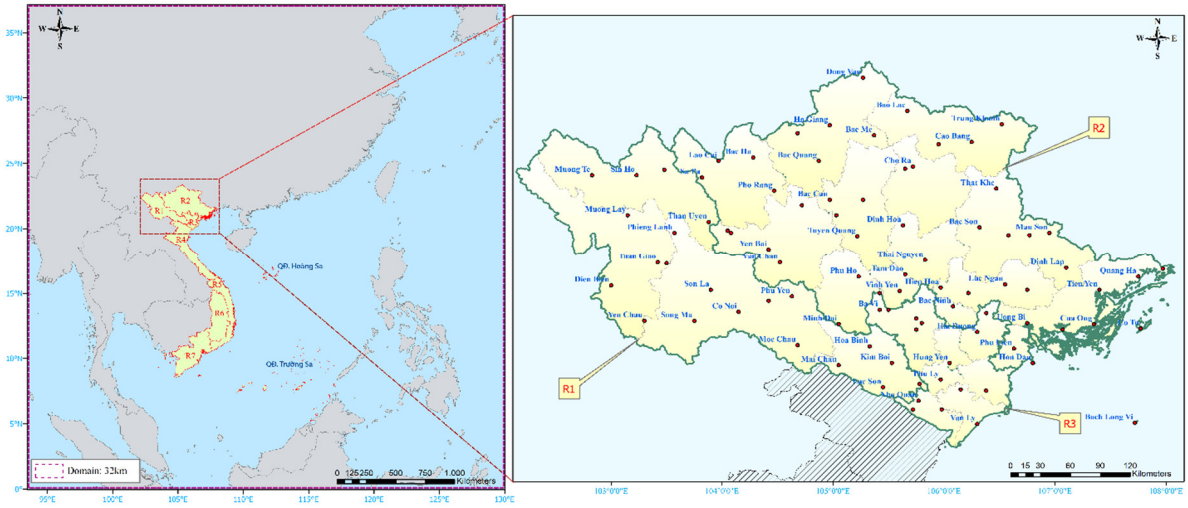

Figure 1. Integal domain of RegCM (left side) and distribution of 84 synoptic station in research region (right side).

Table 1 shows some configuration of the RegCM model. In fact, the RegCM model provides a wide selection of physical parameterization schemes for research purposes. However, the paper does not conduct experimental research and select suitable physical parameterization schemes for the current problem. Hence, the selection of physical parameterization schemes is based on local studies was made. Specifically, the selection of physical parameterization schemes for the RegCM model in this study is based on the research results of Phan Van Tan et al (2014) [14]. The physical configuration is fixed for both of RCP4.5 and RCP8.5 scenarios.

Table 1. The configuration of RegCM model.

Configuration	RegCM (ver. 4.6.2)
Grid center point	20ºN; 110ºE
Grid point	138 x 138
Horizontal resolution	32km
Vertical pressure levels	18
Cumulus parameterization scheme	Grell–AS
Soil parameterization scheme	BATS
Radiation parameterization scheme	CCM3

2.3. Global datasets

In order to have input data (initial and boundary conditions) for the RegCM model, it is necessary to use the climate projection dataset of the global models. In this study, we use estimated data under RCP4.5 and RCP8.5 scenarios from 5 AOGCM that is generated in the Couple Model Intercomparison Project (CMIP). Information about these models is given in Table 2 below. These global datasets were collected from 1986 to 2100 in which period of 1986–2005 was used to calculated the baseline.

Table 2. General information of five AOGCM are used as input data for RegCM model.

Model name	Developer	Resolution	Data link
CNRM–CM5	Centre national de Recherches Meteorologiques, France	1.41×1.40	http://www.umr–cnrm.fr/cmip5/
MPI–ESM	Max Planck Institute for Meteorology, Germany	1.875×1.85	https://www.mpimet.mpg.de/en/science/models/mpi–esm/

Model name	Developer	Resolution	Data link
EC–Earth	EC–Earth consortium, EU	1.125×1.125	http://www.ec–earth.org/
CSIRO	CSIRO, Australia	1.875×1.86	https://data.gov.au/dataset/
GFDL–ESM	GFDL, USA	2.5×2.0	https://www.gfdl.noaa.gov/earth–system–model/

3. Results and discussion

Figure 2 to Figure 6 show the results of projecting the number of abnormal cold surge in winter in the Northern region according to the RCP4.5 and RCP8.5 scenarios for the period 2020–2100 from the RegCM model with input from 5 different global models. From these figures it can be seen that the number of cold surges projected for each winter during 2020–2100 is highly variable between other global inputs as well as between the two RCP scenarios. The frequency of cold spells in the early 21st century is much higher than in the late 21st century. In which, most of the estimated tests show a sudden increase in the number of abnormal cold surges during the period of 2030–2050 according to both scenarios. The sudden increase in period of 2080–2100 was found only when looking at the projected results from the EC–Earth and GFDL–ESM inputs. In comparison with the baseline period (1986–2005), the number of abnormal cold surge projected from the different global input tests and under the 2 scenarios is generally much higher during 2020–2065 and lower during the period of 2070–2100. Some estimates show that there are some years with very larger sudden increase (more than 25 abnormal cold surges in comparison with normal).

The difference between the number of abnormal cold surge occurring in the same year between scenarios and between different global inputs is on average about 3–4 events. There is some possibility that the deviation between the two scenarios is very large such as, for example, in 2022, the expected outcome with input from the global model CNRM–CM5 under the RCP4.5 scenario is only 2 abnormal cold surges, while under the RCP8.5 scenario is 22 abnormal cold surges.

During the first half of the 21st century, the estimated outcome under the RCP4.5 scenario with input from the CNRM–CM5 and CSIRO gives a greater number of abnormal cold surge than in the RCP85 scenario. However, estimates with input from EC–Earth, MPI–ESM and GFDL–ESM models give the opposite result. For the second half of the 21st century, all projections from the global input year show a higher number of abnormal cold surge under the RCP4.5 scenario than under the RCP8.5 scenario, especially is in the last part of the decade (2080–2100).

The changing trend of the number of abnormal cold surge in the whole 2020–2100 period is little change or slight decrease under both scenarios. The results of statistical hypothesis testing show that most of the trends satisfy the statistical hypothesis with the 90% confidence level, but not at the 95 and 99% confidence levels. A rapid downward trend is found in the period 2020–2040 and slight or little change in the remaining years.

Figure 7 shows the results of calculating the ensemble mean variation trend from 5 different global inputs for the RegCM model under the RCP4.5 and RCP8.5 scenarios for the period 2020–2100. A downward trend in abnormal cold surge can be seen in both scenarios in which the decrease in RCP8.5 scenario is faster than in RCP4.5 scenario. This result is completely logical because the RCP8.5 scenario is a high emission scenario that will give a rapid global warming trend, especially in the late 21st century. On average, according to the RCP4.5 scenario, most winters in the period 2020–2100 are expected to have more abnormal cold surge than the baseline period with an average increase of 2–3 events per year.

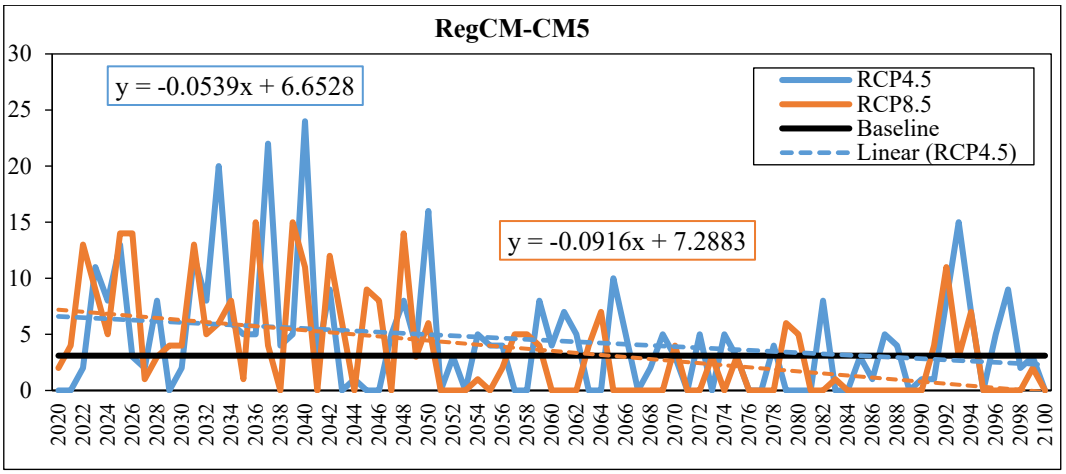

Figure 2. Projection of abnormal cold surge in winter over the northern part of Viet Nam using RegCM model according to RCP4.5 and RCP8.5 scenarios for 2020–2100 period with inputs of CNRM–CM5 global model.

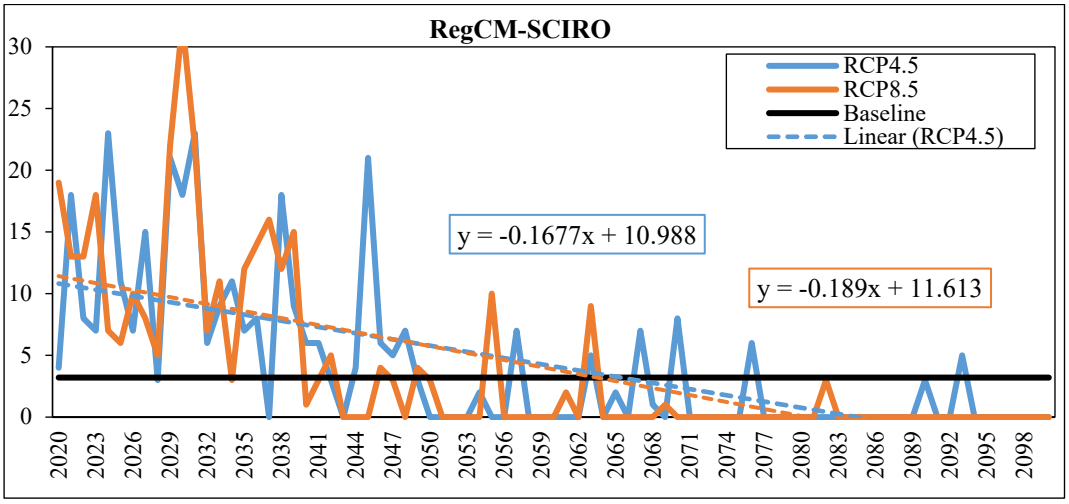

Figure 3. Projection of abnormal cold surge in winter over the northern part of Viet Nam using RegCM model according to RCP4.5 and RCP8.5 scenarios for 2020–2100 period with inputs of SCIRO global model.

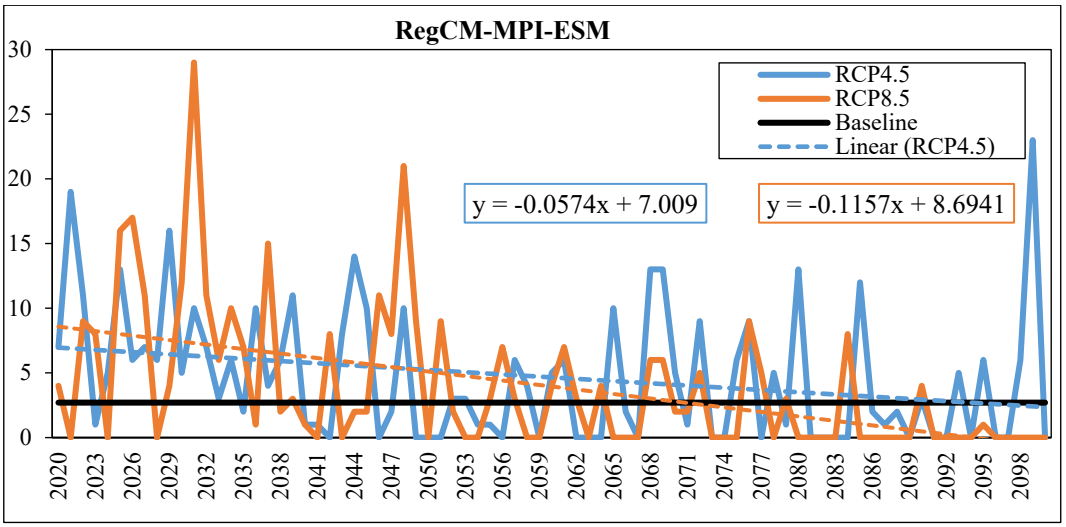

Figure 4. Projection of abnormal cold surge in winter over the northern part of Viet Nam using RegCM model according to RCP4.5 and RCP8.5 scenarios for 2020–2100 period with inputs of MPI–ESM global model.

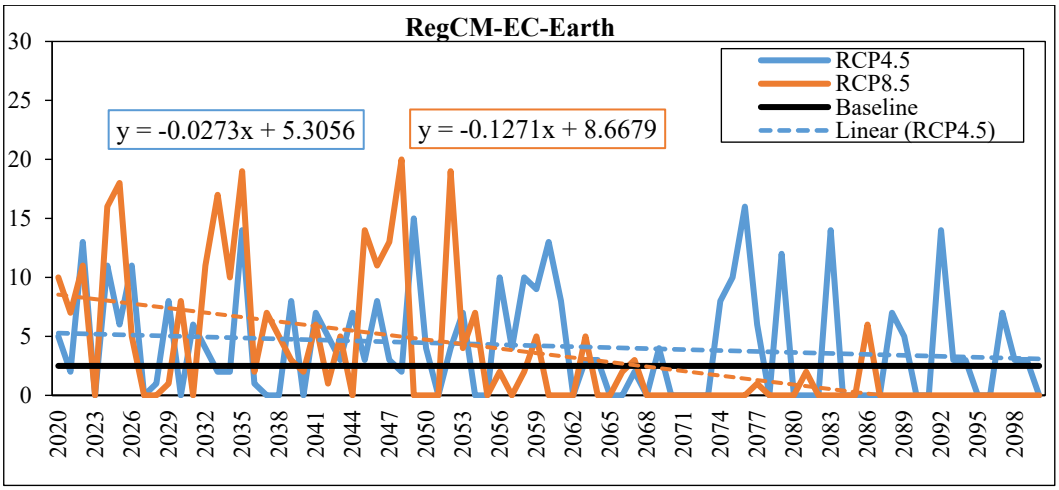

Figure 5. Projection of abnormal cold surge in winter over the northern part of Viet Nam using RegCM model according to RCP4.5 and RCP8.5 scenarios for 2020–2100 period with inputs of EC–Earth global model.

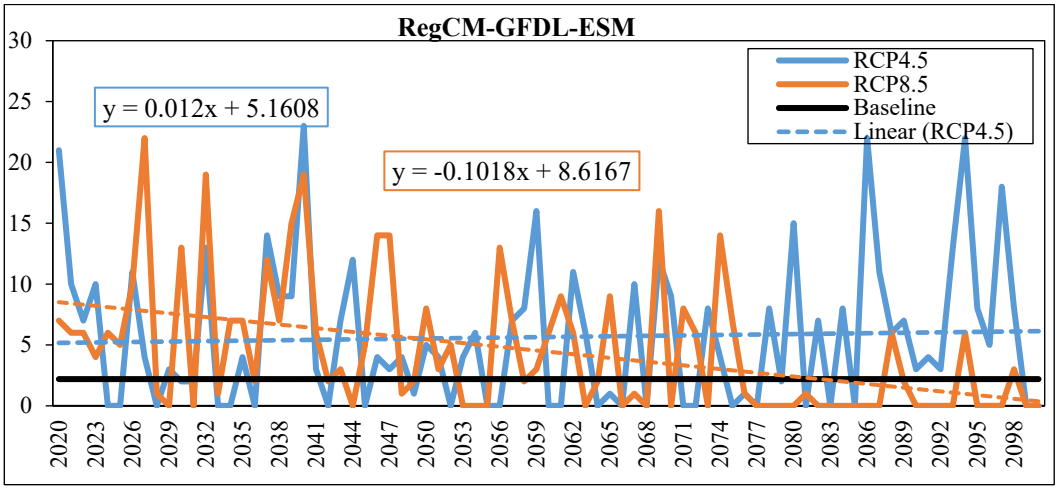

Figure 6. Projection of abnormal cold surge in winter over the northern part of Viet Nam using RegCM model according to RCP4.5 and RCP8.5 scenarios for 2020–2100 period with inputs of GFDL–ESM global model.

However, with the RCP8.5 scenario, the sudden increase compared to the baseline period is only found in the period 2020–2050. For the period 2050–2100, the number of abnormal cold surge decreased faster and less than the baseline period, especially in the late 21st century. In order to take a closer look at the changing trends of abnormal cold surge in winter in the Northern region under the scenarios RCP4.5 and RCP8.5, we calculate the separate changing trends for the 21st century (2045–2065) and the end of the 21st century (2080–2100). Calculation results show that the general trend of abnormal cold surge in winter in the Northern region is decreasing or less changing. With the same global input, the number of abnormal cold surge projected for each year and under the two scenarios is also different with an average difference of 1–2 events. In general, compared with the early 21st century, the number of abnormal cold surge projected under both scenarios is significantly reduced for The changing trend of the number of abnormal cold surge in the whole 2020–2100 period is little change or slight decrease under both scenarios. The results of statistical hypothesis testing show that most of the trends satisfy the statistical hypothesis with the 90% confidence level, but not at the 95 and 99% confidence levels. A rapid downward trend is found in the period 2020–2040 and slight or little change in the remaining years.

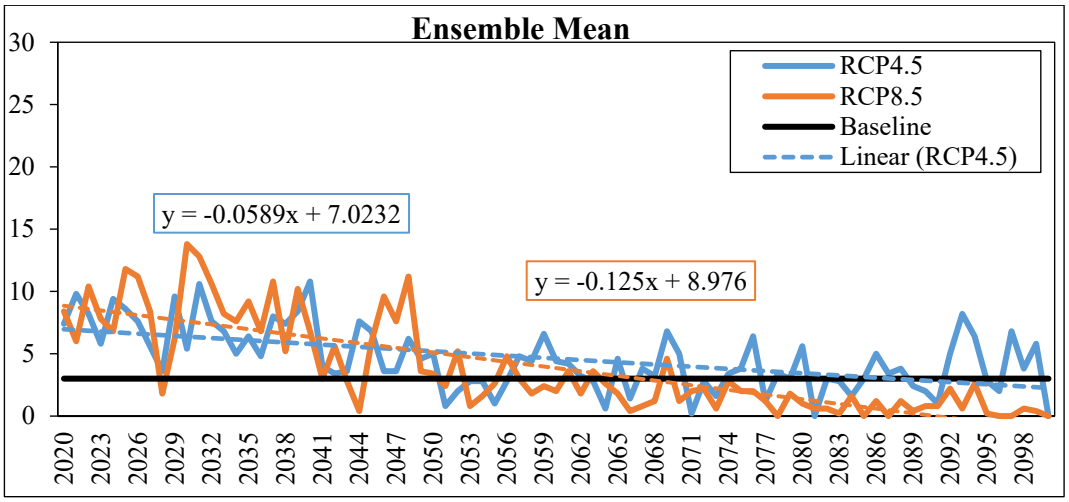

Figure 7. Projection of abnormal cold surge in winter over the northern part of Viet Nam using RegCM model according to RCP4.5 and RCP8.5 scenarios for 2020–2100 period with ensemble mean of five global model.

For the end of the 21st century, the projected outcome is very different between different global inputs as well as between two scenarios with the same global input. Calculation results show that at this stage, abnormal cold surge in the Northern region are almost rare under the RCP8.5 scenarios as seen in the projected results with input from the CSIRO model. The total number of abnormal cold surge expected to occur during this period under the RCP4.5 scenario is much larger than that of the RCP8.5 scenario. Under the RCP8.5 scenario, there are only a few years during this period where there are more abnormal cold surge than the baseline period. Meanwhile, according to the RCP4.5 scenario, about 50–60% of winters in this period have more abnormal cold surge events than in the baseline period. In terms of trend, both scenarios show little change or slight uptrend. Especially in the last 10 years of the 21st century, it can be seen that projections from global inputs show a slight increase trend. The results of the statistical hypothesis testing show that the trends found do not satisfy the statistical hypothesis with the 90% or more confidence level.

4. Conclusion

This article presents the results of projection of abnormal cold surge in winter in the Northern region of Vietnam for the period 2020–2100 based on the regional climate model RegCM under different RCP4.5 and RCP8.5 climate change scenarios are generated from five AOGCM including CNRM–CM5, CSIRO, MPI–ESM, EC–Earth and GFDL–ESM. The magnitude and trend of variation vary considerably between scenarios and between different global inputs. However, if considering the same scenario and AOGCM input, the estimated results from the RegCM model is only quantitatively different (number of occurrences), while in terms of trends it is almost the same. The estimated results show a decreasing trend of abnormal cold surge in winter in the Northern region in the period 2020–2100 under both scenarios RCP4.5 and RCP8.5. The reduction under the RCP8.5 scenario is larger than that of the RCP4.5 scenario. The frequency of abnormal cold surge in the early 21st century is higher than in the middle and late 21st century.

Author Contributions: Conceived and designed the experiments: T.T.L.; Analyzed and interpreted the data: T.T.L.; contributed reagents, materials, analysis tools or data: T.T.L., N.M.L.; manuscript editing: V.V.H.; Performed the experiments: T.T.L.; contributed reagents, materials, analyzed and interpreted the data, wrote the draft manuscript: T.T.L., V.V.H., N.M.L.

Acknowledgements This work was supported by the Ministry of Natural Resources and Environment through the national Project "The impact of climate change on abnormal cold surge and heat wave in the winter at the Viet Nam northern mountain areas to serve for socio-economic development" (code: BDKH.25/16-20).

Conflicts of Interest: The authors declare no conflict of interest.

References

1. Kunkel K.E.; Pritke, R.A.; S.A. Changnon. Temporal fluctuation in weather and climate extremes that cause economic and human health impacts – a review. *Bull. Amer. Meteor. Soc.* **1999**, *80*, 1077.
2. Trenberth, K.E. Observations: Surface and atmospheric climate change, in Climate Change 2007: The Physical Science Basis. *Cambridge Univ. Press, Cambridge, U.K.* **2007**, 235–336.
3. Boyle, J.S.; Chen, T.J. Synoptic aspects of the wintertime East Asian monsoon, in Monsoon Meteorology. *Oxford Univ. Press, Oxford, U.K.* **1987**, 125–160.
4. Alexander, L.V.; Zhang, X.; Peterson, T.C.; Caesar, J.; Gleason, B.; Klein Tank, A. M.G.; Haylock, M.; Collins, D.; Trewin, B.; Rahimzadeh, F.; Tagipour, A.; Rupa Kumar, K.; Revadekar, J.; Griffiths, G.; Vincent, L.; Stephenson, D.B.; Burn, J.; Aguilar, E.; Brunet, M.; Taylor, M.; New, M.; Zhai, P.; Rusticucci, M.; Vazquez-Aguirre, J.L. Global observed changes in daily climate extremes of temperature and precipitation. 111(D5). doi:10.1029/2005jd006290 *J. Geophys. Res*. **2006**, *111(D05109)*, pp.22. https://doi.org/10.1029/2005JD006290.
5. Zhai, P.; Pan, X. Trends in temperature extremes during 1951–1999 in China. *Geophys. Res. Lett.* **2003**, *30(17)*, 1913. https://doi.org/10.1029/2003GL018004.
6. Gong, D.Y.; Ho, C.H. Intra-seasonal variability of wintertime temperature over East Asia. *Theor. Appl. Climatol*. **2004**, *24*, 131–144.
7. Choi, Y.S.; Ho, C.H.; Gong, D.Y.; Jeong, J.H.; Park, T.W. Adaptive change in intra?winter distribution of relatively cold events to East Asian warming. *Terr. Atmos. Oceanic Sci.* **2009**, *20*, 807–816.
8. Walsh, J.E.; Phillips, A.S.; Portis, D.H.; Chapman, W.L. Extreme cold outbreaks in the United States and Europe, 1948–99. *J. Clim.* **2001**, *14*, 2642–2658. https://doi.org/10.1175/1520–0442(2001)014<2642: ECOITU>2.0.CO;2.
9. Takaya, K.; Nakamura, H. Mechanisms of intraseasonal amplification of the cold Siberian high. *J. Atmos. Sci.* **2005**, *62*, 4423–4440. https://doi.org/10.1175/JAS3629.1.
10. Jeong, J.H.; Kim, B.M.; Ho, C.H.; Chen, D.; Lim, G.H. Stratospheric origin of cold surge occurrence in East Asia, *Geophys. Res. Lett.* **2006**, *33*, L14710. https://doi.org/10.1029/2006GL026607.
11. Jeong, J.H.; Ho, C.H. Changes in occurrence of cold surges over East Asia in associated with Arctic Oscillation. *Geophys. Res. Lett.* **2005**, *32*, L14704. https://doi.org/10.1029/2005GL023024.
12. Shabbar, A.; Bonsal, B. An assessment of changes in winter cold and warm spells over Canada. *Nat. Hazards* **2003**, *29(2)*, 173–188.
13. Park, T.W.; Ho, C.H.; Jeong, S.J.; Jeong, Y.S.; Choi, S.K.; Park, S.K.; Song, C.K. Different characteristics of cold day and cold surge frequency over East Asia in a global warming situation. *J. Geophys. Res*. **2011**, *116*, D12118. https://doi.org/10.1029/2010JD015369.
14. Tân, P.V. Nghiên cứu xây dựng hệ thống mô hình dự báo hạn mùa cho một số hiện tượng khí hậu cực đoan phục vụ phòng tránh thiên tai ở Việt Nam. Báo cáo tổng kết đề tài KHCN cấp Nhà nước, mã số ĐT.NCCB–HUD.2011–G/09, 2014, 350.

VIETNAM JOURNAL OF HYDROMETEOROLOGY

Research Article

The impact of Climate Change on the transportation in Binh Thuan Province

Nguyen Van Hong[1*], Vo Thi Nguyen[1]

[1] Sub Institute of Hydrometeorology and Climate Change; nguyenvanhong79@gmail.com; vothinguyen.bb@gmail.com

*Correspondence: nguyenvanhong79@gmail.com; Tel.: +84–913613206

Received: 18 April 2021; Accepted: 29 June 2021; Published: 25 August 2021

Abstract: The paper provides information on the assessment of the impact of the change in temperature and rainfall under the RCP4.5 scenario in the middle and end of 21st century on the transportation in Binh Thuan Province. According to the simulation results, the temperature in Binh Thuan Province increases by 1.29–1.43ºC in the middle of 21st century and 1.77–1.87ºC by the end of the 21st century. Rainfall increases from 8.5–14% in the middle of the 21st century and 9.5–21.6% by the end of the 21st century. This has an impact on road, rail and seaport operations. The roads are at risk of deforming, increasing service and maintenance costs.

Keywords: Temperature; Rainfall; Climate change scenarios; Impacts; Transportation.

1. Introduction

Binh Thuan is the southernmost coastal province of Central Vietnam, with a tropical monsoon climate characterized by high temperature (26.5–27.5ºC), large amount of sunshine and low rainfall (800–1800 mm) without a cold winter. According to a series of statistics at Phan Thiet station in the period of 1984–2019, the temperature tends to increase by 0.2ºC per decade and the rainfall tends to increase by 16 mm per decade. Severe drought in a 6–month dry season in Binh Thuan occurs with a frequency of 7.1% and extremely severe drought occurs with a frequency of 3.7%. On average, there are 0.48 storms and tropical depressions each year directly affecting the province. The sea level at Phu Quy station tends to increase by 5.3 cm per decade. The trends of climate change are becoming more and more obvious; the weather is becoming more complicated with the increase in heavy rains, droughts, high tides, floods, storms, inundation, saltwater intrusion and coastal erosion. Heavy rains accompanied by tornadoes have torn off roofs, damaged houses, and made power poles and roadside trees toppled in recent years in Lac Tanh town, Duc Binh and Duc Thuan communes (Tanh Linh district). The dam of the Ocean Valley project was broken due to the heavy rain in Tien Thanh commune (Phan Thiet), causing rapid flow with mud and sand, resulting in landslides into DT 719 (Provincial Road 719). In addition, the power consumption also increases in the context of the temperature increase [1–6]. Based on the assessment on impacts of climate change and sea level rise [7–10], the study on the results of research on assessing the impacts of climate change in Binh Thuan Province on the transport industry with key sub–sectors (roads, railways and seaports) will have a certain contribution to strengthening the local capacity in responding to climate change.

2. Materials and Methods

2.1. Materials

The temperature and rainfall data at Phan Thiet station and in neighboring provinces of Binh Thuan province in the period of 1984–2019 are used to develop scenarios and verify the climate models. The collected maps are DEM digital elevation maps and maps of the transport sectors [6].

2.2. Methods

The impact of climate change on the Transport sector is evaluated based on the combination of 03 methods including extrapolation of historical monitoring data, numerical model and workshops. The statistics of historical data and data on the impact of climate change and sea level rise are to give an overview of the impacts in the past. The numerical model is used to predict future impacts through extrapolation of monitoring factors. And the analytical method is based on consultation and assessment of experts through the workshop to analyze the impacts of climate change on the subjects under consideration. The three applicable approaches consist of the impact approach, interactive approach, and integrated approach [11–16]. The RCP 4.5 scenario – the climate change scenario – which is used for impact assessment is detailed from the results of regional climate models for Binh Thuan province as show in Table 1.

Table 1. Regional climate models used in the calculation of climate change scenarios for Binh Thuan Province.

No.	Model	Boundary conditions originating from a global model	Resolution	Data retention period	
				Base period	RCP4.5
1	CCAM	ACCESS1–0	10km	1970–2005	2006–2099
2		CCSM4			
3		CNRM–CM5			
4		GFDL–CM3			
5		MPI–ESM–LR			
6		NorESM1–M			
7	RegCM	ACCESS1–0	20km	1980–2000	2046–2065
8		NorESM1–M			2080–2099
9	PRECIS	HadGEM2–ES	25km	1960–2005	2006–2099
10		GFDL–CM3			
11	CLWRF	CNRM–CM5	30km	1980–2005	2006–2099
12		NorESM1–M			

3. Result and discussion

3.1. Impacts of temperature rise

According to the RCP 4.5 scenario, the temperature of the roads located in the study area increases from 1.29–1.43^{o}C in the middle of the century and 1.77–1.87^{o}C by the end of the century. The temperature rise makes the concrete on the pavement soft and expanding, resulting in risks of cracking and rutting of wheel tracks on the asphalt pavement. The North–South railway passing through the province is also suffered from the impacts of the increase in

temperature. The temperature rise also causes the risks of deforming and shortening the life of the train and related equipment. The embankment and breakwater areas (Vinh Tan port, Phan Thiet port) are located in the area where the temperature increases from 1.39–1.4°C; 1.8 –1.81°C in the middle and end of the century respectively. The temperature rises results in the increase in the maintenance costs of embankment systems. The impacts of temperature variation are as shown in Figure 1 and Table 2.

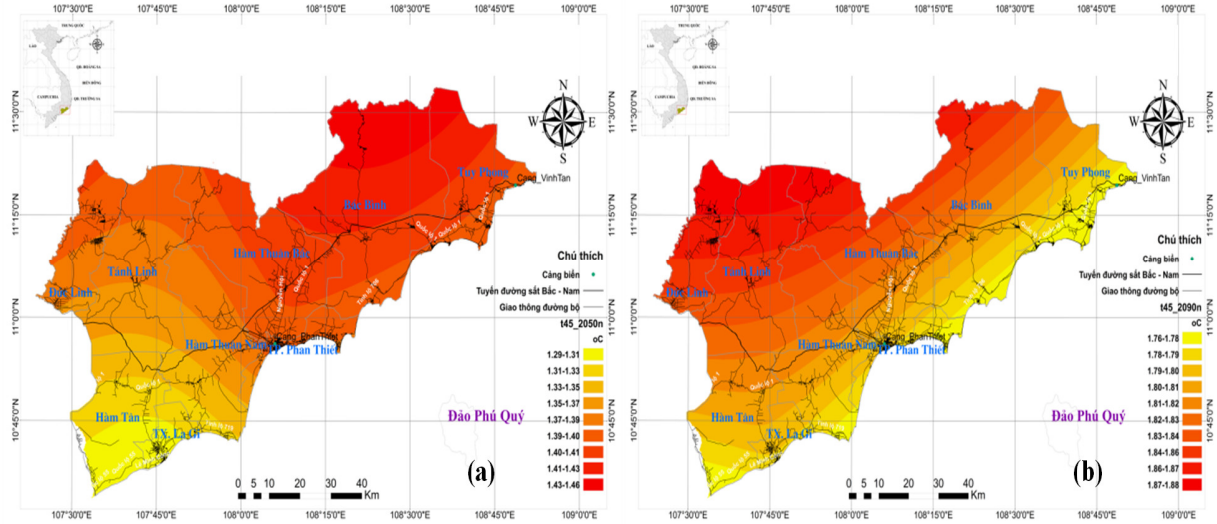

Figure 1. Map of temperature variation under the RCP4.5 scenario for the period: a) mid–21st century; b) the end of the 21st century.

Table 2. Temperature variation at some traffic routes.

Area	Increasing Temperature variation (°C)		
1. Road location			
	Location	Mid–21st century	End of 21st century
Phan Thiet	DT.719 (Tien Thanh, Tien Loi)	1.35–1.39	1.77–1.81
	DT.706B (Phu Hai, Ham Tien)	1.39–1.40	1.79–1.80
La Gi	National Road 55 (Tan Phuoc, Tan Thien, Tan An)	1.29–1.30	1.78–1.80
Duc Linh	DT.720, Ton Duc Thang, Cao Thang (Vo Xu)	1.38–1.39	1.85–1.87
Tanh Linh	DT.710, ĐT.720 (Lac Tanh)	1.36–1.38	1.83–1.86
Ham Tan	National Road 55(Tan Xuan, Tan Ha, Song Phan, Tan Nghia	1.29–1.35	1.79–1.82
Ham Thuan Nam	DT.712 (Tan Thuan, Thuan Nam), DT 719 (Tan Thuan, Tan Thanh)	1.32–1.35	1.77–1.80
Ham Thuan Bac	National Road 1 (Hoa Thang, Ham Duc, Hong Son, Hong Liem, Phu Long)	1.39–1.42	1.79–1.82
Bac Binh	National Road 1 (Binh Tan, Song Binh, Phan Thanh, Phan Hiep, Luong Son, Phan Ri Thanh)	1.39–1.43	1.77–1.83
Tuy Phong	National Road 1 (Vinh Tan, Vinh, Phuoc The, Phu Lac, Binh Thanh, Chi Cong, Hoa Minh, Lien Huong)	1.39–1.40	1.79–1.79

Area		Increasing Temperature variation (°C)	
2. North–South Railway			
Phan Thiet	Phan Thiet City	1.39–1.40	1.80–1.81
Tanh Linh	Gia Huynh, Suoi Kiet	1.35–1.36	1.82–1.84
Ham Tan	Tan Phuc, Song Phan	1.30–1.35	1.81–1.82
Ham Thuan Nam	Tan Lap, Ham Cuong, Ham Kiem	1.32–1.39	1.80–1.83
Ham Thuan Bac	Ham Hiep, Ham Liem, Ham Chinh, Hong Son, Hong Liem, Ma Lam	1.38–1.42	1.79–1.82
Bac Binh	Phan Hoa, Phan Hiep, Hai Ninh, Phan Thanh, Song Binh, Song Luy, Binh Tan, Luong Son	1.39–1.43	1.77–1.89
Tuy Phong	Phong Phu, Phu Lac, Vinh Hai, Vinh Tan	1.39–1.41	1.79–1.80
3. Areas adjacent to the coast			
Phan Thiet	Phan Thiet Port	1.39–1.40	1.80–1.81
La Gi	Lagi Port	1.29–1.30	1.78–1.79
Tuy Phong	Vinh Tan Port, Phan Ri Cua Port	1.39–1.41	1.79–1.80

3.2. Impacts of the increasing rainfall

According to the RCP 4.5 scenario, rainfall in the roads located in the study area increases from 8.5%–14% in the middle of the 21st century and 9.5%–21.6% at the end of the 21st century. The increased rainfall disrupts traffic, delays construction activities, and weakens or washes away soil and leads to overload for the supporting sewer systems. The North–South railway passing through the province is also affected by the increase in rainfall. Heavy rains can delay and disrupt trains, cause risks to the drifting and damage to the track and risk to the safety of the devices. In the middle of the century, rainfall in the areas of Phan Thiet port, Lagi fishing port, Vinh Tan port has an increase from 8.9% to 13.7% and an increase from 9.5% to 21.3% by the end of the century. The impacts of temperature variation are detailed as show in Figure 2 and Table 3.

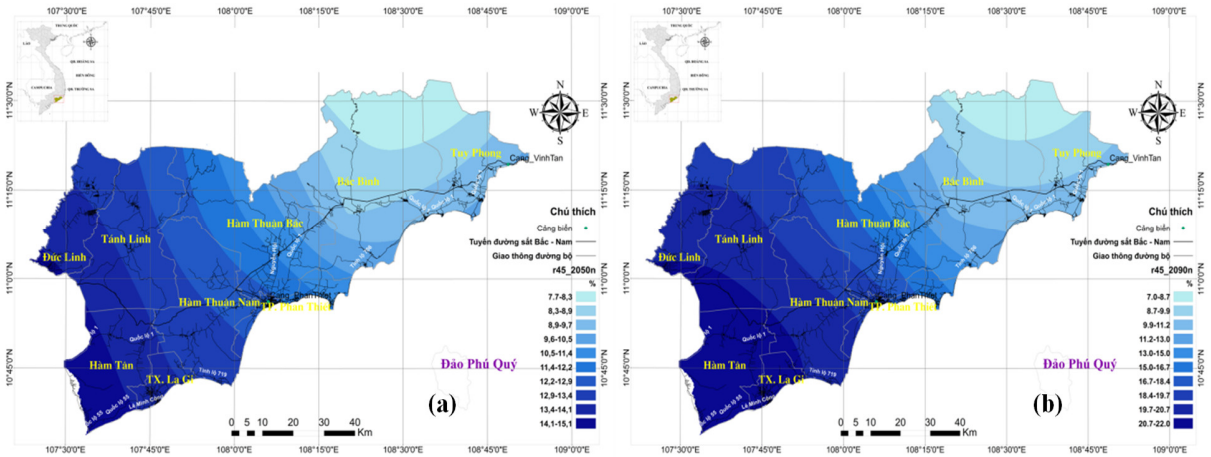

Figure 2. Rainfall verification map under the RCP4.5 scenario for the period: a) mid–21st century; b) the end of the 21st century.

Table 3. Temperature variation at some traffic points.

Area	Increasing Rainfall (%)		
1. Road			
	Location	Mid–21st century	End of 21st century
Phan Thiet	DT.719 (Tien Thanh, Tien Loi)	12.5–13.0	19.3–20.1
	DT.706B (Phu Hai, Ham Tien)	11.3–12.2	16.5–17.9
La Gi	National Road 55 (Tan Phuoc, Tan Thien, Tan An)	13.5–14	21.9–21.5
Duc Linh	DT.720, Ton Duc Thang, Cao Thang (Vo Xu)	13.4–13.8	19.7–20.3
Tanh Linh	DT.710, ĐT.720 (Lac Tanh)	12.9–13.4	19.6–21.2
Ham Tan	National Road 55(Tan Xuan, Tan Ha, Song Phan, Tan Nghia	13.4–13.9	20.8–21.6
Ham Thuan Nam	DT.712 (Tan Thuan, Thuan Nam), DT 719 (Tan Thuan, Tan Thanh)	13.1–13.5	20.2–21.1
Ham Thuan Bac	National Road 1 (Hoa Thang, Ham Duc, Hong Son, Hong Liem, Phu Long)	9.5–12.7	12.1–19.3
Bac Binh	National Road 1 (Binh Tan, Song Binh, Phan Thanh, Phan Hiep, Luong Son, Phan Ri Thanh)	8.5–9.4	9.6–15.2
Tuy Phong	National Road 1 (Vinh Tân,Vinh Hao, Phuoc The, Phu Lac, Binh Thanh, Chi Cong, Hoa Minh, Lien Huong)	9.2–9.8	9.5–11.2
2. North–South Railway			
Phan Thiet	Phan Thiet City	12.2–12.5	17.9–19.3
Tanh Linh	Gia Huynh, Suoi Kiet	12.9–13.4	19.6–21.2
Bac Binh	Phan Hoa, Phan Hiep, Hai Ninh, Phan Thanh, Song Binh, Song Luy, Binh Tan, Luong Son	8.5–9.4	9.6–15.2
Ham Tan	Tan Phuc, Song Phan	13.4–13.9	20.8–21.2
Ham Thuan Bac	Ham Hiep, Ham Liem, Ham Chinh, Hong Son, Hong Liem, Ma Lam	9.5–12.7	12.1–19.3
Ham Thuan Nam	Tan Lap, Ham Cuong, Ham Kiem	12.5–13.5	18.1–21.1
Tuy Phong	Phong Phu, Phu Lac,Vinh Hai,Vinh Tan	8.9–9.8	9.5–10.1
3. Areas adjacent to the coast			
Phan Thiet	Phan Thiet Port	12.5–12.8	17.9–19.3
La Gi	Lagi Port	13.5–13.7	21.0–21.3
Tuy Phong	Vinh Tan Port, Phan Ri Cua Port	8.9 –9.2	9.5 – 10.1

4. Conclusion

The climate change will pose impacts on transport sector in Binh Thuan Province inclusive of traffic routes (roads, railways, and waterways), areas adjacent to the coast and embankments in Binh Thuan province. The temperature rise poses risks of deforming on the railway, causing distortion for rail signals and deduction in life cycle of train and related devices. The base–temperature rise and high value of temperature shall be one of the factors causing risks of concrete cracks, cracking and rutting of wheel tracks of asphalt pavement, reducing the service life of the building and increasing costs for service and maintenance. The increase in rainfall can lead to the delay and interruption of transport routes, landslides, and leave debris on the road causing danger during transportation. Heavy rain may cause the risk of flooding, directly affecting traffic works, increasing erosion of road surface and roadbed. In addition, traffic routes, train stations, bus stations and railway lines may also be affected causing impacts on the travel process.

Author Contributions: N.V.Hong. and V.T.Nguyen. discussed the original idea of the draft. N.V.Hong. analysed and designed the input data. V.T.Nguyen. wrote and edited the manuscript. N.V.Hong. analysed the output data. Both authors reviewed and submitted the final version of manuscript. All authors have read and agreed to the published version of the manuscript.

Acknowledgments: The authors would like to thank the Project "Development of climate change action plans for the Construction, Industry and Trade, Transport, Tourism and some localities in Binh Thuan Province" for their support in the implementation of the article.

Conflicts of Interest: The authors declare that there are no conflict of interest.

References

1. Hưng, N.Q.; Khánh, L.Đ.; Liên. N.T. Application of Variable Infiltration Capacity Model (Vic) for Calculatingdrought Iindicators for Binh Thuan Province. *Tạp chí Các khoa học về trái đất và Môi trường* **2018**, *34(1S),* 41–49.
2. Vinh, P.Q.; Hương. P.T.H. Đánh giá hạn nông nghiệp tỉnh Bình Thuận theo kịch bản Biến đổi khí hậu. *Tạp chí Các khoa học về trái đất* **2012**, *34(4)*, 513–523.
3. Sơn, N.T. Đánh giá tình hình hạn hán tại tỉnh Bình Thuận giai đoạn 1984–2016. *Tạp chí Khoa học Nông nghiệp Việt Nam* **2018***, 16(4)*, 339–350.
4. Tân, P.V.; Thành, N.Đ. Biến đổi Khí hậu ở Việt Nam: Một số kết quả nghiên cứu, thách thức và cơ hội trong hội nhập quốc tế. *Tạp chí Các khoa học về trái đất* **2013**, *29(2)*, 42–55.
5. Huy, H.A.; Linh, P.M.; Đại, H.V. Extreme natural disasters challenges and opportunities in south central region in context of climate change. *Tạp chí Khí tượng Thủy văn* **2020**, *712*, 23–29.
6. Sub–Institute of Hydrometeorology and Climate Change. Development of climate change action plans for the Construction, Industry and Trade, Transport, Tourism and some localities in Binh Thuan province, 2019.
7. Vietnam Institute of Meteorology, Hydrology and Climate Change. Guidelines for assessing climate change impacts and identifying adaptation solutions, Vietnam Publishing House of Natural Resources, Environment and Cartography, 2011.
8. Ministry of Natural Resources and Environment, Vietnam. Circular 08/2016/TT–BTNMT providing detailed regulations on impact assessment of climate change and the national climate assessment, 2016.

9. CIEM, DOE and UN University. Impact of climate change on economic growth and development in Vietnam, Statistical Publishing House, 2012.
10. Asian Development Bank (ADB). Summary on Climate Change Impacts and Response Plan: transport sector (Road), energy sector, urban planning, 2015.
11. Ministry of Natural Resources and Environment, Vietnam. Updated results for Scenarios of climate change and sea level rise for Viet Nam, 2016.
12. IPCC. Climate Change: The Scientific Basis. Contribution of Working Group I to the Fourth Assessment Report of the Intergovernmental Panel on Climate Change, Cambridge University Press, Cambridge, United Kingdom and New York, NY, USA, 2007.
13. IPCC. The Physical Science Basis. Contribution of Working Group I to the Fourth Assessment Report of the Intergovernmental Panel on Climate Change, 2007.
14. IPCC. Fifth Assessment Report: Climate Change 2013 – The Physical Science Basis. Cambridge University Press, Cambridge, UK, 2013, pp. 1535.
15. IPCC. The Physical Science Basis. Contribution of Working Group I to the Fifth Assessment Report of the Intergovernmental Panel on Climate Change, 2013.
16. IPCC. Managing the Risks of Extreme Events and Disasters to Advance Climate Change Adaptation, A Special Report of Working Groups I and II of the Intergovernmental Panel on Climate Change, Cambridge University Press, 2012.

VIETNAM JOURNAL OF HYDROMETEOROLOGY

Rerearch paper

Application of machine learning method–decision tree to classification of oil use sentinel 2

Ha Phong Doan[1*], Thanh Bang Nguyen[1], Dang Hung Tran[1], Dao Xuan Hoang[1], Tran Anh Doan[1]

[1] Vietnam Institute of Meteorology Hydrology and Climate Change (IMHEN); doanhaphong@gmail.com; bangnt29@gmail.com; danghung2261991@gmail.com; hoangdx81@gmail.com; dtrananh2612@gmail.com

*Corresponding author: doanhaphong@gmail.com; Tel.: 84–913212325

Received: 27 February 2021; Accepted: 15 June 2021; Published: 25 August 2021

Abstract: Decision tree classification algorithms have significant potential in classifying remote sensing data. This article's approach method using decision tree technology to classify remote sensing images with the representative object as oil spill. First, this paper discusses the algorithmic structure and algorithmic theory of the decision tree. Second, the build of decision tree classification algorithm with 10 branches for oil spill classification using Sentinel 2 image data based on the JavaScript application's online interface (API) called Code Editor. Decision tree technology has several advantages for remote sensing applications due to their relatively simple, clear and intuitive classification structure.

Keywords: Decision Tree; Classification; Models; Machine Learning; Remote sensing image; Oil Spill.

1. Introduction

Remote sensing techniques in detecting oil spills based on remote sensors are widely used in the world. There are many types of remote sensing materials that have supported in monitoring and detecting polluting oil spill locations. Radar technology can monitor a wide area, day and night regardless of rainy/ cloudy weather due to an infrared device that detects oil spill at night and a UV laser (fluorosensor laser). Therefore, most oil spill maps are used radar technology.

In the Caspian Sea region of Azerbaijan, a stochastic model of oil spills risk leading to deterioration of water quality and coastal ecosystems was established by using satellite imagery. More than 411 satellite images obtained by sensors SENTINEL–1, LANDSAT–8, RADARSAT, ENVISAT and ERS from 1996 to 2017 are used for semi–automatic detection and classification of oil spills and slicks. Natural oil slicks are classified based on object orientation and visual interpretation. Parameters such as size, shape are determined, oil slick location takes into account the interaction between factors such as wind speed and current direction, depth and main source of emissions at the seabed. The pixel values in the combined pollution hazard model are positively correlated with the observed frequency of oil spills during the research period, contributing to improving the reliability of the modeling method [1].

The SANCHI tanker collision accident in January 2018 in the South China Sea shows that traditional techniques using synthetic aperture radar or daylight optics do not provide timely and complete information about the incident. Therefore, a Visible Infrared Imaging Radiometer Suite (VIIRS) and day/ night Automatic Indentification System (AIS) were used. The path and position can also be built as a numerical model, with an average error

from the origin < 15 km. While high–resolution optical images taken 4 days after the tanker sank show a much larger area of oil spill (> 350 km^2). In this case the VIIRS night data is the only satellite data that has proven effective in detecting the orbital drift and daily position of the ship, while all other sensor satellites can not observe or obscured. Together with digital equipment to detect oil tankers and other sensors to re–map the oil spill trajectory [2]. Sentinel–3 satellite with OLCI probe has also been used to track and monitor the Sanchi collision by combining close to the true color of channels 10,5,1 as shown in Figure 1.

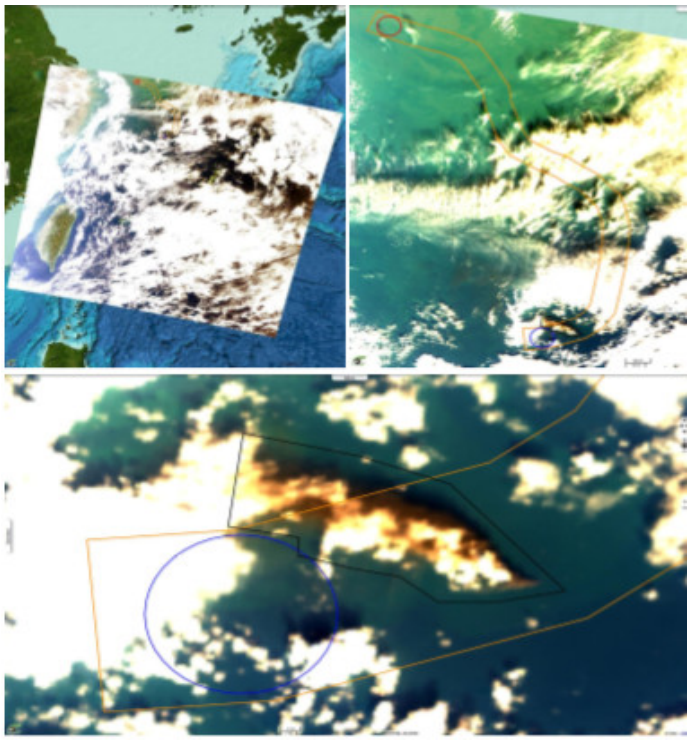

Figure 1. Sentinel–3 OLCI acquired on 14 Jan 2018 at 01:38:58 GMT [2].

Based on the reflection of the sun on the sea surface, it can be difficult to distinguish an oil stain. However, observed by the 300 m resolution Sentinel–3 image, the position of the boat and the cargo burning fiercely a few hours before sinking, an oil slick away from the sinking area was shown on this complex image.

Research on oil spills in the Deepwater Horizon area, used Synthetic Aperture Radar (SAR) within 10 km of the coast with suitable weather conditions to detect oil. In case of large oil spills occurred, SAR satellites will collect spill location data and provide oil spill feedback from one or more images per day, helping to estimate the trajectory of the oil spill. The combination of oil stains in shallow water will be affected by the current, wind direction and wave direction affecting the oil drift. By collecting and analyzing sequence of time SAR images in the same location, the speed and trajectory of oil drift in coastal areas can be estimated. The simplest oil spill model can be built, simulating the movement of oil on the ocean surface by tracking the motion of a large number of particles moving with velocities that are a combination of ocean surface velocities and speed of winds [3].

The results of satellite monitoring of the oil spill in the Barents Sea 2015–2016 also used SAR images from the European space satellite Sentinel–1A and Sentinel–1B. To efficiently analyze the SAR images, a site–based GeoMixer application–specific geographic approach was used. Dedicated Geoportal with a large volume of oceanographic, geographic and watershed information, including oil and gas infrastructure and coastlines. This tool with data from AIS has shown that the main sources of oil pollution (spill from 0.5 to 90 km^2) are freight transport and fishing vessels from which an overview map of the

oil spill was developed of reportred. Most surface oils are detected in the summer, which is a typical seasonal dynamic. Over time, single cases of large oil spills at sea were observed. Oil spill distribution maps based on SAR images provide assistance in obtaining new information on the extent and sources of oil contamination.

Thus, with the development of Remote Sensing technology in oil pollution detection, in addition to the advantages of Radar sensors, optical sensors (near infrared at night, visible, ultraviolet rays) must still be used. purple) to obtain as much information about oil pollution at sea as possible, combined with the information of the oil decoder [4].

If using a large number of satellites of all kinds, it is possible to build an oil orbit according to the corresponding time (from 15 to 60 days), combined with wave and wind data, which can serve for source tracing oil–based relatively accurately [1–4].

Oil pollution of unknown origin on the coast of Vietnam is usually pollution in two forms: visible to the naked eye: patches, streaks, oil patches, rocks, hydrated oil lumps floating in close waters or rocks, oil lumps that have been ored to varying degrees located onshore , yards; not visible to the naked eye: the form is soluble in water or deposited in sediment with content exceeding the limits allowed in coastal seawater standards [5].

Based on the results of research on the state–level topic [6] two types of ultra–high–frequency satellite imagery materials are ENVISAT ASAR and ALOS PALSAR, with a total of 110 scenes (2007). The number of ENVISAT ASAR images ordered is 10 scenes, at a processing level of 1B. The number of photos ALOS PALSAR ordered was 80 scenes, a processing level of 4.2. In addition, 20 ENVISAT ASAR images collected from the Department of Environmental Protection – Ministry of Natural Resources and Environment are also used to assist in the detection of oil stains at sea [7].

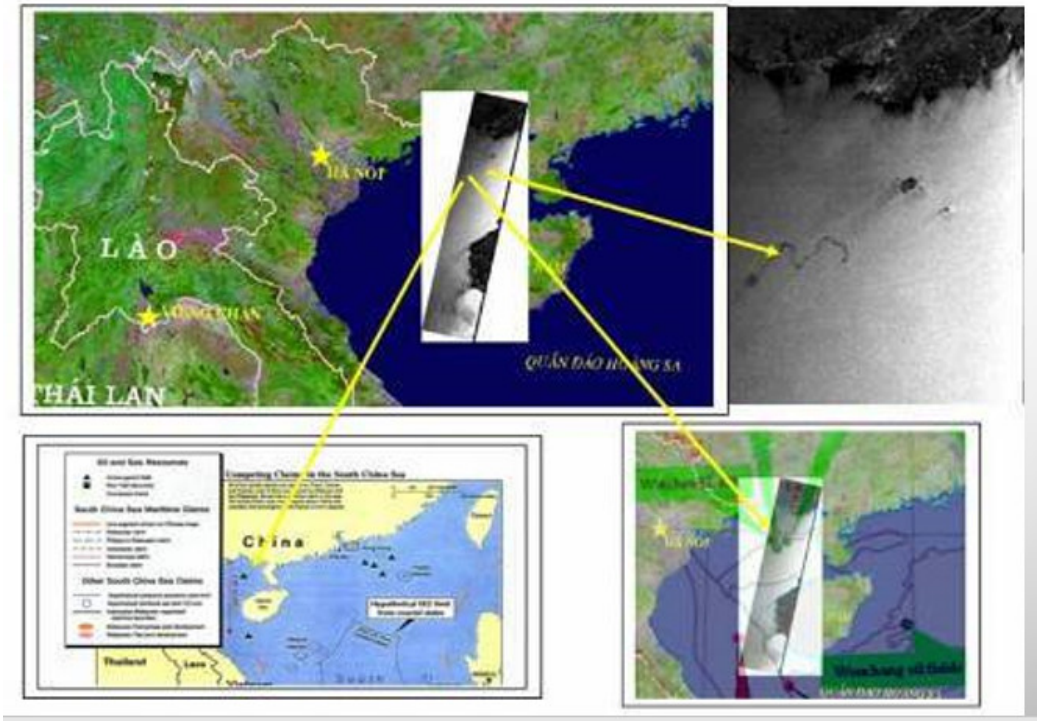

Figure 2. The source of oil pollution comes from the area where the oil field is located.

The source of oil pollution comes from the oil field area in southern China (in the Gulf of Tonkin region), the central coordinates of the polluted region about: Latitude 108°45' and latitude 20°50'. Envisat Asar satellite image number: ASA_IM Orbit 25179 Track 75, Swath I1. Collection time: December 24, 2006 at 02:48.64 (UTC). 147 ENVISAT ASAR scenes, 49 ALOS PALSAR scenes (December 2006 to April 2007) were used in the identification of oil pollution sources [8].

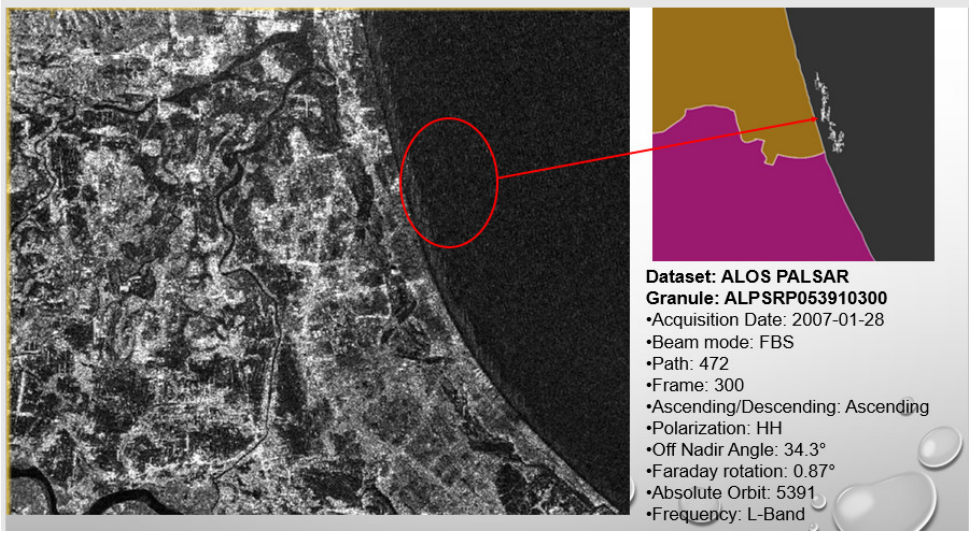

Figure 3. ALOS PALSAR satellite image dated January 28, 2007 Cua Dai Beach – Hoi An (Quang Nam), Non Nuoc (Da Nang). Oil pollution area and interpretation in red circle [8].

On January 30, 2007, the oil clumps and oil carpet stretched nearly 20 km from the sea area of Da Nang to Quang Nam, off the coast, the spreading oil slick was still floating on the water. Many black oil blocks began disintegrated and floated on the sea. Figure 3 shows the oil slick detected after treatment, starting for 6 months of major oil spills occurring in 20 coastal provinces of Vietnam.

Thus, the use of remote reconnaissance in monitoring and monitoring the location of oil spills of unknown origin (has been conducted in Vietnam in case of oil spills with particularly serious consequences, from the time of the oil spill to the detection occurs in 1 month) with a very large number of satellite images (approximately 200 scenes of all kinds have been selected). In particular, mainly using radar images of all kinds (image resolution from 10–30 m, suitable for the establishment of a ratio of 1: 50,000, serving a provincial scale), image processing and data extraction does not keep up with the requirements of location determination, not combined with the back–time model. Optical fars telescopes are almost uns mentioned and used appropriately in determining the trajectory, and specifications of oil spills.

Remote sensing information classification and exploitation play as an important role in the field of remote sensing technology. In the remote sensing classification application, traditional classification methods such as supervised classification, unsupervised classification and expert classification are all based on spectrum image features. However, since the image itself has the phenomenon of the same object having different spectra, and different objects have the same spectrum, classification methods based only on the ground spectral features always included many false classifications and omit errors. Numerous studies show that a classification combined with image spectrum and other supporting information can greatly improve the accuracy of a classification [9].

A random forest classifier is a group classifier that produces multiple decision trees, using a randomly selected subset of training samples and variables [10]. Due to the accuracy of this classifier has been used in this research. Decision trees classification as a supervised classification method that exploits spatial data, solves previous classification problems and rules, as well as making use of certainty ecological and remote sensing knowledge and the results are always closely related to experience and expertise. It has the classification rules by the decision research process and does not need to satisfy the normal distribution [11]. It can use the knowledge of the earth in the GIS database to help with the classification and improve the accuracy of the classification [12].

Currently, decision tree classification has been applied in the field of land use, land use change as capture and scoping remote sensing images [13]. In the United States, the USGS and EPA, the departments have agreed to put in place the US land cover database plan and decision tree classification technology not only to be applied in soil classification but also in urban density information and urban density class information extraction. Land classification accuracy reached 73–77% and urban density information extraction accuracy is from 83% to 91% and canopy accuracy is 78–93% [14]. The mapping efficiency has been improved by 50% and can meet the requirements of large–scale soil classification data production.

Decision tree research method is one of the data mining methods to find classification problems in reality. It can classify the rules of decision tree expression form. The great advantage of the decision tree is that the research does not require a user with huge background knowledge [15]. As long as the input data examples can be represented by "attribute–result" and use this algorithm to learn. Categorizing the data obtained by the decision tree is easy to show and apply. Currently, foreign scholars have used decision trees to gather knowledge and apply them in spatial research and analysis.

Recently, sentinel 2 optical satellite with a resolution of 10 m is a source of high–resolution free remote images as well as low image repeat (5 days) is a valuable resource for us to monitor and monitor oil spills so it is necessary to develop a method of classification of oil spills from satellite images. Sentinel 2 with new classification algorithms and suitable for this satellite image.

Therefore, the purpose of the study is to test the application of the decision tree machine learning algorithm in oil spill classification using Sentinel 2 satellite images, as well as determine the best number of branches for this classification.

2. Materials and Methods

2.1. Description of study site

In this study, remote sensing data which is Sentinel 2 optical satellite data is used to detect oil spills in the coastal area of Binh Dinh province in May 2020. The reseach site located in Binh Dinh – a coastal province in central Vietnam. The province's territory stretches for 110 km in the North–South direction, with an average width of 55 km (50 km at the narrowest point, 60 km at the widest place). The North borders Quang Ngai province with a common boundary line of 63 km (the northernmost point has coordinates: 14°42'10" North, 108°55'4" East). The South borders Phu Yen province with a common boundary of 50 km (the southernmost point has coordinates: 13°39'10" North, 108°54'00" East). The West borders Gia Lai province with a common boundary line of 130 km (the westernmost point has coordinates: 14°27' North, 108°27' East). The East borders the East Sea with a coastline of 134 km, the easternmost point is Nhon Chau commune (Cu Lao Xanh) in Quy Nhon city (coordinates: 13°36'33" North, 109°21' East). Binh Dinh is considered as one of the gateways to the sea of the Central Highlands provinces and southern of Laos (Figure 4).

2.2. Research data

This study will test the recognition and classification using a decision tree algorithm for an oil spill accident in Binh Dinh Province, Vietnam. Multispectral optical satellite images show a sharp contrast to the surrounding oil–free water, which depends on several factors such as the shape of the sun observed, the type of oil, and the thickness. The Sentinel–2 satellite consists of 13 spectral channels, a near–infrared band at 10 m resolution, six red/short–wave infrared bands at 20 m, and three atmospheric correction bands at 60 m.

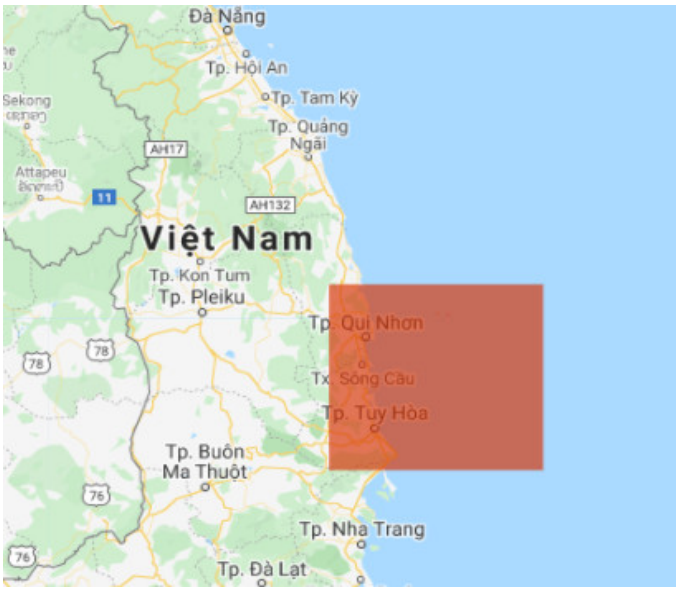

Figure 4. Binh Dinh coastal area.

Table 1. Sentinel 2 used images.

Research area	Date	Sensor Type	Name
Binh Dinh coastal	12/5/2020	Sentinel 2A	S2A_MSIL1C_20200512T030551_N0209_R075_T49PCR_20200512T061450
Binh Dinh coastal	12/5/2020	Sentinel 2A	S2A_MSIL2A_20200512T030551_N0214_R075_T49PBS_20200512T073119

2.3. Arithmetic Decision Tree

A decision tree is a method that can be inductive by training patterns and building a decision tree or decision rule and then use them to categorize data [16]. A decision tree composed of a root node, a series of inner nodes and leaf nodes. Each node can have only one primary node and two or more sub nodes. Nodes are connected by branches. Each inner node corresponds to an experimental property or property group, and every side corresponds to any possible value of the property. A node corresponds to a class attribute value, and a different node can correspond to the same class attribute value. Decision trees not only can be represented by trees, but also as a group of IF–THEN rules. Each line from the root to the leaf corresponds to a rule, and the rule's condition is, optionally, all of the node's attribute values. And the result of the rule is the class attribute of the leaf node on the road. Compared with decision attributes, the rules are simpler and more convenient to understand, to use, repair and can form the basis of the expert system [17]. Therefore, the rule is being used more and more in practical application.

2.3.1. Classification and Regression Tree (Cart)

Classification and regression tree is a common tree growth algorithm. It was presented by Breiman, etc. and it is a supervised classification method. It trains the sampler to build a binary tree and decode it for classification [18]. This feature is to take advantage of the full binary structure, in other words, the root node includes all patterns. The root node is divided into two subnodes according to defined division rules. This process repeats again in the child node and becomes a regression process until the subnode cannot divide into two subnodes [19]. Building the CART thinking training is based on a whole sampled data, building a multi–level and multi–leaf node tree to reflect the relationship between the nodes and then cutting the tree to create a series of subtree and selecting suitable trees in order to classify the data. In detail, the process involved building a tree and pruning a tree.

a) Tree Development

The distinction of tree nodes is named a branch and it corresponds to a subset of the training patterns. The branch of the root node corresponds to the entire training pattern. Then classification is the partition training sampling process. Therefore, the process of building a tree is to query properties to create partition rules. In this paper, CART adopts an index called "impurity level of the node": i (N) represents the impurity level of node N. When the data is from the same type, i (N) = 0; when the categories of data are evenly distributed, i (N) will be very large. The partition rule is created based on the minimum value of the impurity level function. Here two impurity functions are introduced.

- "Entropy impurity" also known as information impurity:

$$i(N) = -\sum_j P(w_j)\log_2 p(w_j) \quad (1)$$

where P (wj) is the calculation probability calculation for sampling data mode wj that node N belongs to the entire sampling process. According to the entropy parameters, if all data come from the same type then the impurity level is 0; or other impurity level is greater than zero; when all category data appear with the same probability calculation, entropy is the maximum value.

- VAR is the "Gini impurity level". According to nodes sampled from different categories and it is related to the total distribution variance, the below formula is given.

$$-\sum_{i\neq j} P(w_i)P(w_j) = 1 - \sum_j P^2(w_j) \quad (2)$$

The meaning of "Gini impurity level" is to represent the error rate of catalog creation in node N. When given a tree has grown to node N and the node is property queried, a heuristic thinking method has visible is to select the query with the fastest reduction in noise. Reduced impurity levels may be noted:

$$\Delta i(N) = i(N) - P_L i(N_L) - (1-P_L) i(N_R) \quad (3)$$

Include NL and NR as separate left and right buttons; i (NL), i (NR) are the individual impurity level. L P is the probability that when query T is passed, the tree grows from N to NL. And the optimal query value S is the maximum value of Δi (T) [20].

b) Reduce Branches

If we consisted in building the tree until all leaf nodes reach the minimum impurity level. The data will be over–sorted and the tree will degrade into a convenient lookup table. It may not be good for the overall performance of interfering lamps due to the larger Bayes error. Conversely, if the branches stop too early, the sampling training error will not be small enough resulting in a very poor type efficiency. One main method of stopping the branches is pruning, which can also prevent the tree from growing too big. In this paper, the following indicators are adopted to achieve the goal.

$$\cos t = \alpha.size + \sum_{leaf \quad node} i(n) \quad (4)$$

where cost is denoted the cost function of the tree weighted error probability and the sum of the complex penalty. Size is expressed from the number of leaf nodes to the weight complexity of the tree classifier, α is denoted as an index of complexity.

According to equation (4), pruning can be done in two steps:

(1) In all sibling leaf nodes, compare t cos after the associated leaf nodes.

(2) Delete the leaf node that has the most t cos. If t cos has not decreased, nothing will be done [21].

Repeat the above process until you cannot continue pruning. During pruning, the training error inferred with leaf nodes increases; The test error deduced at the start and

reached the minimum and then rolled up gradually affected by the training patterns. Use independent data to test and select a subtree with minimum test error as decision tree. This paper applies the heuristics–cross validation technique to select the best tree has 10 cross validations. The training samples are divided into ten subsets that are equal in number and not the same. The classifier will train the data 10 times, and each time the nine subset groups are trained, and one test is the validation set for estimating the test error. The estimated test error is the mean of the ten groups [22].

2.3.2. Enhancement Method – New Applied Techonology in Decision Trees

In decision tree classification design, an enhancement technology was widely used in the mid–1990s in the field of machine learning to improve the accuracy of the classifier. This method can increase the accuracy of the sampled classifier which is difficult to discern. At the same time, this technology can cut down on the sensitivity that the categorization algorithm affects data noise and training sampling error. Reinforcement is a learning method that can increase the accuracy of any learning algorithm, and it can strengthen a weak learning algorithm into a strong learning algorithm. Its theory is probably derived from an approximate learning model. It can leverage a number of mathematical algorithms to generate a wide range of basic classifiers [23]. Every basic classifying training depends on the classification results generated by the old classifier and ends up failing training samples with great weight so that they pay more attention during the next learning process. Finally, the classifier has a vote weighting for all base classifiers and receives the final results and reduces the signal classifier error and improves the classification accuracy. Freund and Schapire came up with the most pragmatic boosting algorithm–AdaBoost followed the basic theory of reinforcement in 1995 and is widely applied.

2.4. Applying Oil Spill Analysis Test Construction Algorithm for an Area

This article uses Google Earth Engine (GEE) software. Google Earth Engine works through a JavaScript Application Online Interface (API) called Code Editor. On this interface, users can write and run scripts/ scripts to share and repeat the processes of analyzing and processing geospatial data. Code Editor helps users to perform all functions available in Earth Engine. The process of constructing oil spill analysis method for Sentinel 2 image is shown in detail in Figure 5.

First, we declare Sentinel 2 data set as input data set for analysis. Thus, we filtered data by boundary, according to the date when the oil spill occurred, as well as filtered the scene with less clouds. After filtering the image, it is necessary to create a data set for training between the oil–free inlet. Conduct a very detailed and accurate sampling as well as the more samples, the better the output. After creating the training data set, the decision tree will be sorted according to Cart algorithm. The classification results are corrected by resample until best results are obtained. This process is also the process of selecting the best number of branches for the classification process. Using the trial and error method, with 10 branches the classification result is the most accurate. Finally, extract oil spill results and make final manual calibration using Arcmap software.

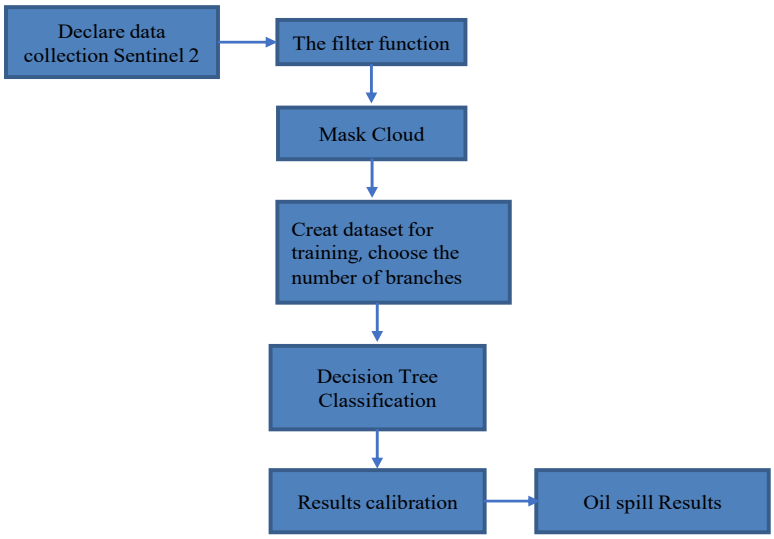

Figure 5. A Method of Constructing a Classification of Decision Trees On GEE.

3. Results and discussion

Run time series analysis 2020 in the coast of Binh Dinh Province detects the oil spill on May 12 in detail (Figure 6).

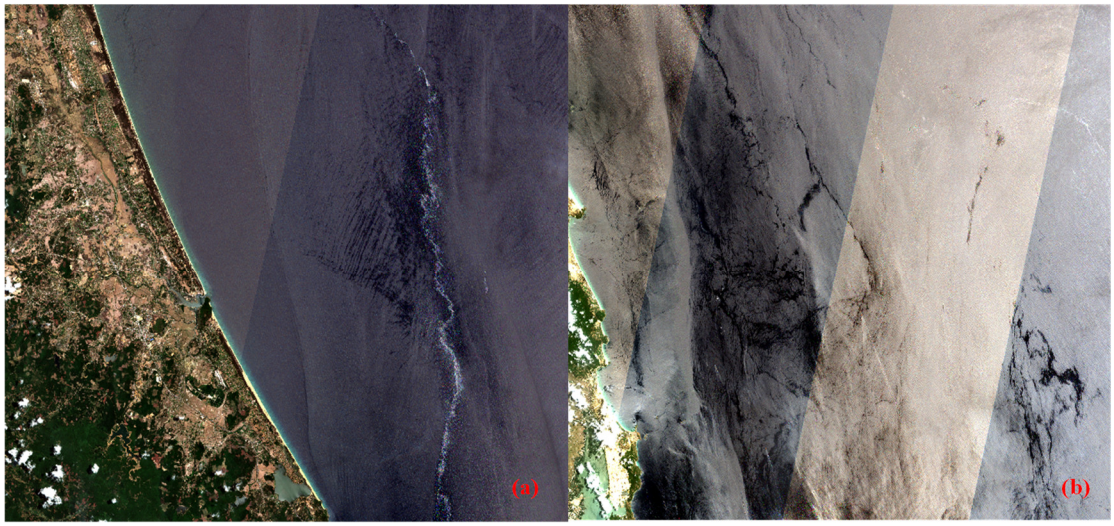

Figure 6. (a) and (b) 2 locations noticed oil spill on Sentinel 2 photo at the coast of Binh Dinh on May 12, 2020.

Create training datasets with 41 elements in google earth engine (Figure 7).

```
▾ FeatureCollection (41 elements, 2 columns)
    type: FeatureCollection
  ▾ columns: Object (2 properties)
      LC: Integer
      system:index: String
  ▾ features: List (41 elements)
    ▸ 0: Feature 1_0 (Polygon, 1 property)
    ▸ 1: Feature 1_1 (Polygon, 1 property)
    ▸ 2: Feature 1_2 (Polygon, 1 property)
    ▸ 3: Feature 1_3 (Polygon, 1 property)
    ▸ 4: Feature 1_4 (Polygon, 1 property)
    ▸ 5: Feature 1_5 (Polygon, 1 property)
    ▸ 6: Feature 1_6 (Polygon, 1 property)
```

Figure 7. Training datasets information.

The final oil spill result is shown as (Figure 8).

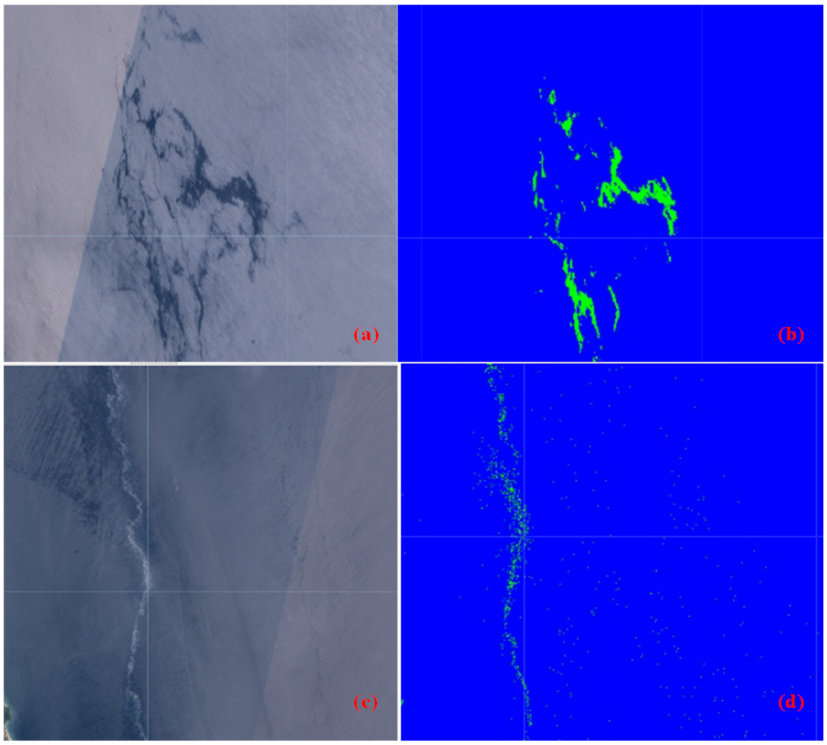

Figure 8. (a–d) The results of classification of two Sentinel 2 images on May 12, 2020

The results of classification were decent, the research was able to detect oil spills using Sentinel 2 images. As can be seen in Figures 8b and 8d, the oil spills areas were highlighted as green in contrast with the blue color of our seawater surface.

4. Conclusion

The advantage of the decision tree algorithm used in remote sensing data classification is that it can show the lack of the MLC algorithm when processing complex distributed data sets. Decision trees offer more flexibility and powerful with data distribution and categorization markup functions. Therefore, evenwhen the distribution of remote sensing image data characteristics is very complex or the source data size has different distributions and statistical ratios, the decision tree classification method can obtain the best classification results.

With the development of artificial intelligence technology and theory, the research of remote sensing image classification has reached to a higher level. Geographic knowledge and support for geographic decision–making can promote the accuracy of remote sensing image classification, extracting information and expert systems is a good approach to solve this problem. The article successfully researched and applied to classify oil spills is a good example to promote in–depth studies on the application of decision tree algorithm in resource and environmental management.

A big problem to be solved in the classification problem using the decision tree algorithm is the optimal number of branches for our problem. In the framework of the new paper, the trial and error method is applied with low accuracy, so it is necessary to develop a new method to give more accurate results.

Author Contributions: Conceptualization, methodology, validation, formal analysis; investigation and project administration: H.P.D; resources, data curation, software, draft preparation: T.B.N and D.H.T; writing–original, writing–review and editing, visualization: X.H.D and T.A.D.

Acknowledgements: This research was funded by the Viet Nam Ministry of Natural Resources and Environment (MONRE), grant No: TNMT.2018.05.39. The authors would like to thank the members of Hydrology–Meteorology and Climate Change Technology Research Division, Vietnam Institute of Meteorology Hydrology and Climate Change for discussions that improved the quality of the publication.

Competing interest statement: The authors declare no conflict of interest.

Reference

1. Bayramov, E.; Kada, M.; Buchroithner, M. Monitoring oil spill hotspots, contamination probability modelling and assessment of coastal impacts in the Caspian Sea using SENTINEL–1, LANDSAT–8, RADARSAT, ENVISAT and ERS satellite sensors. *J. Oper. Oceanogr.* **2018**, *11*, 27–43.
2. Sun, S.; Lu, Y.; Liu, Y.; Wang, M.; Chuanmin Hu, C. Tracking an Oil Tanker Collision and Spilled Oils in the East China Sea Using Multisensor Day and Night Satellite Imagery. *Geophys. Res. Lett.* **2018**, *45(7)*, 3212–3220. https://doi.org/10.1002/2018GL077433.
3. Garcia–Pineda, O.; Holmes, J.; Rissing, M.; Jones, R.; Wobus, C.; Jan Svejkovsky, J.; Mark Hess, M. Detection of Oil near Shorelines during the Deepwater Horizon Oil Spill Using Synthetic Aperture Radar (SAR). *Remote Sens.* **2017**, *9*, 567. https://doi.org/10.3390/rs9060567.
4. Ivanov, A.Y.; Filimonova, N.A.; Kucheiko, A.Y.; Evtushenko, N.V.; Terleeva, N.V. Oil spills in the Barents Sea based on satellite monitoring using SAR: spatial distribution and main sources. *Int. J. Remote Sens.* **2017**, *39*, 4484–4498. https://doi.org/10.1080/01431161.2017.1371869.
5. Nhân, N.H. và cs. Thử nghiệm mô hình OILSAS – công cụ trợ giúp ứng phó sự cố tràn dầu trên vịnh Vân Phong, tỉnh Khánh Hòa. *Tuyển tập Nghiên cứu Biển* **2014**, *20*, 19–29.
6. Dương, N.Đ. Ô nhiễm dầu trên vùng biển Việt Nam và biển Đông. Đề tài KC.09.22/06–10, 2010.
7. Dương, N.Đ.; Thu, H.L.; Anh, L.V.; Anh, N.K. Ô nhiễm dầu trên vùng biển Việt Nam và kế cận. *Tạp chí các Khoa học về Trái đất* **2013**, *35(4)*, 424–432.
8. Khánh, N.Q. và cs. Ứng dụng công nghệ viễn thám kết hợp với GIS phục vụ giám sát sự cố ô nhiễm dầu ở Việt Nam. *Tạp chí Môi trường* 2014, 7, 13–15.
9. Song, Y.Y.; Lu, Y. Decision tree methods: applications for classification and prediction. *Shanghai Arch Psychiatry* **2015**, *27*, 130–135.
10. Jenhani, I.; Amor, N.B.; Elouedi, Z. Decision trees as possibilistic classifiers. *Int. J. Approximate Reasoning* **2018**, *48*, 784–807.
11. Fouad, M.M. A Decision Tree Classification Model for University Admission System. *Int. J. Adv. Computer Sci. Appl.* **2012**, *3*, 184–186.
12. Zeng, X.; Yuan, S.; Li, Y.; Zou, Q. Decision Tree Classification Model for Popularity Forecast of Chinese Colleges. *J. Appl. Math.* **2014**, 675806. https://doi.org/10.1155/2014/675806.
13. Dai, Q.Y.; Zhang, C.P.; Wu, H. Research of Decision Tree Classification Algorithm in Data Mining. *Int. J. Database Theory Appl.* **2016**, *9*, 1–8.
14. Patel, H.H.; Prajapati, P. Study and Analysis of Decision Tree Based Classification Algorithms. *Int. J. Computer Sci. Eng.* **2018**, *6(10)*, 74–78.
15. Zhong, Y. The analysis of cases based on decision tree. Proceeding of the 7th IEEE International Conference on Software Engineering and Service Science (ICSESS), 2016.
16. Lian, H.; Yang, Y. Study on the Test Data Fault Mining Technology Based on Decision Tree. *Procedia Comput. Sci.* **2019**, *154*, 232–237.

17. Ivanov, A. Decision Trees for Evaluation of Mathematical Competencies in the Higher Education: A Case Study. *Mathematics* **2020**, *8(5)*, 748. https://doi.org/10.3390/math8050748.
18. Zimmerman, R.K.; Balasubramani, G.K.; Nowalk, M.P.; Eng, H.; Urbanski, L.; Jackson, M.L.; Jackson, L.A.; McLean, H.Q.; Belongia, E.A.; Monto, A.S.; Malosh, R.E.; Gaglani, M.; Clipper, L.; Flannery, B.; Wisniewski, S.R. Classification and Regression Tree (CART) analysis to predict influenza in primary care patients. *BMC Infect. Dis.* **2016**, *16(1)*, 503. https://doi.org/10.1186/s12879-016-1839-x.
19. Lemon, S.C.; Roy, J.; Clark, M.A.; Friedmann, P.D.; Rakowski, W. Classification and regression tree analysis in public health: Methodological review and comparison with logistic regression. *Ann. Behav. Med.* **2003**, *26*, 172–181.
20. Machuca, C.; Vettore, M.V.; Krasuska, M. et al. Using classification and regression tree modelling to investigate response shift patterns in dentine hypersensitivity. *BMC Med. Res. Method.* **2017**, *17*, 120. https://doi.org/10.1186/s12874-017-0396-3.
21. Denisko, D.; Hofman, M.M. Classification and interaction in random forests. *PNAS* **2018**, *115*, 1690–1692.
22. Basu, S.; Kumbier, K.; Brown, J.B.; Yu, B. Iterative random forests to discover predictive and stable high–order interactions. *PNAS* **2018**, *115*, 1943–1948.
23. Riddick, G. Predicting in vitro drug sensitivity using Random Forests. *Bioinf.* **2011**, *27*, 220–224.

VIETNAM JOURNAL OF HYDROMETEOROLOGY

Research Article

The advantage of using satellite data together with the hydraulic model in flood hazard assessment: A case study in Ca River downstream

Van Anh Truong[1], Anh Quan Duong[2*], Ngoc Quy Bui[2], Van Hiep Pham[2], Danh Duc Nguyen[2], Xuan Quang Truong[3], Thi Mai Anh Tran[4]

[1] Faculty of Meteorology and Hydrology, Hanoi University of Nature resources and Environment; tvanh@hunre.edu.vn
[2] Faculty of Geomatics and Land Administration, Hanoi University of Mining and Geology; duonganhquan@humg.edu.vn
[3] Faculty of Informatics, Hanoi University of Nature resources and Environment; txquang@hunre.edu.vn
[4] Faculty of Resources management, Thai Nguyen University of Agriculture and Forestry; tranthimaianh@tuaf.edu.vn

*Correspondence: duonganhquan@humg.edu.vn; Tel: +84–344779968

Received: 10 May 2021; Accepted: 08 July 2021; Published: 25 August 2021

Abstract: In Vietnam, the Central area faced the highest frequency of flood; in 2020, 13 tropical depressions landed in Vietnam, 8 of them came to the Central area within more than one month, from the 7th October to 15th November caused a loss estimated at 30000 billion in Vietnam Dong(VND), and 249 people died. Flood management in this area is a crucial task for local authorities. In flood management, flood simulation is the critical task needed for every flood management strategy. Many methods can make the flood simulation. In those methods, hydraulic modeling is the widest apply in Vietnam. This method shows its advantages in many aspects, but they also have limitations compare to other methods. The hydraulic model can predict floods with complex conditions and multi–input. In this study, flood simulation is made by applying hydraulic modeling. The study area is downstream of the Ca river basin, affected area by flood in Central Vietnam. The flood simulation is made with four flood scenarios in MIKE packages: 1%, 2%, 5%, and 10%, representing the flooding return period of 100, 50, 20, and 10 years. The flood simulation provides flood map based on the modeling result. Those data is validated and compare with flood areas from satellite images in the study area. The study shows the advantages and disadvantages of hydraulic modeling in flood simulation and flood mapping from satellite images. There is a very high potential of using the hydraulic model together with satellite data for flood hazard assessment.

Keywords: Flood mapping; Hydraulic model; MIKE; River basin flood; Sentinel 1.

1. Introduction

Flood and inundation is a most dangerous disaster in Vietnam [1]. Flood prediction for flood management is essential to work, especially downstream of rivers, coastal areas. Those areas are high population density, high development with the concentration of economic values but strongly affected by the flood, combined with heavy rainfall and high tides. Ca river is the biggest river basin in North Central of Vietnam, the flood is frequently occurred

in this area, especially the downstream. Therefore, Ca's downstream area is attractive in flood studies.

Flood prediction is the essential value in flood risk assessment and flood management. The flood prediction can be made by simulation in hydraulic modeling or flood susceptible modeling in GIS. Both of them have advantages and disadvantages. The GIS modeling methods commonly use Multi–criteria analysis (MCA)with several criteria and define flood hazard by combining them in GIS environment [2–6]. Using GIS modeling, the flood can be drawn based on criteria as DEM, land use data, hydraulic network, infrastructures. Other characteristics of a flood as frequency, duration, and velocity, are challenging to simulate in GIS. On the other hand, the hydraulic model simulation can provide valuable characteristics for flood risk assessment and preparedness. In Vietnam, there are several pieces of research applied the flood simulation, MIKE package dominated in flood modeling in Vietnam, the researches can be found from North [7] to Central coastal [8–9] to the Highland [10], some using SWAT [11] or FLO2D [12], Quasi2D [13], Probabilistic model (POT) [14]. The flood simulation started by designing flood scenarios. A flood simulation was designed by one of two designing methods: Flood frequency analysis (FFA) and Rainfall–Runoff analysis (RRA) [15].

The first method is based on the statistical analysis of flow monitoring data. This method is applied to define a maximum flow point in the flood model. The second one designs a flood by estimating runoff based on rainfall data analysis in the basin area. This design can be used to find the maximum flood area and hydraulic characteristics of a flood. In the developed countries like the USA and the developed countries, the FFA method is widely used in flood designing because they have a very dense flow monitoring system covering all areas of a river basin [16–18]. However, for the less developed countries like Vietnam, applying the FFA is challenging because lacking monitoring data. In order to overcome the data problem, many research pieces suggest that using the RRA is suitable for the basin with lesser monitoring data [19].

Some technical standards were issued in the flood prediction design in Vietnam, such as TCVN 9845:2013 (Flood characteristic calculation) [20] and TCVN 7957:2008 (Hydraulic network and construction) [21], are tricky to apply in flood prediction of river basins. The flood simulation design is recently based on historical events to reference and extend to flood frequencies. In this design, the rainfall in the river basin is considered the main factor of flooding. This study uses a hydraulic model to predict floods by applying the MIKE package and the RRA method. The modeling is applying for downstream of the Ca River basin.

The SAR data have been using in flood monitoring for a long time. However, in recent years, the open data from European Space Agency (ESA) boosted Sentinel 1 data in research [22–23]. Many researchers have used Sentinel 1 in the GEE platform for flood monitoring, from urban [24–25] to river basin scale [26–28]. In Vietnam, the SAR application is commonly used for flood monitoring, from the Mekong delta [29–30]to the Red River delta [31–32]. In this study, the Sentinel 1 data automatically processed in GEE by applying the UN–SPIDER practice for flood monitoring [33].

2. Materials and methodology

2.1. Study area

According to [34], the Ca River is one of the most significant rivers in the center–north of Vietnam; it is an international river with 531 km length, and the basin area is 27,000 km^2. The river flows from Lao to Vietnam and lying in Thanh Hoa, Nghe An, and Ha Tinh provinces before reaching the sea at the Cua Hoi river mouth. The river basin received 1100–2500 mm annually, precipitation concentrated in May to October in upstream and August to

November downstream. The flood season occurred from April to November with several tributaries.

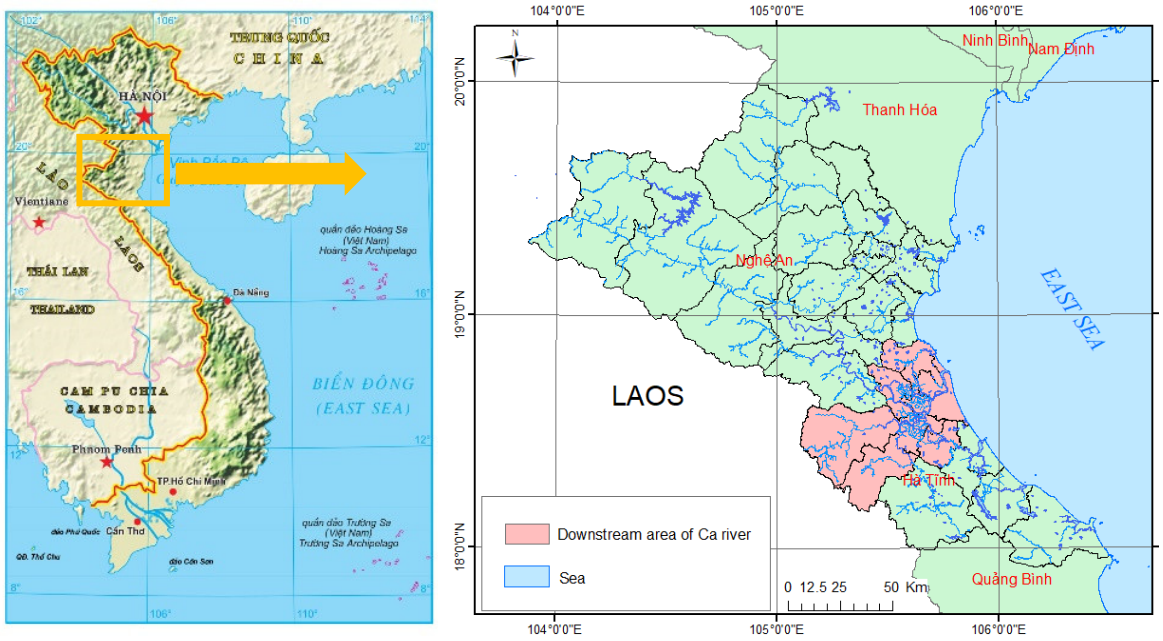

Figure 1. The downstream of Ca River.

Flood in this river basin is one of the most damaging disasters. From 1990 to 2010, the statistics showed the loss from flood only is 3300 billion VND, in 2011 and 2012, the loss from flooding about ~ 1000 billion VND each year, then from 2013 to 2016, the loss is ranged from 150 to 500 Billion VND (http://phongchongthientai.mard.gov.vn).

2.2. Data collection

The data used in the study include:

- Observed rainfall, discharge and water level from 1987–2017 have been collected for model calibration and validation and design scenarios.
- Topographic maps from MONRE with a scale of 1:10000 and 1:5000, river cross–sections from 2001–1014 collected from Vietnamese Disaster Management Authority.
- Land use map dated 2015 from MONRE.
- Data of disaster risk reduction infrastructure: dykes, dams, pumps, gates, etc., collected from the Disaster management authority in 2017.
- Infrastructure and transportation data from Open Streetmap 2017.
- Sentinel 1 data from GEE with the time of acquiring is 25th September 2020 for non–flood and 15th October 2020, and 2nd November 2020 for floods.

2.3. Modeling methodology

Figure 2 presents the workflow of the modeling process. The workflow includes five steps and using three groups of data (Meteorological–hydrological; hydraulic works and infrastructures; DEM).

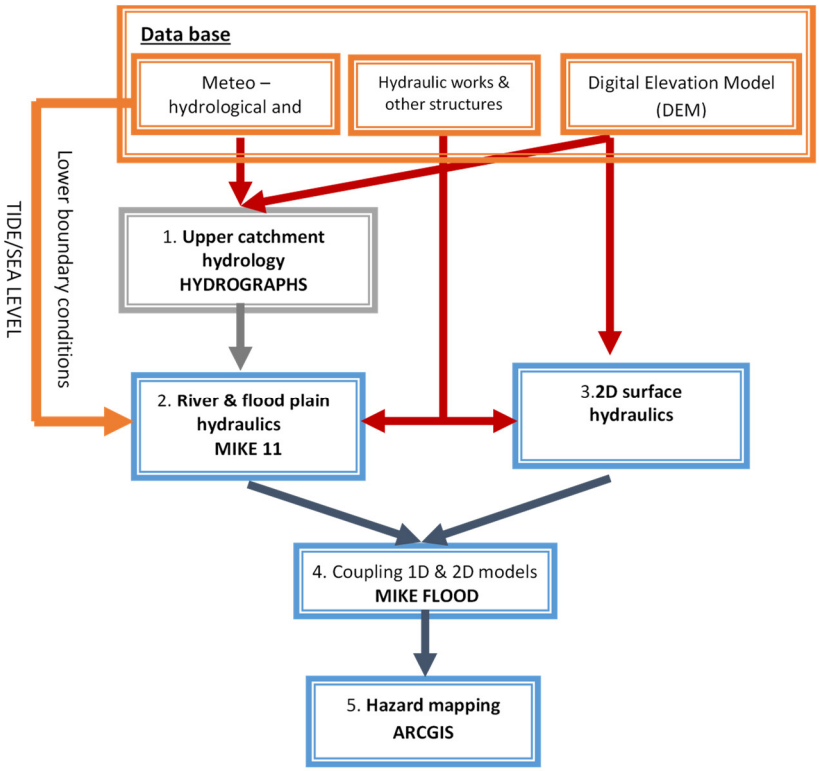

Figure 2. Modeling process.

2.3.1. Sub–basin defined

The boundary conditions needed for the one dimension (1D) hydraulic model are upstream, downstream, and lateral boundaries. Usually, the upstream and lateral boundaries are discharged, while downstream boundaries are water levels. Rainfall–runoff models are usually applied to estimate the inflows and their influences and confluences in relevant sub–basins to identify upstream and lateral boundaries. In this study, sub–basins are defined based on the following criteria: (1) Strategic hydraulic works in the system such as reservoirs, hydropower, and division nodes; (2) Influences and confluence streams discharge into modeled river network; and (3) Lateral boundaries of modeled rivers account for every 20% of the total basin area.

For flood analysis, the 1D hydrodynamic model is set up for the lower part of the basin from the reservoir to the sea. Furthermore, the lateral flows from other sub–basins along the leading river network need to be estimated. Therefore, the whole basin is divided into 27 sub–basins, as shown in Figure 3.

All hydrological features are identified for each sub–basin, including basin area, main river length, riverbed slope, basin slope, lowest/ highest/ medium elevation of the basin. The distribution of meteorological and hydrological stations in the basin is present in Figure 4.

In this study, the Intensity–Duration–Frequency (IDF) curves are used to established designed rains, in which the rainfall layer is used instead of the intensity to make it easier in later stages, calculated by the equation (1).

$$h=a\times t^{n} \quad (1)$$

where h is the rainfall layer (mm) with the period of rain; a, n are parameters calculated from the data series; and i=h/t is the intensity of rain.

The IDF curve series are calculated using this procedure for different repetitions: 10 years, 20 years, 50 years, 100 years, and 200 years for each station with data available in the basin, as shown in Figure 5.

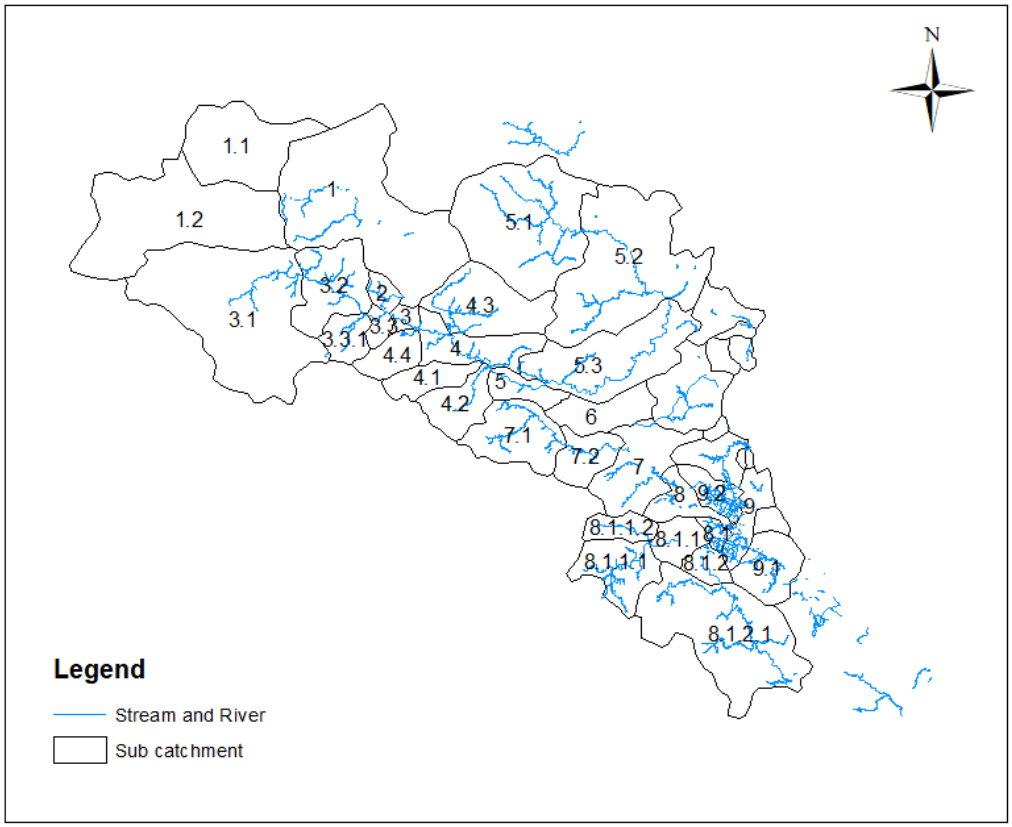

Figure 3. Sub–basins defined for flood analysis.

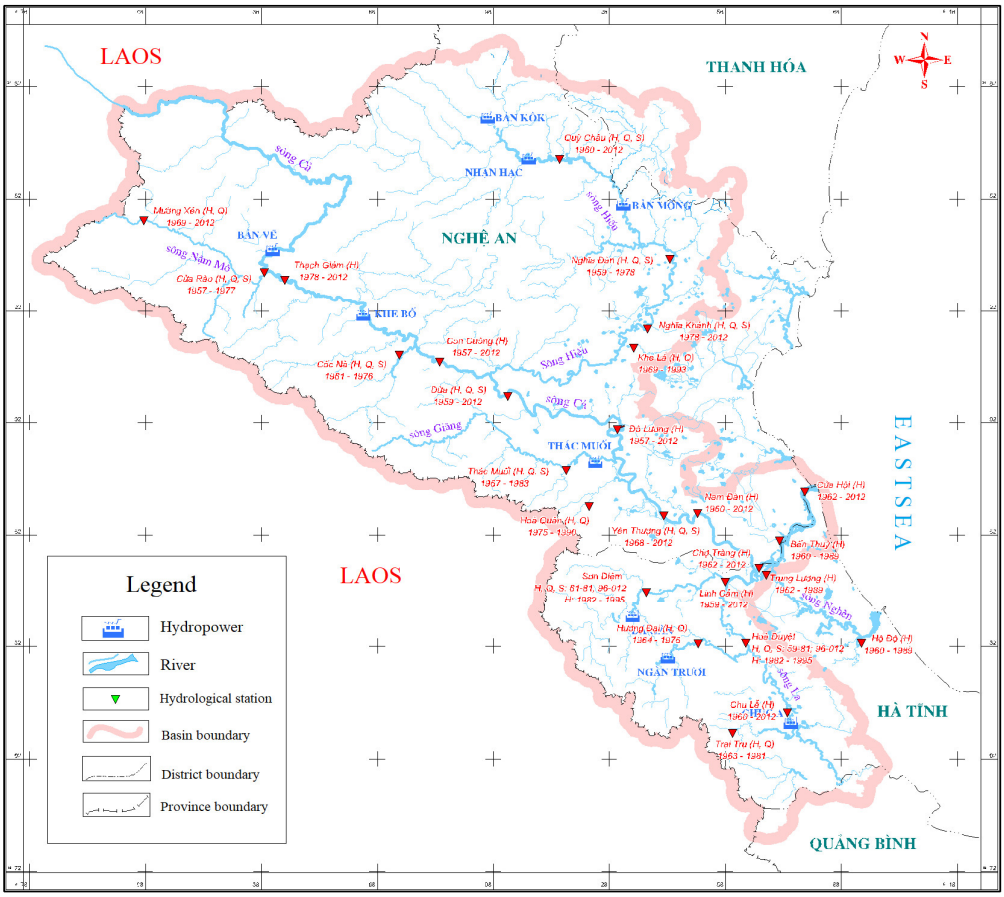

Figure 4. Hydrological and meteorological station in the river basin.

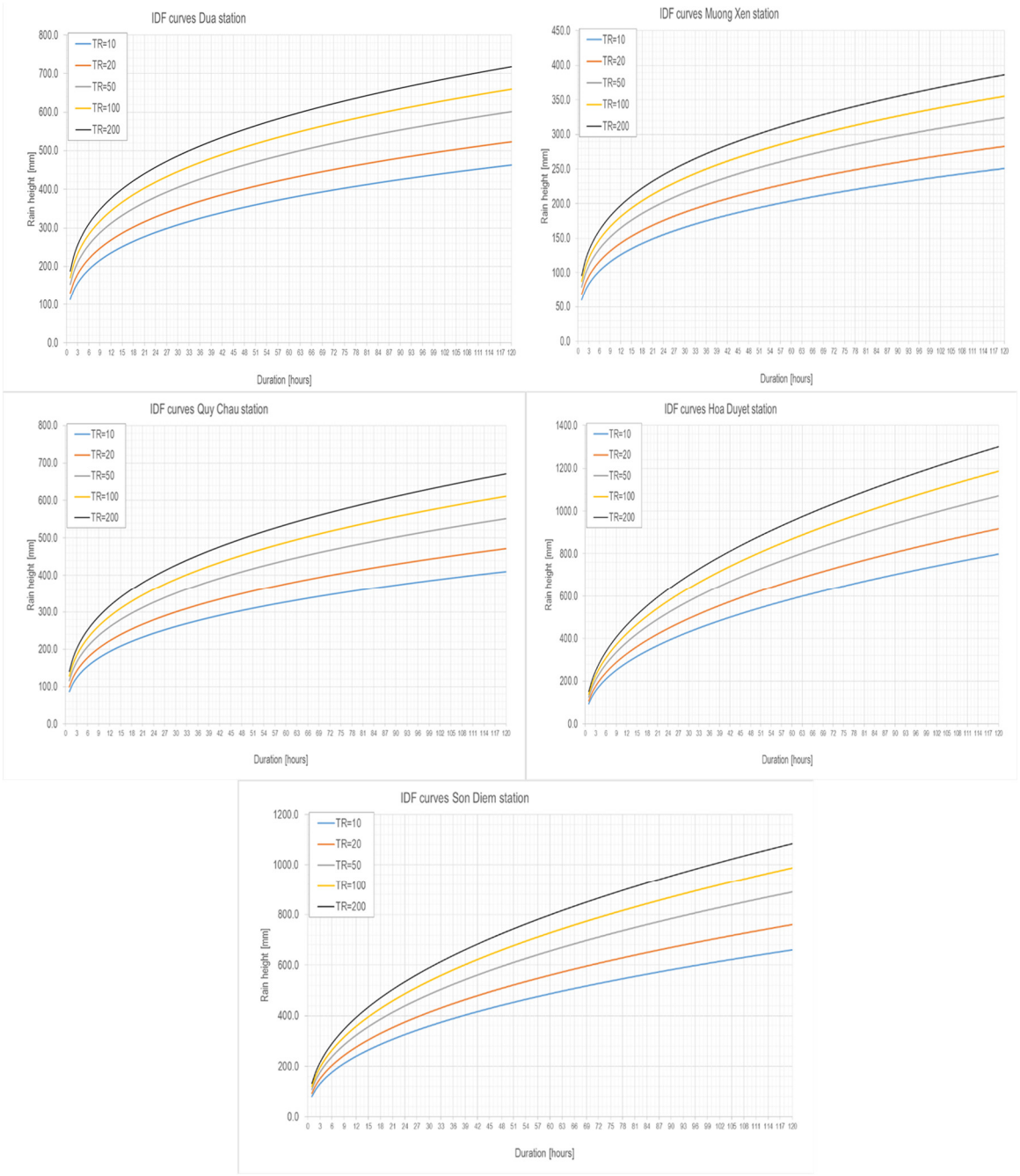

Figure 5. Hydrological and meteorological station in the river basin.

2.3.2. The design hydrograph flood

Design flood process lines are constructed from design rainfalls with a rainfall time equal to concentrating water in the basin by applying a rainfall–runoff model. According to this method, the shape of the flood process line is a shape triangle with a total flow time twice the sub–basin's water concentration time.

a) Sub–basins of characteristics

As stated above, for each sub–basin, the main parameters from available DEM are defined as an area, average and minimum elevation, river length (of the main branch), river slope, hillsides average slope. These values were estimated for the entire basin upstream of each river closing section, not only for the added area of a single sub–basin. The other parameters, runoff coefficient and Curve Number (C.N) coefficient of each sub–basin, were

estimated from the land use map considering that land use is classified into seven types: cropland, forestland, grassland, settlement, water, other uses, and no data.

b) Runoff concentration–time of each sub–basin

For each sub–basin, the concentration–time is computed using Giandotti [35] and Soil Conservation Service (SCS) formula [36] as expressed:

$$t_c = \frac{4\sqrt{A} + 1.5L}{0.8 \times \sqrt{Hmed} - Hmin} \quad (2)$$

$$t_c = \frac{0{,}342}{0{,}6} \cdot \frac{L^{0,8} \cdot (S+1)^{0,7}}{\sqrt{y}} \quad (3)$$

where A is the sub–basin area (km^2); L is main river length (km); H_{med}, H_{min} are the average and minimum basin elevation (m); S is the potential maximum retention (S=(1000/CN–10) *25,4) (mm); y is the slope of the average hillside (%).

Giandotti formula is used for most sub–basins; The formula has been established for mountainous basins covering an area of 140 km^2 to 70,000 km^2, so this is a suitable formula for the study basins. Smaller sub–basins, especially sub–basins in the downstream area, where there is a slight slope of the study area, are more accurately described with the SCS formula created for small rural basins.

In this analysis, the following rule provided the most representative results:

River slope < 2%, area < 100 km^2: SCS formula.

River slope < 2%, area > 100 km^2: average value between the two formulas.

River slope > 2%: Giandotti formula.

This methodology is the most effective, and Vietnamese formulas found in local regulation do not apply to this large basin area (because they are developed for small basins).

c) ARF values assigned for each sub–basin

According to various R.P. (100, 50, 20, 10), for each sub–basin, critical rainfall height is evaluated based on the IDF curves ($h = axt_n$), considering a duration t equal to concentration–time tc. An area reduction factor is applied to resulting height, considering the USWB formula (from U.S. Weather Bureau with coefficients recalibrated [36]):

$$ARF(t,A) = 1 - (1 - e^{-0.01298A}) \times e^{-0.6786 \times t^{0.332}} \quad (4)$$

d) Flood peaks of relevant frequencies for each sub–basin

The flood peak discharge is computed using a simple rainfall–runoff model as the rational method (or kinematic method). Thus the flood peak for a given return period (R.P) will be computed as:

$$Q[m^3/s] = \frac{\phi \times h \times A}{3.6 \times t_c} \quad (5)$$

where Φ is the runoff coefficient, h the rainfall height for given R.P. (reduced by ARF coefficient as stated above), A is the basin area, and tc the basin concentration time.

e) Hydrograph of relevant frequencies for each sub–basin

According to flood peak estimation methodology, the schematic flood hydrograph is developed with an isosceles triangular shape, with a duration equal to double the concentration time. This can be smoothed using UHM module of MIKE software, i.e., with SCS model, with parameters calibrated to obtain the same flood peak resulting from the previously described methodology. However, this passage is not necessary, as the two shapes are very similar, considering that the triangular hydrograph will soon smoothen due to hydraulic propagation in the MIKE11 model. The triangular shape is easier to combine to define the lateral contribution of downstream sub–basins, as described in the following point.

The basic flow is included if necessary for modeling purposes; this is not necessary when the designed rain period is long and focuses on the hydrograph's upper boundary (large volume). However, each basin's minimum flow rate can be determined based on the low

flow's average annual flow value. Note: this basic flow is not included in hydrological calculations, except only used to increase the flow at the foot of the hydrograph up to the minimum value.

Hydrographs are defined for every Return Period (R.P.) (scenario) and every sub–basin with a closing section within modeled branches.

f) Upper and lateral boundaries with relevant frequencies

The contribution of sub–basins downstream the same main (modeled) river branch has been added as the difference between the hydrological (theoretical) triangular hydrographs computed for two consecutive closing sections. This contribution (lateral discharge) was added as distributed along the model cross–sections between the two closing sections or concentrated if there is a relevant tributary in this sub–branch.

g) Lower boundary

The lower boundary uses the tide level measured at Hoi mouth. In scenario simulation, the aggregate sea level value is related to the model and is determined as the high tide cycle; In some scenarios, the sea levels are increased by storm surge values is taken from previous research. In this study, a frequency curve of sea level during storm surge is based on Vietnam Standard TCVN 9901: 2014 for irrigation works – Requirements for sea dike design. According to this national standard, sea level at Cua Hoi, in Nghi Xuan Ha Tinh district (MC25). Tide is taken from the tidal regulation function of this region.

2.3.3. Scenarios

In this study, the scenarios are constructed based on a combination of design–heavy rains and tidal water cases, as shown in the table 1 . The core of these combinations is to consider the impact of heavy rains and different tidal regimes, creating flood areas with the most significant depth and inundation. First, consider the combination of high–frequency floods and low–frequency tides (scenarios 1 and 2). Next, consider the combination of low–frequency floods with low and high tide (3A, 3B, 4A, 4B). Therefore, there are six design scenarios summarized in Table 1.

Table 1. Scenarios according to each calculation timeline.

Scenario	Simulation mode	R.P. (Frequency)	Downstream boundary conditions (sea level *)
1	Unsteady	100 years (1%)	20 years (5%)
2	Unsteady	50 years (2%)	20 years (5%)
3A	Unsteady	20 years (5%)	10 years (10%)
3B	Unsteady	20 years (5%)	100 years (1%)
4A	Unsteady	10 years (10%)	10 years (10%)
4B	Unsteady	10 years (10%)	100 years (1%)

After all scenarios and parameters are set, the model setup in the MIKE package includes the following tasks:

- Setup the 1D model in Mike 11
- Setup the (2 dimensions) 2D model in MIKE 21
- Combining MIKE 11 and MIKE 21 to create MIKE FLOOD.
- Calibration and validation of the model in MIKE NAM
- Compare with flood data processed from Sentinel 1 satellite by Google Earth

2.4. Flood monitoring with Sentinel 1 in Google Earth Engine.

2.4.1. Workflow of flood mapping by UN–SPIDER

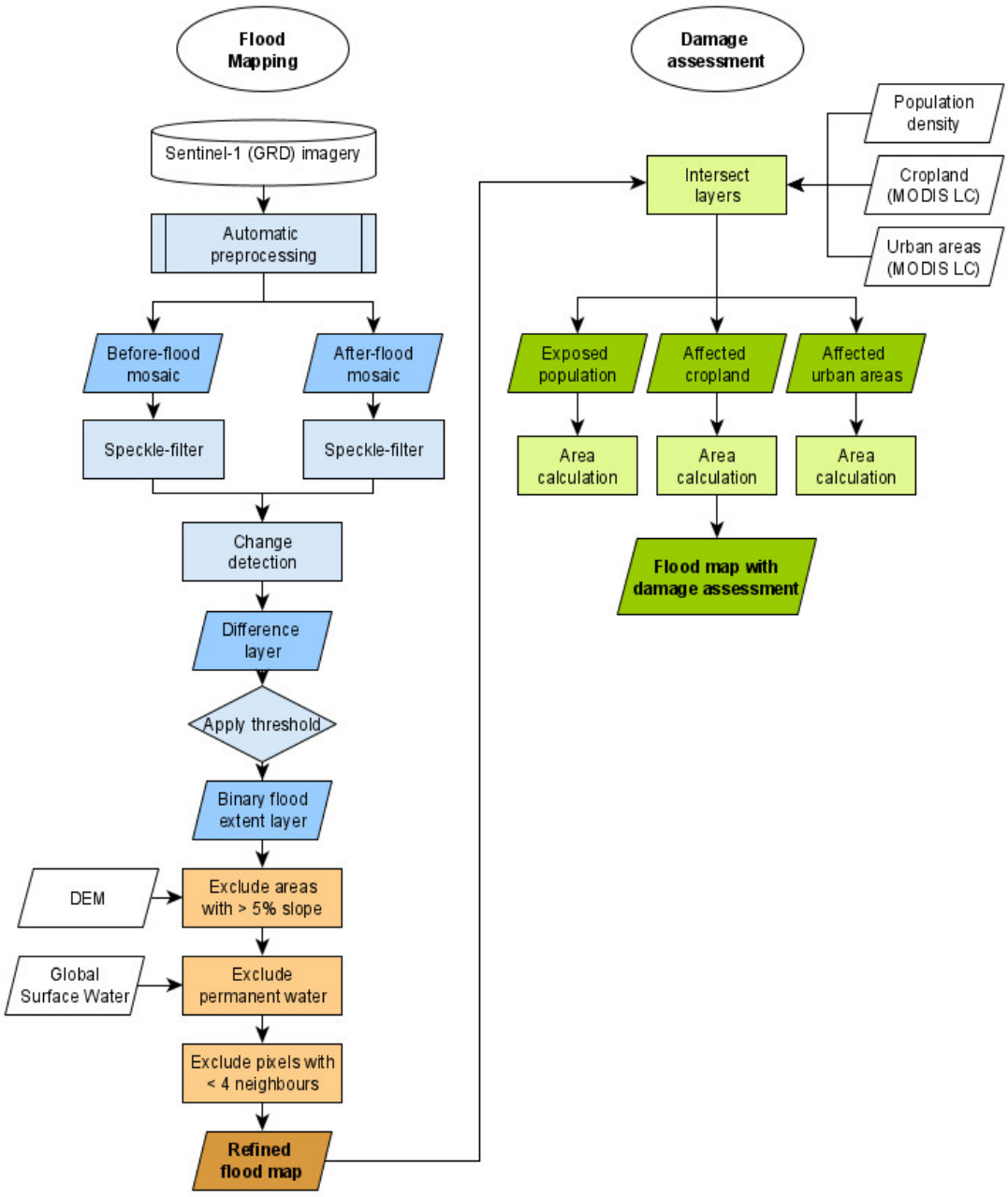

Figure 6. Flood mapping in GEE using Sentinel 1 data (Source UN–SPIDER).

The workflow of flood mapping in GEE (figure 6) is an automation process with pre–define code (Javascript). All of the code and data run on cloud computing inside the GEE. The user needs to define the boundary of the study area, the time frame of the flood that occurred. The processing of satellite images is in cloud computing. This workflow gives fast, on–time flood maps of natural floods. Those data will be used to compare with flood simulation results to help improve the accuracy of the flood model.

2.4.2. Selection of data

The floods in the Ca river basin in 2020 are occurred in 2 periods: 12 to 18th October, 28 to 04th November. The Sentinel data in these periods need to available to perform the flood mapping. The following table (Table 2) describes the flood information and corresponded data available.

Table 2. Flood periods and availability of Sentinel data.

No	Period			Sentinel1 date
	Start	Peak	End	
1	14th October	17th October	18th October	15th October
2	27th October	28–29th October	4th November	2nd November

In this research, there are only two available data set of Sentinel 1 for two periods of flood, and those data are not in peak flood dates.

3. Result and discussion

3.1. Model calibration and validation

The rainfall–runoff model has been calibrated with the flood event in 2013, and the result shows well with Nash coefficient ranging from 0.7 (Muong Xen) to 0.91(Hoa Duyet). The peak errors are minor than 5%, and the total volume errors are minor than 10%, as shown in Figure 7 below.

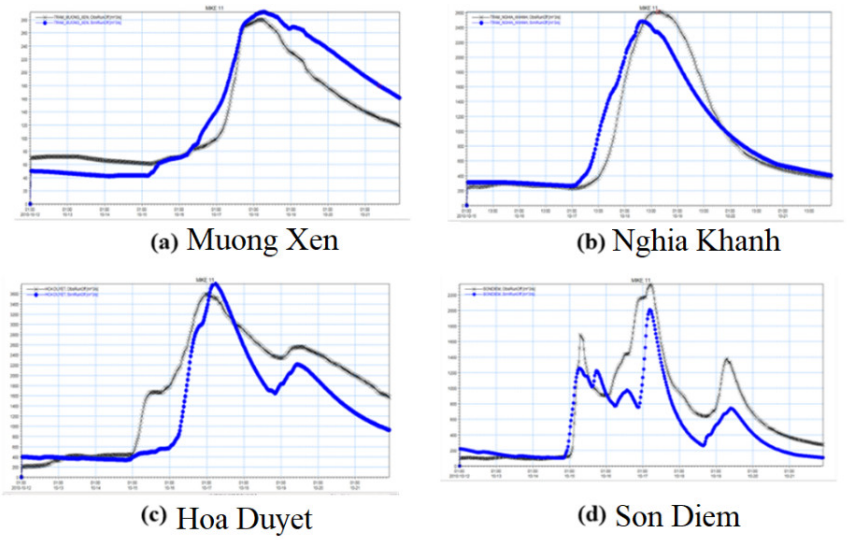

Figure 7. Model calibration.

The flood model has been validated with the same event in 2013 using 13 flood marks. The results are acceptable, as in figure 8 below.

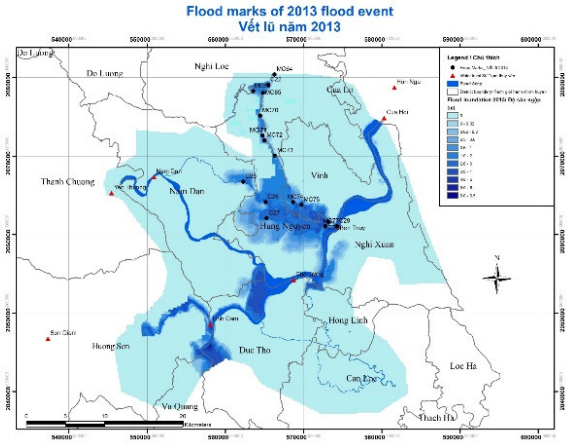

No	ID	X (m)	Y (m)	H^{obs}[m]	H^{est} [m]	$H^{est} - H^{obs}$ [m]
1	C25	588491	2067554	3.84	4.3	0.46
2	C26	591364	2064961	3.23	2.85	-0.38
3	C27	591492	2062894	3.65	3.29	-0.36
4	C29	600483	2061904	2.99	3.34	0.35
5	MC65	591000	2078885	2.45	2.6	0.15
6	MC70	590636	2075984	2.33	2.6	0.27
7	MC71	590945	2073445	3.40	3.55	0.15
8	MC72	591194	2072822	3.48	3.78	0.30
9	MC73	592534	2070874	3.89	4.21	0.32
10	MC74	594864	2064950	4.01	4.21	0.20
11	MC75	595940	2064607	4.00	4.31	0.31
12	MC76	599369	2062448	3.10	3.70	0.60
13	MC77	598999	2061909	1.99	2.24	0.25

Figure 8. Model validated.

3.2. Flood modeling

Hydrological modeling provides the result as a set of models and floodwater depth. The results of 1D and 2D models are shown as hydraulic networks as the following figure 10. The 1D model considers 12 rivers and 320 cross–sections in modeling to ensure the model's quality and accuracy. This model also includes hydraulic constructions and the main transportation infrastructure in the study area. The 2D model is constructed with more detailed with all transportation infrastructures, gates, and hydraulic structures in the Ca river's lower basin. The water depth data are a mesh of triangular polygons with water lever information. The data include six defined scenarios and mapping in GIS software (Figure 10).

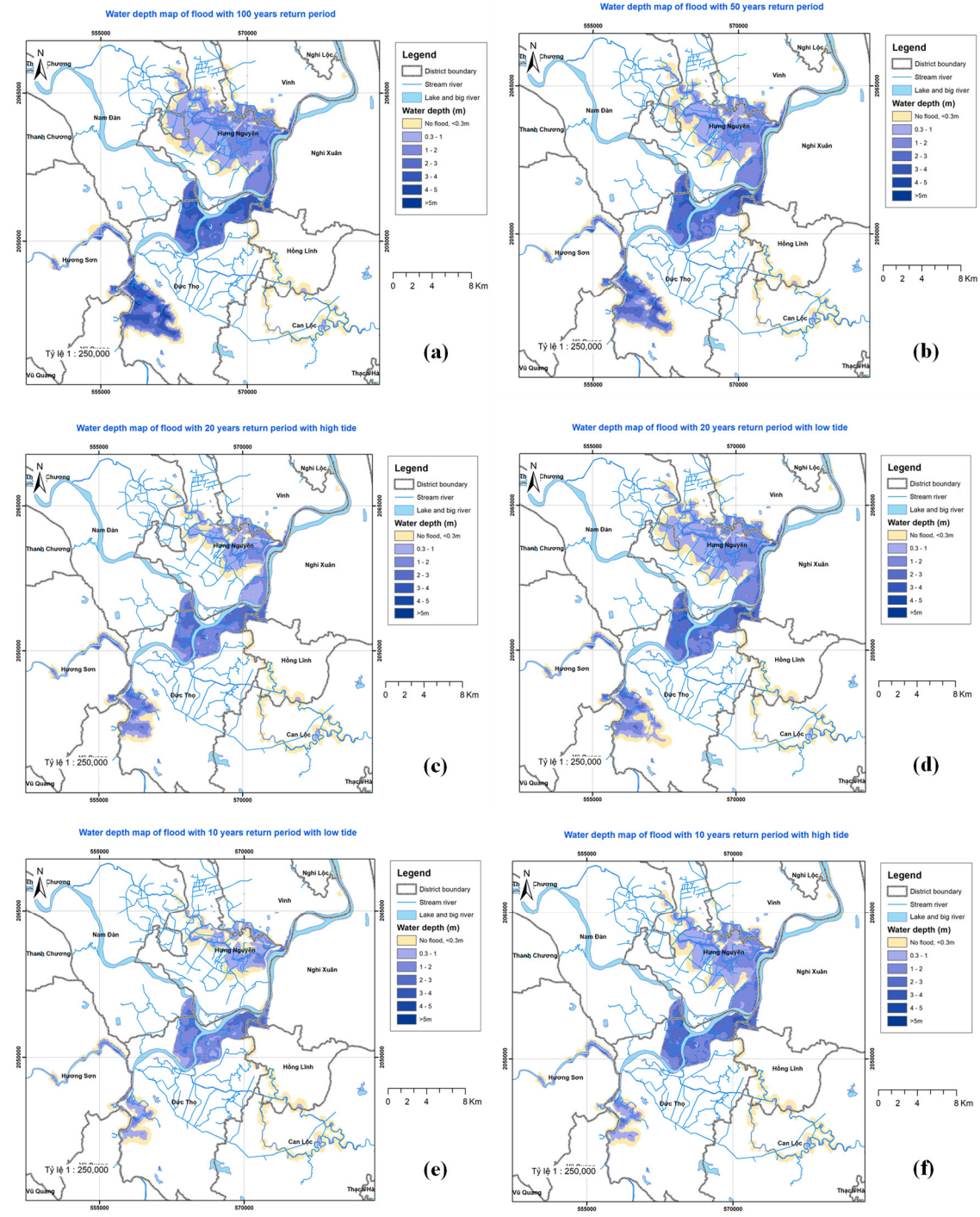

Figure 10. Result of hydraulic modeling (Scenario 1, 2, 3A, 3B, 4A, 4B from right to left and top–down).

3.3. Flood mapping by using Sentinel 1 data in GEE

The results of flood data from Sentinel 1 are created, as in Figures 11 and 12.

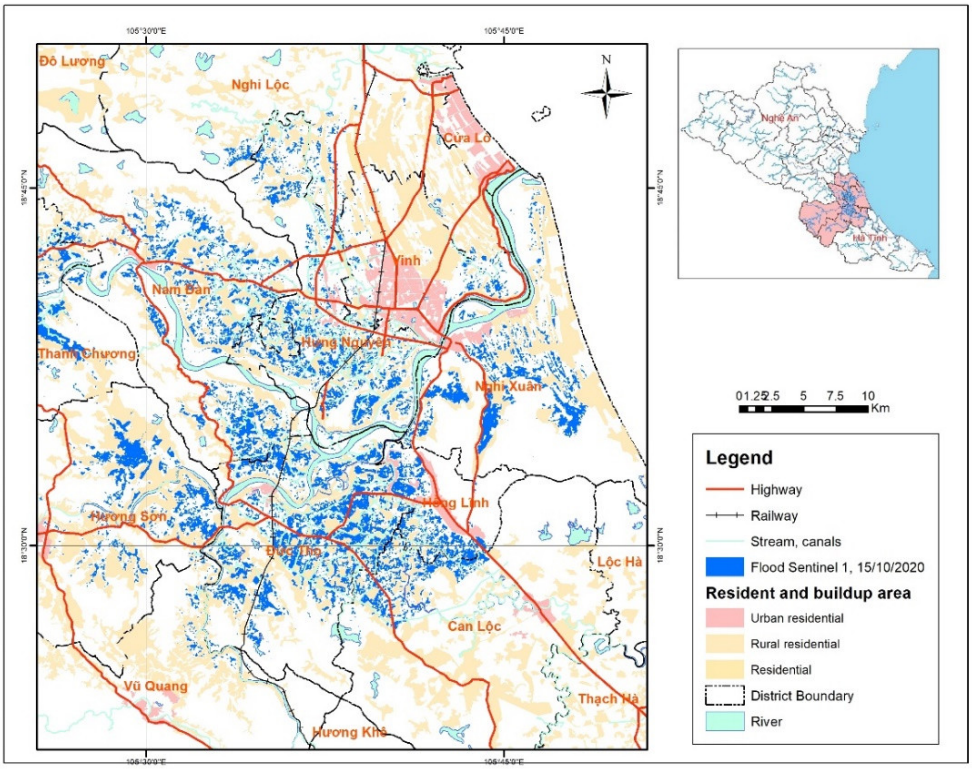

Figure 11. Flood data from Sentinel 1 date 15/10/2020.

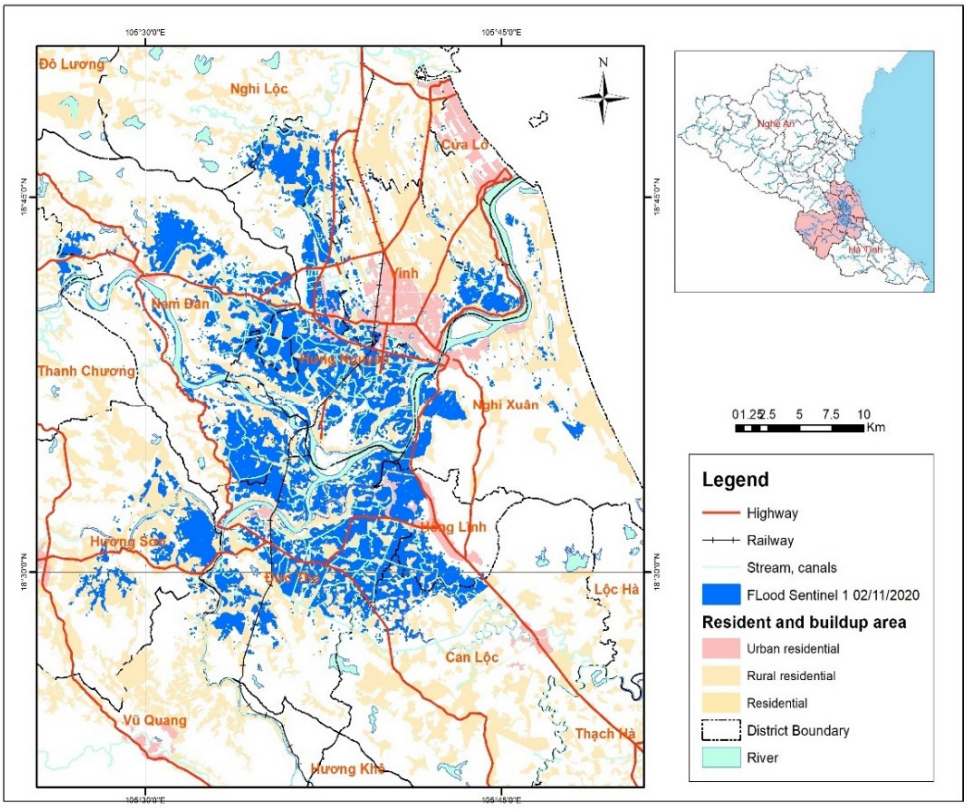

Figure 12. Flood data from Sentinel 1 date 02/11/2020.

Because of the difference in time and peak of the flood, the flood extent of the 2nd November data is more extensive than 15th October. On the other hand, the distribution of floods is similar in both flood maps.

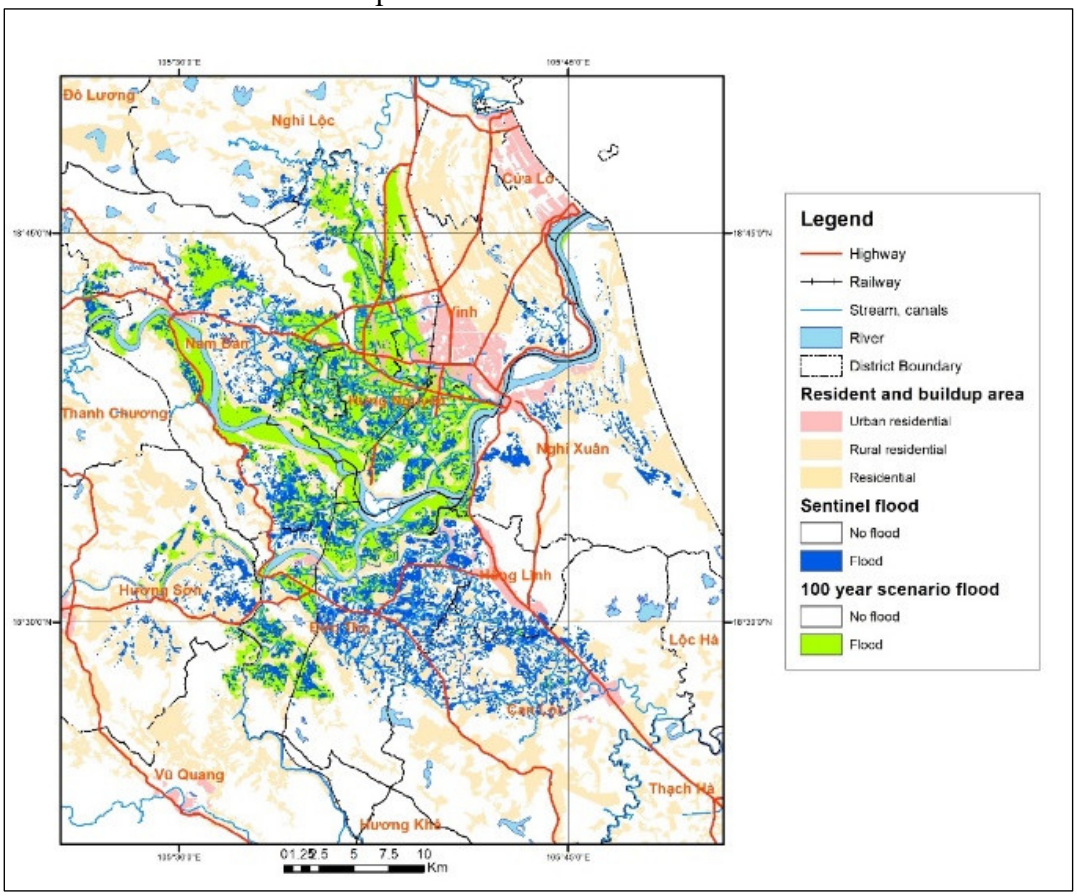

Figure 13 Compare the result of 100 years return period with flood data from Sentinel 1 date 17/10/2020.

Figure 13 provides a better comparison between the results of flood simulation and satellite image processing. Compare to the flood map provided by flood simulation modeling; the flood extends from Sentinel1 data are larger. The most significant difference is the Huong Son, Duc Tho, and Hong Linh district areas in Ha Tinh Province. Modeling considers all water a free run from the river, but in reality, the rainfall was concentrated in the field, making flood inside the dyke system. That means the modeling may not present a good accuracy of the flood. Most of the modeling is based on input data, which have low quality or out of date. It is tough to model all hydraulic systems, and the cost of data processing is unacceptable.

The flood mapping from satellite data is fast, accurate, and automated compared to the traditional flood modeling by simulation software. Nevertheless, the satellite data depend on the revisit time frame of the satellite; the peak flood dates rarely are the same as data acquiring dates. This problem may solve very soon with new satellites coming in the next few years. The combination of flood simulation and flood monitoring by satellite is very potential; the satellite can be used as validation and calibration sets for flood simulation.

4. Conclusion

The result shows that modeling the flood is needed for flood risk assessment. The modeling output is useable but limited in risk assessment, especially in disaster risk management. The hydraulic modeling can be applied in other river basins to help authorities understand the flood and plan the response strategies.

The hydraulic modeling is enormously dependent on input data. In this study, the DEM taken from the 1:5000 topographic map and infrastructure taken from the Open street map may not provide an exact flood map. That suggested the following study should using better quality of data.

The Sentinel1 flood mapping was limited by the revisiting time of the satellite; the data acquired may not in the peak time flood, which may give an underestimated flood extend. On the other hand, the flood mapping from the satellite images can be done rapidly, automatically in free cloud computing of GEE. These advantages give this method a priority in an emergency, search and rescue, post–flood recovery tasks.

Author's contributions: D.A.Q. is the first author, written most of the paper; T.V.A., T.X.Q. contribute the modeling in MIKE; B.N.Q. response to the review and graphic design; P.V.H., T.T.M.A., N.D.D. build the maps.

Acknowledgment: The paper results from research project No T20–11 from Hanoi University of Mining and Geology.

Conflicts of Interest: The authors declare no conflict of interest.

References

1. Thuc, T. Vietnam Special Report on Managing the Risks of Extreme Events and Disasters to Advance Climate Change Adaptation. Vietnam Pulishing House of Natural Resources, Environment and Cartography 2015.
2. Shadmehri Toosi, A.; Calbimonte, G.H.; Nouri, H.; Alaghmand, S. River basin–scale flood hazard assessment using a modified multi–criteria decision analysis approach: A case study. *J. Hydrol.* **2019**, *574*, 660–671.
3. Youssef, A.M.; Hegab, M.A. Flood–Hazard Assessment Modeling Using Multicriteria Analysis and GIS: A Case Study—Ras Gharib Area, Egypt. *Spatial Modeling in GIS and R for Earth and Environmental Sciences* **2019**, 229–257.
4. Nhung, L.H.; Perminov, A.V.; Kozyr, I.E. Modeling of Floods and Flood Control Water Reservoirs for Evaluation of Inundation da Nang Province of Vietnam. *Procedia Eng.* **2016**, *154*, 1319–1323.
5. Chau, V.N.; Holland, J.; Cassells, S.; Tuohy, M. Using GIS to map impacts upon agriculture from extreme floods in Vietnam. *Appl. Geogr.* **2013**, *41*, 65–74.
6. Le, T.V.H.; Nguyen, H.N.; Wolanski, E.; Tran, T.C.; Haruyama, S. The combined impact on the flooding in Vietnam's Mekong River delta of local man–made structures, sea level rise, and dams upstream in the river catchment. *Estuar. Coast. Shelf Sci.* **2007**, *71*, 110–116.
7. Phạm, V.B. Flood hazard mapping for Ninh Binh province. Center For Participatory Irrigation Management, **2019**, 1–46.
8. Duong, V.N.; Gourbesville, P. Model Uncertainty in Flood Modelling. Case Study at Vu Gia Thu Bon Catchment – Vietnam. *Procedia Eng.* **2016**, *154*, 450–458.
9. Vo, N.D.; Gourbesville, P.; Vu, M.T.; Raghavan, S.V.; Liong, S.Y. A deterministic hydrological approach to estimate climate change impact on river flow: Vu Gia–Thu Bon catchment, Vietnam. *J. Hydro–Environment Res.* **2016**, *11*, 59–74.
10. Dang, D.D.; Ngo, A.Q.; Nguyen, H.S.; Nguyen, N.T. Flood mapping for the downstream area of Dak Bla river. *Tạp chí Khoa học và Công nghệ Thủy Lợi* **2018**, 1–9.
11. Khuong, D.V.; Linh, N.M. Application of the SWAT model to assess the importance of forests in flood control in the Vu Gia–Thu Bon river basin. *J. Water Resour. Sci. Technol.* **2012**, 7, 56–63 (in Vietnamese).
12. Vu, T.T.; Ranzi, R. Flood risk assessment and coping capacity of floods in central Vietnam. *J. Hydro–Environment Res.* **2017**, *14*, 44–60.

13. Van Khanh Triet, N.; Viet Dung, N.; Merz, B.; Apel, H. Towards risk–based flood management in highly productive paddy rice cultivation–concept development and application to the Mekong Delta. *Nat. Hazards Earth Syst. Sci.* **2018**, *18*, 2859–2876.
14. Apel, H.; Martínez Trepat, O.; Nghia Hung, N.; Thi Chinh, D.; Merz, B.; Dung, N.V. Combined fluvial and pluvial urban flood hazard analysis: Concept development and application to Can Tho city, Mekong Delta, Vietnam. *Nat. Hazards Earth Syst. Sci.* **2016**, *16*, 941–961.
15. Wright, D.B.; Ramirez–cort, F.; Ishizawa, O.A.; Rogelis, M.C. Methods in flood hazard and risk assessment. 1–20.
16. UK Centre for Ecology & Hydrology, Flood Estimation Handbook. 1999. Online Available: https://www.ceh.ac.uk/services/flood–estimation–handbook (Accessed: 10–May–2021).
17. Castellarin, A. European procedures for flood (FloodFreq, COST Action ES0901) FloodFreq – ES0901. 2010, 22–24.
18. McKerchar, A.I.; Macky, G. Comparison of a regional method for estimating design floods with two rainfall–based methods. *J. Hydrol.* **2001**, *40*, 129–138.
19. Calver, A.; Stewart, E.; Goodsell, G. Comparative analysis of statistical and catchment modelling approaches to river flood frequency estimation. *J. Flood Risk Manag.* **2009**, *2*, 24–31.
20. Ministry of Science and Technology. TCVN 9845:2013 Calculation of flood flow characteristics. 2013.
21. Ministry of Science and Technology. TCVN 7957:2008 Drainage and sewerage – External Networks and Facilities – Design Standard, 2008, 3–98.
22. Klein, T.; Nilsson, M.; Persson, A.; Håkansson, B. From open data to open analyses—new opportunities for environmental applications? *Environ.* **2017**, *4(2)*, 1–17.
23. Turner, W. Free and open–access satellite data are key to biodiversity conservation. *Biol. Conserv.* **2015**, *182*, 173–176.
24. Tavus, B.; Kocaman, S.; Gokceoglu, C.; Nefeslioglu, H.A. Considerations on the Use of Sentinel–1 Data in Flood Mapping in Urban Areas: Ankara (Turkey) 2018 Floods. *ISPRS – Int. Arch. Photogramm. Remote Sens. Spat. Inf. Sci.* **2018**, *XLII–5,* 575–581.
25. Mason, D.C.; Dance, S.L.; Cloke, H.L. Floodwater detection in urban areas using Sentinel–1 and WorldDEM data. *J. Appl. Remote Sens.* **2001**, *15(3)*, 1–22.
26. Singha, M. Identifying floods and flood–affected paddy rice fields in Bangladesh based on Sentinel–1 imagery and Google Earth Engine *ISPRS. J. Photogramm. Remote Sens.* **2020**, *166*, 278–293.
27. Conde, F.C.; De Mata Muñoz, M. Flood monitoring based on the study of Sentinel–1 SAR images: The Ebro River case study. *Water* **2019**, *11*, 1–25.
28. Uddin, K.; Matin, M.A.; Meyer, F.J. Operational flood mapping using multi–temporal Sentinel–1 SAR images: A case study from Bangladesh. *Remote Sens.* **2019**, *11(13)*, 1581.
29. Nguyen, T.H.D.; Nguyen, T.C.; Nguyen, T.N.T.; Doan, T.N. Flood inundation mapping using Sentinel–1A in An Giang province in 2019. *Vietnam J. Sci. Technol. Eng.* **2020**, *62*, 36–42.
30. Dinh, D.A.; Elmahrad, B.; Leinenkugel, P.; Newton, A. Time series of flood mapping in the Mekong Delta using high resolution satellite images Time series of flood mapping in the Mekong Delta using high resolution satellite images. *IOP Conf. Ser.: Earth Environ. Sci.* **2019**, *266*, 012011.
31. Phan, A.; Ha, D.N.; Man, C,D.; Nguyen, T.T.; Bui, H.Q.; Nguyen, T.T.N. Rapid assessment of flood inundation and damaged rice area in Red River Delta from

Sentinel 1A imagery. *Remote Sens.* **2019**, *11(17)*, 2034.
32. Duc, P.B.; Tran, T. Potential Of Sentinel–1 SAR Observations To Monitor Floods In The North Vietnam. *Int. J. Sci. Technol. Res.* **2020**, *9(4)*, 326–331.
33. UN–SPIDER. In Detail: Recommended Practice: Flood Mapping and Damage Assessment using Sentinel–1 SAR data in Google Earth Engine. *UN*, **2021.** Online Available:https://un–spider.org/advisory–support/recommended–practices/recommended–practice–google–earth–engine–flood–mapping/in–detail.
34. Hoang, N.Q.; Phan, T.D. Water resource and water quality in Ca river basin. *VN J. Hydrometeorol.* **2003**, *507*, 26–31.
35. Giandotti. Previsione delle piene e delle magre dei corsid'acqua. Istituto Poligrafico dello Stato **1934**, *8*, 107–117.
36. USDA–SCS. Urban Hydrology for Small Watersheds. Technical Release 55. Washington, DC, **1986**.

VIETNAM JOURNAL OF HYDROMETEOROLOGY

Research Article

Degradation of perfluorooctanoic acid in aqueous solution with sulfate radicals generated in the UV/sodium sulfate system

Huu–Tuan Do[1*], Lan–Anh Phan Thi[2, 3], Thuy Hanh Pham[1]

[1] Faculty of Environmental Sciences, VNU University of Science, Vietnam National University, Hanoi, 334 Nguyen Trai, Thanh Xuan, Hanoi, Vietnam; tuandh@vnu.edu.vn, hanhph.0901@gmail.com

[2] VNU Key Laboratory of Analytical Technology for Environmental Quality and Food Safety Control (KLATEFOS), VNU University of Science, Vietnam National University, Hanoi, 334 Nguyen Trai, Thanh Xuan, Hanoi, Vietnam; lananh@vnu.edu.vn

[3] Center for Environmental Technology and Sustainable Development (CETASD), VNU University of Science, Vietnam National University, Hanoi, 334 Nguyen Trai, Thanh Xuan, Hanoi, Vietnam; lananh@vnu.edu.vn

*Correspondence: tuandh@vnu.edu.vn; Tel.: +84–2438584995

Received: 12 May 2021; Accepted: 19 July 2021; Published: 25 August 2021

Abstract: Perfluorooctanoic acid ($C_7F_{15}COOH$, PFOA) is a persisted organic pollutant widely used in industry in recently. It is widespread occurrence in the environment and because of its ability to bioaccumulate. PFOA is reported toxic and carcinogenic to animals such as rats, fishes, monkeys, and even humans. Photodegradation PFOA solution in presence Na_2SO_4 was studied in this study. PFOA was photodegraded about 93% after 24 h by using a combination of UV 254nm irradiation and Na_2SO_4 30mM, while under only UV irradiation, 43% of PFOA was photodegraded. Na_2SO_4 30mM was the concentration that photodegradation PFOA reached highest efficiency. The optimal temperature for PFOA degradation is 25°C.

Keywords: Perfluorooctanoic acid; Photodegradation; Treatment; Radical scavenger.

1. Introduction

Perfluorooctanoic acid ($C_7F_{15}COOH$, PFOA) is a contaminant widely used in industry in recently. It is very stable in the natural environment due to its strong C–F bonds (110 kcal/mol) [1–2]. It contains both hydropholic and hydropholic polar structure, so it is used as a surface treatment agent in photolithography, an emulsifying agent in polymer synthesis, a fire retardant, and is one component of paper coating [3]. PFOA has been detected in aquatic environments and animals, and has been demonstrated to exhibit bioaccumulative and biomagnificative effects [4]. They are toxic and carcinogenic to animals such as rats, fishes, monkeys, and even humans [3–6]. Therefore, there is interest in developing methods for PFOA removal.

The treatment technologies of PFOA are interested recently. Some advanced oxidation processes (AOPs) in critical conditions have been developed to degrade PFOA. The noticeable treatment technologies are either photo–based approaches, such as: photolysis, photochemical and photocatalysis [7–11] sonochemical treatment [12–15] or microwave–hydrothermal treatment [16–17]. The key factor in these treatment reactions are one–electron

oxidants such as persulfate [8–16] periodate [10], or photocatalysts such as heteropolyacid [7], TiO_2 [9, 11], have been used to decompose PFCAs under UV–irradiation.

This study explored the effect of the presence of sulfate radicals on the degradation rate of PFOA undergoing UV–irradiation. The effects of sulfate concentration, solution temperature and the radical scavengers on the degradation rate of PFOA were investigated.

2. Materials and methods

2.1. Materials

The perfluorooctanoic acid (PFOA, $C_7F_{15}COOH$, 96% purity) was from Aldrich. Sodium Sulfate Anhydrous (Na_2SO_4, 100% purity) was from Nacalai Tesque. Acetic acid 99%, ammonium acetate 97%, methanol, and tert–BuOH was from Merck, Germany.

2.2. Experimental procedures

A stock solution of 250 ppm PFOA was prepared by diluting the chemicals into the desired volume of Milli–Q water. This solution was stored in a 4°C refrigerator and used for all following experiments; the solution concentration was adjusted accordingly. The Na_2SO_4 solution was prepared at a concentration of 100mM and stored at 4°C. The photodegradation experimental was setup in a dark close carton box. A 1 L closed double–layered glass reactor with a low–pressure mercury vapor quartz lamp (254 nm, 11 W, Aquapro, Taiwan) was placed in the middle of reactor. The reaction temperature was controlled at 25°C by a circulating water bath (B204, Firstek Scientific Co. Ltd., Taiwan). The Na_2SO_4 solutions were mixed well with PFOA solution by a magnetic stirrer. The samples were taken at various intervals and filtered by Millipore syringe filters with a 0.22 μm pore size (Millipore, Ireland) to analyze the concentration of PFOA remain.

2.3 Samples analysis

The LC–MS/MS (8040 Shimadzu, Japan) system was equipped with a column (Poroshell 120, EC.C18 (2.1 mm I.D. × 150 mm L, 2.7 μm) and guard column EC–C18, Agilent, USA was used to analyze samples. The mobile phase consisted of a binary mixture of A (2 mM.L–1 ammonium acetate in water with methanol in a ratio of volume is 9 and 1) and solvent B (methanol) at flow rate of 0.25 ml.min–1. The gradient, the start with 50%B in 2 min increased to 95% B for 18 min and linearly at 95% B for 4 min then ramped to 50%A for 3 min. Total running time was 27 min. The inject volume was 2μL. The MS system was running with an electrospray ionization source in negative mode (ESI) at 3.5kV. The PFOA degradation efficiency was calculated via following equation:

$$\text{PFOA degradation (\%)} = \frac{C}{C_0} x100 \quad (1)$$

where C and C_0 are the PFOA concentration at the sampling and the initial time (ppm), respectively.

3. Results and Discussion

3.1. Photodegradation of PFOA

The photodegradation of PFOA was carried out with 1ppm PFOA in DI water. The photodegradation efficiencies of direct photolysis and photolysis in the solution with Na_2SO_4 were compared in figure 1. Red circle shows the experimental results of PFOA photodegradation in Na_2SO_4 (30mM) solution and black square for case without Na_2SO_4. When the solution with 50 ppm PFOA was decomposed with direct photolysis under 254 nm irradiation for 24 h, the decomposition efficiency of PFOA reached 41.3%. Na_2SO_4 (30mM)

containing solution showed higher PFOA degradation efficiency. The PFOA photodegradation reached 92.3% under UV irradiation assisted Na_2SO_4. This result implies that Na_2SO_4 act as an efficient oxidant for PFOA degradation when combined with the effects of H_2O_2 and UV irradiation.

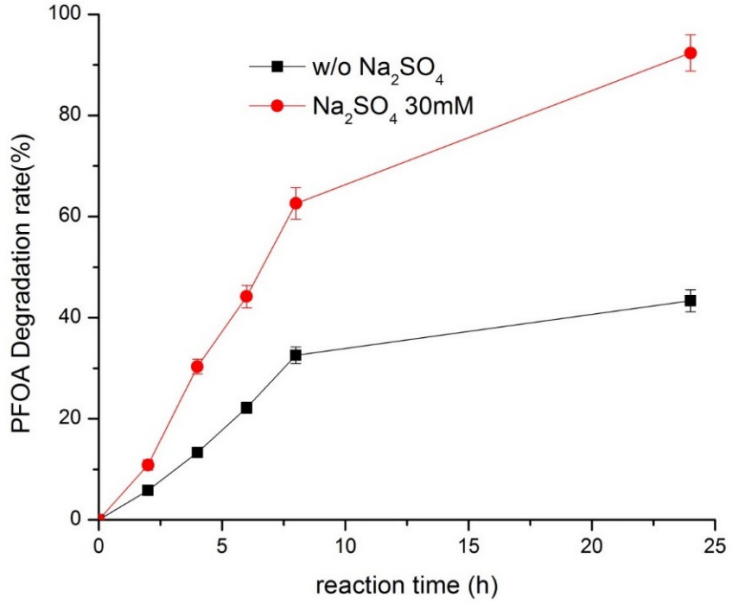

Figure 1. Photodegradation of PFOA with and without Na_2SO_4.

3.2. Degradation of PFOA by different Na_2SO_4 concentration

Degradation of PFOA by different Na_2SO_4 concentration, from 20 mM to 50 mM Na_2SO_4 used to investigate the effluence on degradation efficiency. Figure 2 shows the degradation efficiencies of PFOA at different initial Na_2SO_4 concentrations. The highest degradation efficiency reaches at 40 mM Na_2SO_4 solution. The degradation efficiency increased with increasing Na_2SO_4 concentrations from 20 mM to 40 mM and decreased at 50 mM Na_2SO_4 solution.

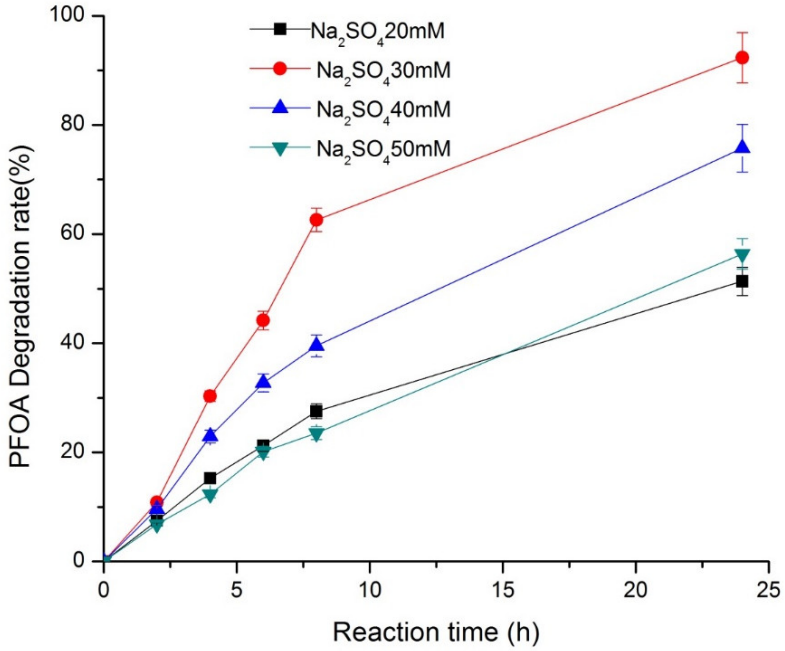

Figure 2. Photodegradation of PFOA by different Na_2SO_4 concentration.

3.3. Degradation of PFOA by Na_2SO_4 presence of t–BuOH

To investigate SO_4•– radical affection on PFOA photodegradation, tert–butanol (t–BuOH), a typical hydroxyl radical inhibitor, was added in PFOA/Na_2SO_4 decomposition solution. t–BuOH, a typical •OH inhibitor, has been used to inhibit the activity of •OH. The effect of radical scavenger t–BuOH on PFOA decomposition was illustrated in figure 3. With UV/Na_2SO_4, the degradation of PFOA in the presence of t–BuOH was considerably reduced to about 45% after 24 hours irradiation. The reaction rate without t–BuOH was 1.5 times faster that with t–BuOH in the UV/Na_2SO_4 system. Comparison with previous literatures [12–13], this results are in a fair agreement with those conclusion. That confirms t–BuOH is an effective radical scavenger in the UV/Na_2SO_4 system.

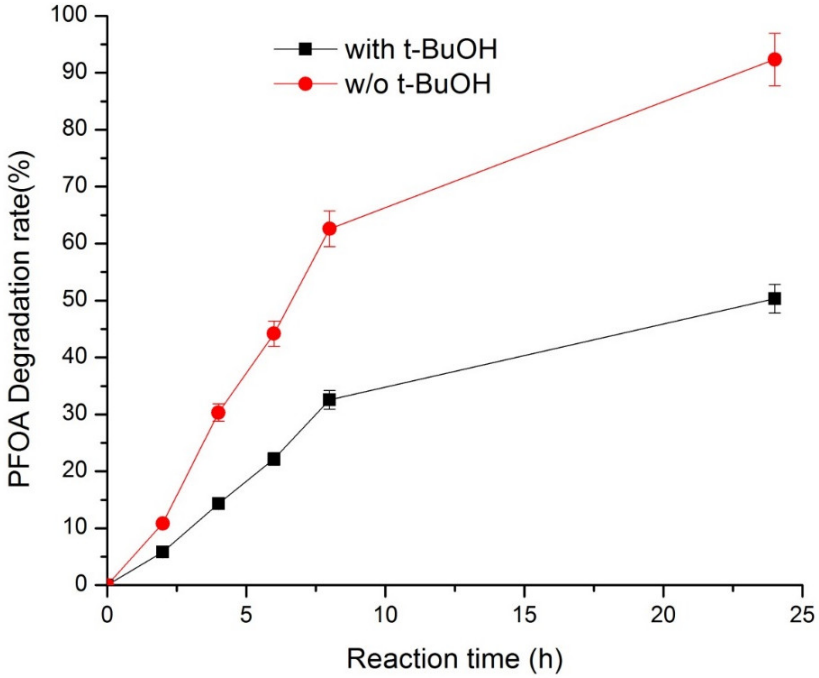

Figure 3. Photodegradation of PFOA effluent by radical scavenger t–BuOH.

3.4. Degradation of PFOA affected by reaction temperature

Solution temperature was controlled by water bath cycle at 15, 25, 35, and 45°C to evaluate the effects of solution temperature on the photodegradation of PFOA.

The result of photodegradation of PFOA affected by reaction temperature was shown in figure 4. UV/Na_2SO_4 system, the highest photodegradation rate was observed at 25°C. At 15°C, 35°C and 45°C, the photodegradation efficienies of PFOA were lower than those at 25°C. These results imply that the sulfate assisted UV treatment works best under ambient temperatures (25°C), while higher temperatures have an adverse effect irrespective of sulfate addition.

4. Conclusion

This study investigated the efficiency of PFOA photodegradation by UV/Na_2SO_4 system with different Na_2SO_4 concentrations, solution temperature levels, and presence of radical scavenger t–BuOH. The rate of PFOA degradation depend heavily on Na_2SO_4 dose. The effficiency of PFOA degradation in UV/Na_2SO_4 solution showed higher than it in UV irradiation only. The highest PFOA degradation efficiency obtains at Na_2SO_4 30mM, 25°C. The degradation of PFOA in the presence of t–BuOH was reduced. Photodegradation shows promised technique in treatment PFOA and other POPs, the presence of oxidants like SO_4^{2-}

(Na_2SO_4) will improve the efficiency of photodegradation. This study demonstrated that PFOA degradation can be effectively achieved through sulfate-assisted photochemical treatment at room temperature.

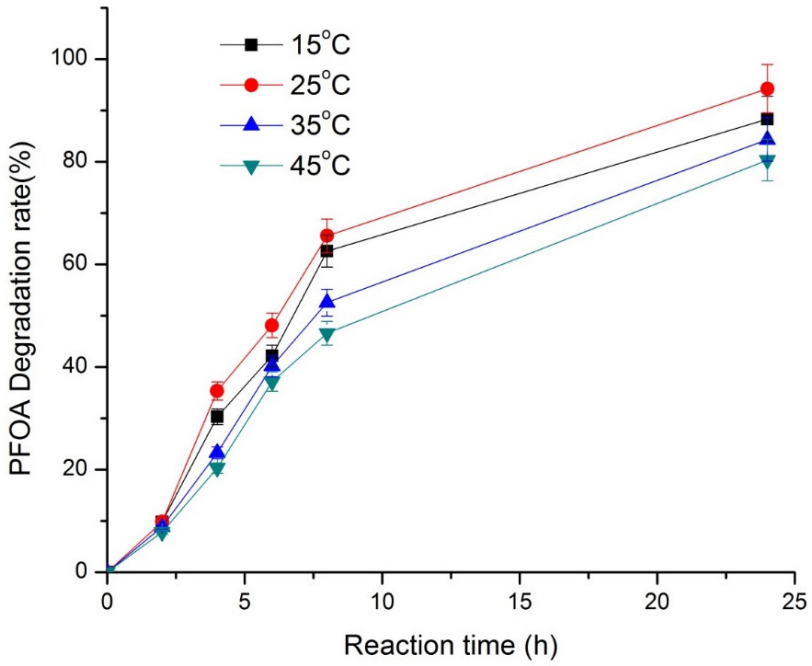

Figure 4. Photodegradation of PFOA at different temperature levels.

Acknowledgement

This research is funded by Vietnam National Foundation for Science and Technology Development (NAFOSTED) under grant number 104.99–2018.37.

Author Contributions: The experiment was conducted by H.T.D., L.A.P.T., T.H.P.; the paper was written by H.T.D., L.A.P.T.

Conflicts of Interest: The authors declare no conflict of interest.

References

1. Key, B.D.; Howell, R.D.; Criddle, C.S. Fluorinated Organics in the Biosphere. *Environ. Sci. Technol.* **1997**, *31(9),* 2445–2454.
2. So, M.K.; Taniyasu, S.; Yamashita, N.; Giesy, J. P.; Zheng, J.; Fang, Z.; Im, S. H.; Paul K. S. L. Perfluorinated Compounds in Coastal Waters of Hong Kong, South China, and Korea. *Environ. Sci. Technol.* **2004**, *38(15)*, 4056–4063.
3. Kudo, N.; Kawashima, Y. Toxicity and toxicokinetics of perfluorooctanoic acid in humans and animals. *J. Toxicol. Sci*. **2003**, *28(2)*, 49–57.
4. EFSA. Opinion of the Scientific Panel on Contaminants in the Food chain on Perfluorooctane sulfonate (PFOS), perfluorooctanoic acid (PFOA) and their salts. *EFSA J.* **2008**, 653.
5. USEPA. Revised draft hazard assessment of perfluorooctanoic acid and its salts. http://www.fluoridealert.org/wp–content/pesticides/pfoa.epa.nov.4.2002.pdf, **2002**.
6. Kennedy, G.L.Jr.; Butenhoff, J.L.; Olsen, G.W.; O'Connor, J.C.; Seacat, A.M.; Perkins, R.G.; Biegel, L.B.; Murphy, S.R.; Farrar, D.G. The toxicology of perfluorooctanoate. *Crit. Rev. Toxicol.* **2004**, *34(4)*, 351–384.
7. Hori, H.; Hayakawa E.; Einaga, H.; Kutsuna, S.; Koike, K.; Ibusuki, T.; Kiatagawa, H.; Arakawa, R. Decomposition of Environmentally Persistent Perfluorooctanoic

Acid in Water by Photochemical Approaches. *Environ. Sci. Technol.* **2004**, *38(22)*, 6118–6124.

8. Hori, H.; Yamamoto, A.; Hayakawa, E.; Taniyasu, S.; Yamashita, N.; Kutsuna, S.; Kiatagawa, H.; Arakawa, R. Efficient Decomposition of Environmentally Persistent Perfluorocarboxylic Acids by Use of Persulfate as a Photochemical Oxidant, *Environ. Sci. Technol.* **2005**, 3*9(7)*, 2383–2388.
9. Estrellan, C.R.; Salim C.; Hinode, H. Photocatalytic decomposition of perfluorooctanoic acid by iron and niobium co–doped titanium dioxide. *J. Hazard. Mater.* **2010**, *179(1)*, 79–83.
10. Cao, M.H.; Wang, B.B.; Yu, H.S.; Wang, L.L.; Yuan, S.H.; Chen, J. Photochemical decomposition of perfluorooctanoic acid in aqueous periodate with VUV and UV light irradiation. *J. Hazard. Mater.* **2010**, *179(1–3)*, 1143–1146.
11. Panchangam, S.C.; Lin, A.Y.C.; Shaik, K.L.; Lin, C.F. Decomposition of perfluorocarboxylic acids (PFCAs) by heterogeneous photocatalysis in acidic aqueous medium. *Chemosphere* **2009**, *77(2)*, 242–248.
12. Hiroshi, M.; Takagi, Y.; Tanaka, M.; Tsuruho, K.; Okitsu, K.; Maeda, Y. Sonochemical Decomposition of Perfluorooctane Sulfonate and Perfluorooctanoic Acid. *Environ. Sci. Technol.* **2005**, *39*, 3388–3392.
13. Lee, Y.C.; Huang, C.M.J.; Kuo, C.P.J.; Lo, S.L. Efficient sonochemical degradation of perfluorooctanoic acid using periodate. *Ultrason Sonochem* **2016**, *31*, 499–505.
14. Sekiguchi, K.; Kudo, T.; Sankoda, K. Combined sonochemical and short–wavelength UV degradation of hydrophobic perfluorinated compounds. *Ultrason Sonochem* **2017**, *39*, 87–92.
15. Hu, Y.B.; Lo, S.L.; Li, Y.F.; Lee, Y.C.; Chen, M.J.; Lin, J.C. Autocatalytic degradation of perfluorooctanoic acid in a permanganate–ultrasonic system. *Water. Res.* **2018**, *140*, 148–157.
16. Lee, Y.C.; Lo, S.L.; Chiueh, P.T.; Chang, D.G. Efficient decomposition of perfluorocarboxylic acids in aqueous solution using microwave–induced persulfate. *Water. Res.* **2009**, *43(11)*, 2811–2816.
17. Lee, Y.C.; Lo, S.L.; Chiueh, P.T.; Liou, Y.H.; Chen, M.L. Microwave–hydrothermal decomposition of perfluorooctanoic acid in water by iron–activated persulfate oxidation. *Water. Res.* **2009**, *44(3)*, 886–892.

VIETNAM JOURNAL OF HYDROMETEOROLOGY

Research Article

Mapping the residual tidal ellipse from Vung Tau–Bac Lieu, Viet Nam by using a numerical model in curvilinear coordinate

Tran Thi Kim[1,2,4], Nguyen Khac Thanh Long[3,4], Nguyen Thi Thu Hong[1], Nguyen Ky Phung[5], Nguyen Thi Bay[3,4*]

[1] Ho Chi Minh City University of Natural Resources and Environment; ttkim@hcmunre.edu.vn
[2] Institute of Environment and Natural Resources, Vietnam National University Ho Chi Minh City; ttkim@hcmunre.edu.vn
[3] University of Technology; ntbay@hcmut.edu.vn
[4] Vietnam National University Ho Chi Minh City; ntbay@hcmut.edu.vn
[5] Institute of Computational Science and Technology; kyphungng@gmail.com

*Correspondence: ntbay@hcmut.edu.vn; Tel.: +84–902698585

Received: 12 June 2021; Accepted: 21 July 2021; Published: 25 August 2021

Abstract: Tidal currents are often the dominant source of current variability and play an important role in shaping coastal bottom topography. In this paper, the authors applied a hydraulic model in curvilinear coordinates to calculate 4 main tidal constituents, namely K_1, O_1, M_2 and S_2 in a region from Vung Tau–Bac Lieu, Viet Nam. The hydraulic model with the two–dimensional orthogonal curvilinear grid has the advantage of increasing the accuracy of the results at the domain boundary. The numerical method of this model derives from the solution of the Reynolds system of equations averaged over depths in the curvilinear coordinate systems. The model verification is implemented based on the equilibrium of the tidal currents of energy. The result of this model is used to map ellipse constituents and help understand more about the tidal deposition from Vung Tau to Bac Lieu, Viet Nam. The results recorded that the residual tidal ellipse M_2 from Vung Tau–Bac Lieu, the greatest ellipses are M_2, followed by the tidal constituents K_1, O_1 and S_2. This rotation of the ellipse is almost the same with clockwise.

Keywords: Ellipse constituents; Tidal constituents; Numerical model; Curvilinear co–ordinates.

1. Introduction

The tidal regime at a certain location is determined according to the period of tidal fluctuations. There are two basic types of tides, semi–diurnal and diurnal. With a semi–diurnal tide, there are two high tides and two low tides in a day, while a diurnal tide has only one rise and one low tide in a day Tides propagate in the hydrosphere as long waves, with periods of many hours, wavelengths thousands of kilometers, and small amplitudes (compared to wavelengths) and are called tidal constituents. The properties of the component tidal constituents depend on the magnitude and period of gravitational change between the earth's surface, the moon and the sun. There are 396 significant tidal components, the basic tidal constituents are: semi–diurnal constituents (symbols M_2 and S_2), diurnal constituents (symbols O_1 and K_1) [1]. For each tidal constituent the tip of the current velocity vector describes an ellipse. Within each period of the respective tidal constituent a full rotation is executed [2].

The studies of tidal characteristics, particularly, tidal ellipse has been studied by many researchers. [3] calculated and compared the tidal flow results from the model and the observation for New Zealand region. The results showed that the M_2 tidal constituent is the dominant component of currents in this region, and the model gives the best results for this constituent. The tidal ellipse of M_2 constituent shows the strongest tidal currents in Cook Strait, near Stewart Island and parts of Hauraki Bay. [4] applied a two–dimensional vertically integrated hydrodynamic model to simulate the hydrodynamics in the Tagus estuary and the model developed from the SIMSYS2D model. The result of the model was the tidal hydrodynamic regime of the Tagus estuary by analysing the amplitude, phase, tidal ellipse parameters of both semi–diurnal and diurnal constituents. [5] studied the characteristics of tidal current and tidal residual current in Chunsu Bay, Yellow Sea, Korea based on numerical modeling experiments – ECOM3D. The model results have been verified through measurement data, amplitude and phase analysis of 4 main tidal constituents (M_2, S_2, K_1 and O_1) of current velocity and sea level. [6] extracted high–frequency tidal variability from HF Radar Data in the northwestern Bay of Bengal and analyzed tidal harmonic by using the T_Tide tool. The constituents S_4, MS_4 and M_3 (M_4, $2SM_6$ and M_6) at nearshore location (offshore) was identified, which are due to the non–linear interaction of tidal currents with bathymetry. In 2019, Ahmed and Siddiqa used the Tide and Wave Recorder TWR–2050 along with Flow Quest 600 and ADCP to record tidal levels in coast of Karrachi, Pakistan. The ellipses were used to analyze the tidal current characteristics. In the study region, semi–diurnal tide prevails [7].

In Viet Nam, [8] published a paper in 2007 which calculated tidal currents in the North Danger Reef by using finite element method (FEM) with shallow water equations, mainly continuity and momentum equations to partially solve the problems of bottom topography, boundary conditions, etc. using the finite difference method (FDM). The result shows the characteristics of ellipse for 4 main tidal constituents (K_1, O_1, M_2, S_2) and tidal currents. [9] calculated the tidal wave propagation along the Mekong Deltaic coast by using Delft3S–FLOW model for the hydrodynamic regime and the astronomical phases and amplitudes were analyzed, using Delft3D–TIDE tool. The tidal ellipses of the M_2 semi–diurnal constituent show strong currents occurring on the eastern coast of the Mekong Delta, while weak currents occur near the western coast. The residual current increased in the southeastern of the shallow area of the Mekong Delta is strongest along the Ca Mau peninsula up to about 10–15 cm/s. In addition, a geographical distribution map of tidal characteristics in the entire East Sea Viet Nam has been developed.

For nearshore areas, curvilinear coordinate models show many advantages. Because the velocity field is calculated on a curved grid (which is usually built along shorelines), the simulation results in areas with complex topography are better. Furthermore, the hydraulic model with the two–dimensional orthogonal curvilinear grid has the advantage of increasing the accuracy of the results at the domain boundary. In general, the studies show that tidal currents in the shallow waters are influenced by topography. This study focuses on building an ellipse map of tidal currents from Vung Tau to Bac Lieu where is strongly influenced by the semi–diurnal tidal regime by a curvilinear coordinate model. In the nearshore, the friction is calculated as a matrix inversely proportional to the depth. The results of ellipse for 4 main constituents K_1, O_1, M_2 and S_2 are essential information about the semi–diurnal tidal characteristics in this region.

2. Material and method

2.1. Material

The Southern region, Viet Nam is affected by two different tidal systems originating from the East Sea and the Southwest Sea. Therefore, the tidal regime in the coastal strip

from Vung Tau to Ca Mau Cape is irregular semi–diurnal tide. In this study, ellipses will be established for this semi–diurnal zone. The study area is the coastal area from Vung Tau to Bac Lieu (Figure 1a), geographically located from 106.009° to 106.84° East longitude and 8.91° to 9,63° North latitude.

The domain consists of four boundaries: three liquid boundaries (Boundary 2, 3 and 4) are the East Sea boundaries; the solid boundary is the coastline of the Hau Estuary (Boundary 1), in which, there are two river boundaries (Figure 1b). A computational mesh (Figure 1b) is a curved perpendicular the computational mesh with a mesh size of 130 x 155 cells with d_x, d_y in the range of 300 meters to 500 meters.

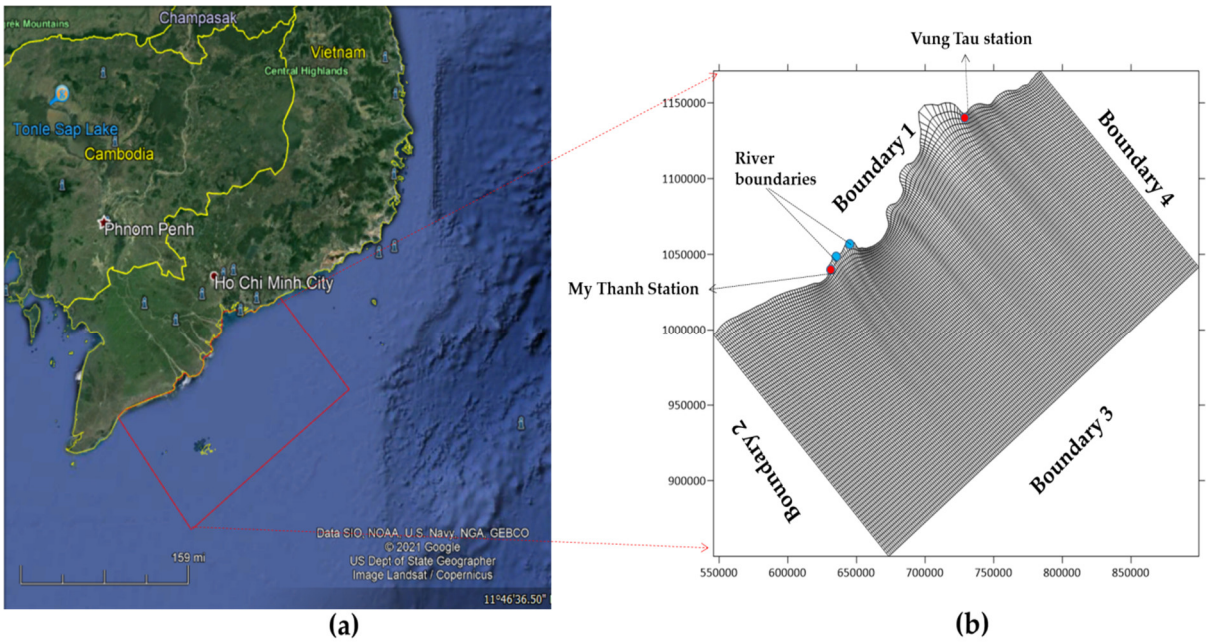

Figure 1. Study area.

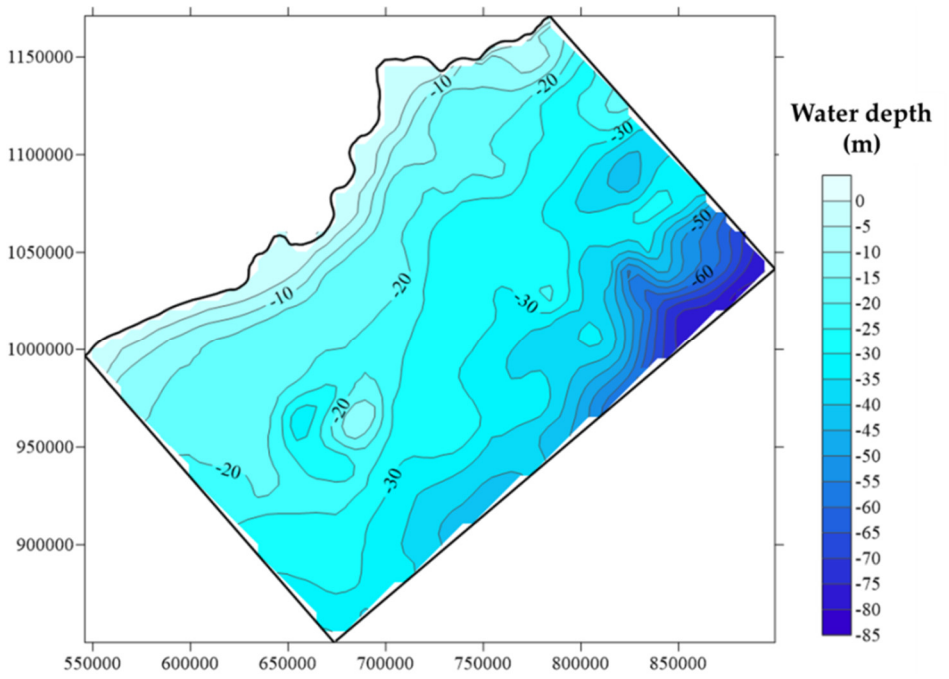

Figure 2. Topography.

Topography: The topographic data (Figure 2) is collected in 2010 from Southern Institute of Water Resources Research, Viet Nam (SIWRR). The parameters in the model are set up: Time step (dt): 72 s, Coriolis: 2.4096 x 10^{-5}, Sigma 7.26 x 10^{-5} (K_1), 6.76 x 10^{-5} (O_1), 14.05 x 10^{-5} (M_2), 14.54 x 10^{-5} (S_2), Tidal constituent period: 8614s (K_1), 92950s (O_1), 44714s (M_2), 43200s (S_2). The density of sea water: 1026 kg/m^3.

The friction bed coefficients for four tidal constituents were set up changing the water depth with the range of 0.026 to 0.058 (Figure 3).

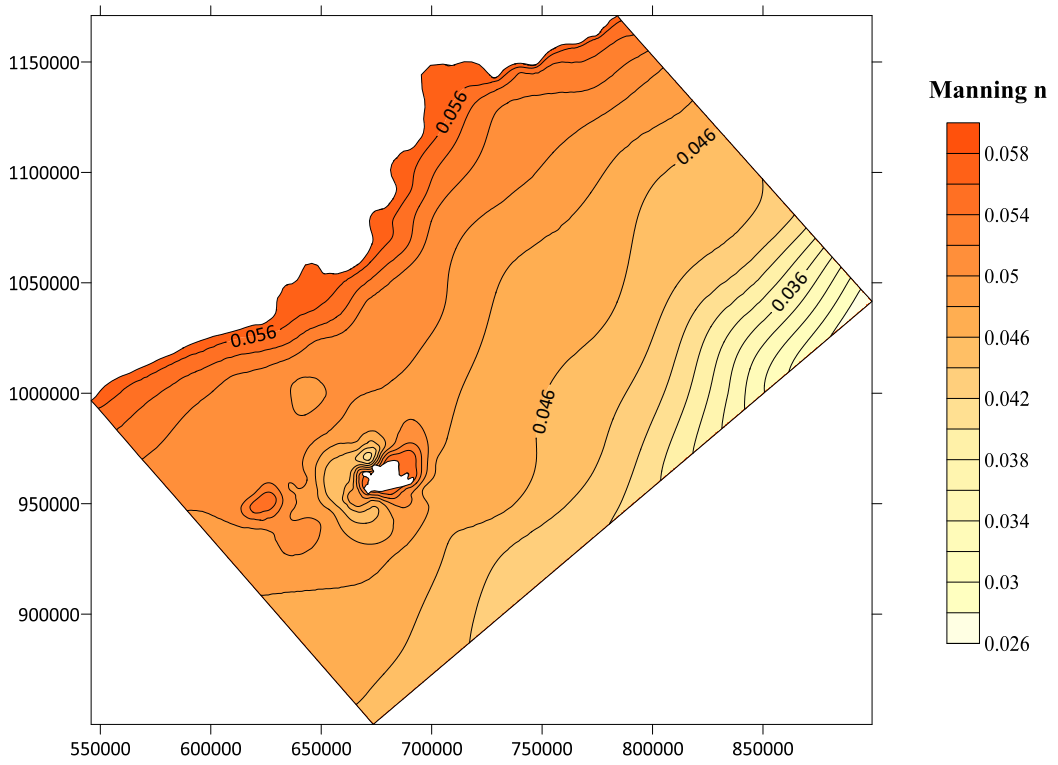

Figure 3. Roughness map.

Boundary conditions: The harmonic constant data for the four tidal constituents were extracted from the DTU10 Global Tide Model for the three open boundaries at sea. For river boundaries, the data is collected the Atlas Viet Nam (1994) for harmonic constant.

2.2. The governing equations in the curvilinear coordinate system

The governing equations in the curvilinear co–ordinates, are constructed based on the Reynolds equation in Cartesian coordinates [8]:

$$\begin{cases} p_\tau + gHJ^{-1}\left(g_{22}\zeta_\xi - g_{12}\zeta_\eta\right) = \Psi_1 \\ q_\tau + gHJ^{-1}\left(g_{11}\zeta_\eta - g_{12}\zeta_\xi\right) = \Psi_2 \\ JH_\tau + p_\xi + q_\eta = 0 \end{cases} \quad (1)$$

where $\tau = t$; $p = JUH$; $q = JVH$; $H = h + \zeta$

U, V are the "contravariant" base vectors of the curvilinear coordinate system.

$$U = J^{-1}\left(uy_\eta - vx_\eta\right); \qquad V = J^{-1}\left(-vy_\xi - vx_\xi\right) \quad (2)$$

$$\Psi_1 = \Psi_{a1} + \Psi_{t1} + \Psi_{k1}; \qquad \Psi_2 = \Psi_{a2} + \Psi_{t2} + \Psi_{k2} \quad (3)$$

$\Psi a_1, \Psi_{a_2}$ are the nonlinear component in curvilinear coordinate system ξ, η.

Ψ_{t_1}, Ψ_{t_2} are the Friction bed component; Ψ_{k_1}, Ψ_{k_2} are the Coriolis component.

$$\Psi_{a1} = -\left[(pU)_{\xi} + (pV)_{\eta} + JH\left(U^2\Gamma^1_{11} + 2UV\Gamma^1_{12} + V^2\Gamma^1_{22}\right)\right] \quad (4)$$

$$\Psi_{a2} = -\left[(qU)_{\xi} + (qV)_{\eta} + JH\left(U^2\Gamma^2_{11} + 2UV\Gamma^2_{12} + V^2\Gamma^2_{22}\right)\right] \quad (5)$$

$$\Psi_{t1} = -\frac{K}{H}|v|p; \qquad \Psi_{t2} = -\frac{K}{H}|v|q; \quad (6)$$

$\Gamma^k_{i,j}$ is the Christoffel symbol type – II is defined as follows: $\Gamma^k_{i,j} = \frac{\partial e_i}{\partial \xi^j} e^k$ (7)

e_1, e_2 are the base vectors of the curvilinear coordinate system ξ, η; e_i, e_j are the "covariant" base vectors $\vec{e}$ [9–10].

The mesh is generated based on the Poisson equations (8) [11–12].

$$\Delta^2\xi = P(\xi,\eta); \qquad \Delta^2\eta = Q(\xi,\eta) \quad (8)$$

where P and Q are the control functions. The solution of this equation system in the domain (ξ, η) is:

$$L(r) = g_{22}r_{\xi\xi} - 2g_{12}r_{\xi\eta} - g_{11}r_{\eta\eta} = -J^2\left(Pr_{\xi} + Qr_{\eta}\right) \quad (9)$$

J is the "Jacobian" of the transformation. $J = x_{\xi}x_{\eta} + y_{\xi}y_{\eta}; \qquad 0 \neq J < \infty$

$$r = x_i + y_j; \qquad g_{22} = x_{\eta}^2 + y_{\eta}^2 = |r_{\eta}|^2;$$
$$g_{12} = x_{\xi}x_{\eta} + y_{\xi}y_{\eta} = r_{\xi}r_{\eta}; \qquad g_{11} = x_{\xi}^2 + y_{\xi}^2 = |r_{\xi}|^2 \quad (10)$$

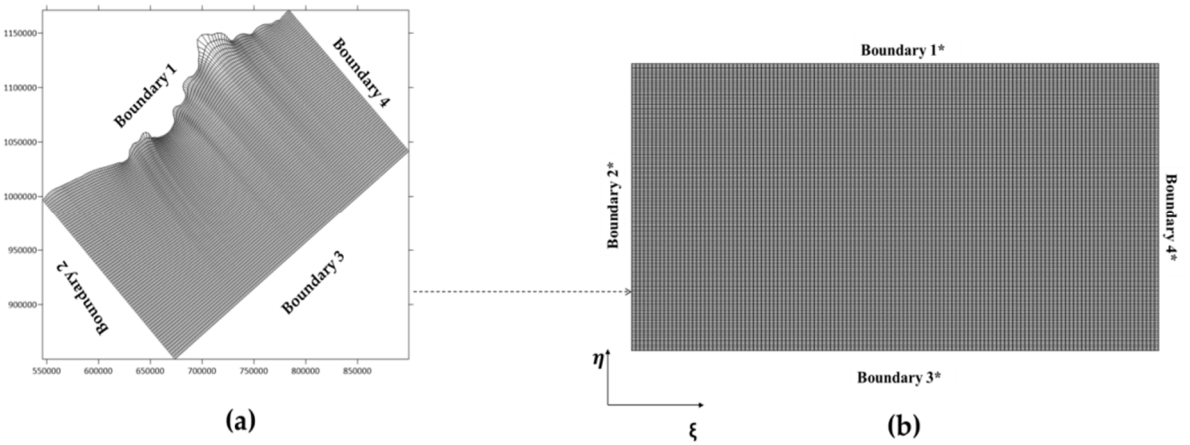

Figure 4. The mesh generation.

The study mesh (Figure 4) is a curved perpendicular mesh with a mesh size of 130 * 155 cells with dx, dy in the range of 300 meters to 500 meters.

Boundary conditions: After setting up the hydraulic model (equation (1) and the mesh generation (equation (9)). The boundary conditions at the liquid boundaries give the form of oscillation of each tidal constituent (K_1, O_1, M_2 and S_2), g_o: Amplitude, frequency and phase of the tidal oscillation. The boundary conditions at the solid boundaries [12]: p = 0 on ξ = const and q = 0 on η = const.

Equation (4) are solved using alternating direction implicit method on C–Arakov grid. The mesh node is at the boundary, on which the velocity component is perpendicular to the boundary. In the algorithm, using the semi–implicit diagram: "gradient" the water level is calculated according to the implicit diagram, while the nonlinear component is solved by an explicit diagram [8, 9, 14].

2.3. Energy balance equation

In defining the energy in the study area, the total energy is a combination between kinetic energy and potential enery. These components are calculated in the below while two energy dissipation due to bottom friction and mesh smoothing is identify by using equations (13) [13].

$$K = \frac{1}{2}\rho \iint_{\Omega*} J^{-1}H^{-1}\mathbf{p}^2 d\Omega * ; P = \frac{1}{2}\rho g \iint_{\Omega*} J\zeta^2 d\Omega * \quad (11)$$

$$W_\xi = \rho \int_{\eta_0} q\left(\frac{J^{-2}H^{-2}\mathbf{p}^2}{2} + g\zeta\right) d\xi \quad (12)$$

$$D_1 = -K\rho \iint_{\Omega*} J^{-2}H^{-3}\mathbf{p}^3 \, d\Omega * ; D_2 = \frac{2}{dt}\iint_{\Omega*} \gamma[\boldsymbol{P}^*\nabla^2 p + \boldsymbol{Q}^*\nabla^2 q] \quad (13)$$

where K is the Kinetic Energy; P is the potential energy; W is the energy flows across the liquid boundary; D_1 is the velocity of energy dissipation due to bottom friction; D_2 is the velocity of energy dissipation when smoothing; P*, Q* are the "convariant" component of velocity vector.

$$\boldsymbol{P}^* = g_{11}U + g_{12}V, \boldsymbol{Q}^* = g_{21}U + g_{22}V \quad (14)$$

3. Results

3.1. Verification model

Total water level data of 4 constituents were extracted at My Thanh station from 10pm on 15/01/2017 to 23pm on 14/02/2017 (Figure 5) which the data is at Vung Tau station from 01am on 01/01/2017 to 23pm on 28/02/2017 (Figure 6).

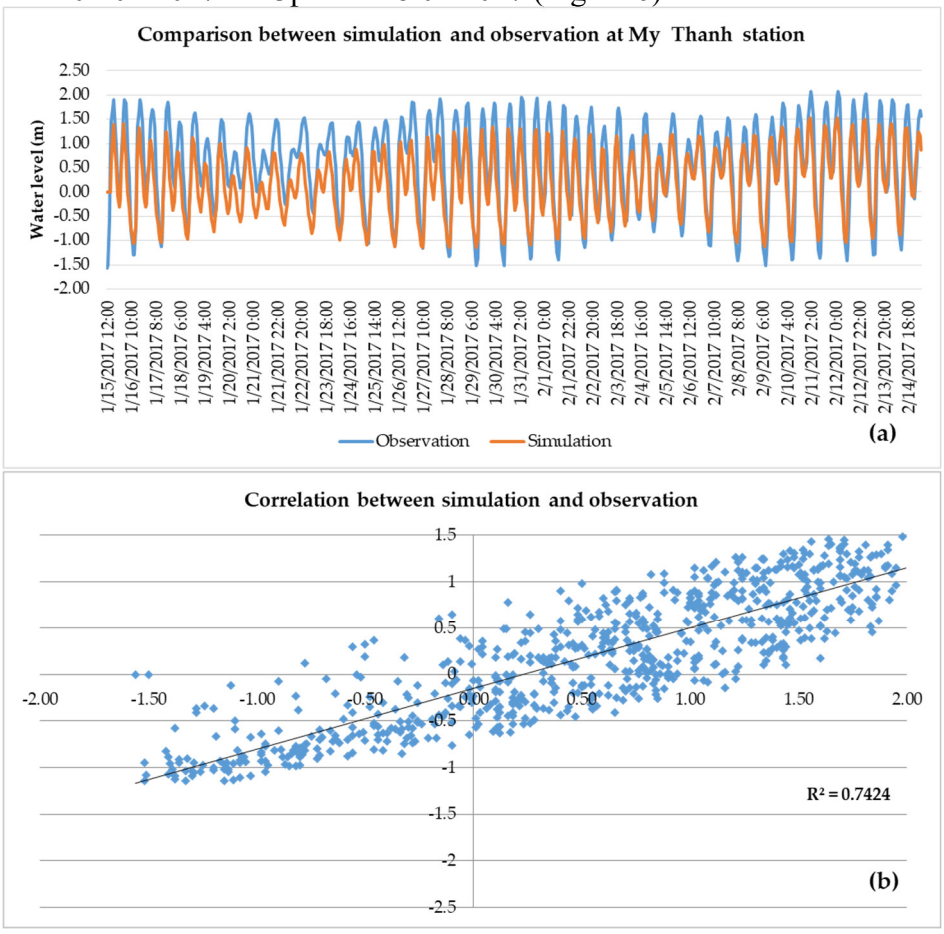

Figure 5. Comparison between simulation and observation at My Thanh station (a) and correlation between simulation and observation (b).

The verifiable results of the water level at My Thanh and Vung Tau station show the correlation coefficient $R^2 = 0.74$, $R^2 = 0.64$ and NSE = 0.6, NSE = 0.58, respectively. The difference in amplitude can be explained that the water level data are extracted from the model is considered for 4 main constituents M_2, K_1, O_1 and S_2, the others have not been considered. However, the phase of the water level is quite consistent with the observation data, which shows the great dominance of 4 constituents in this region.

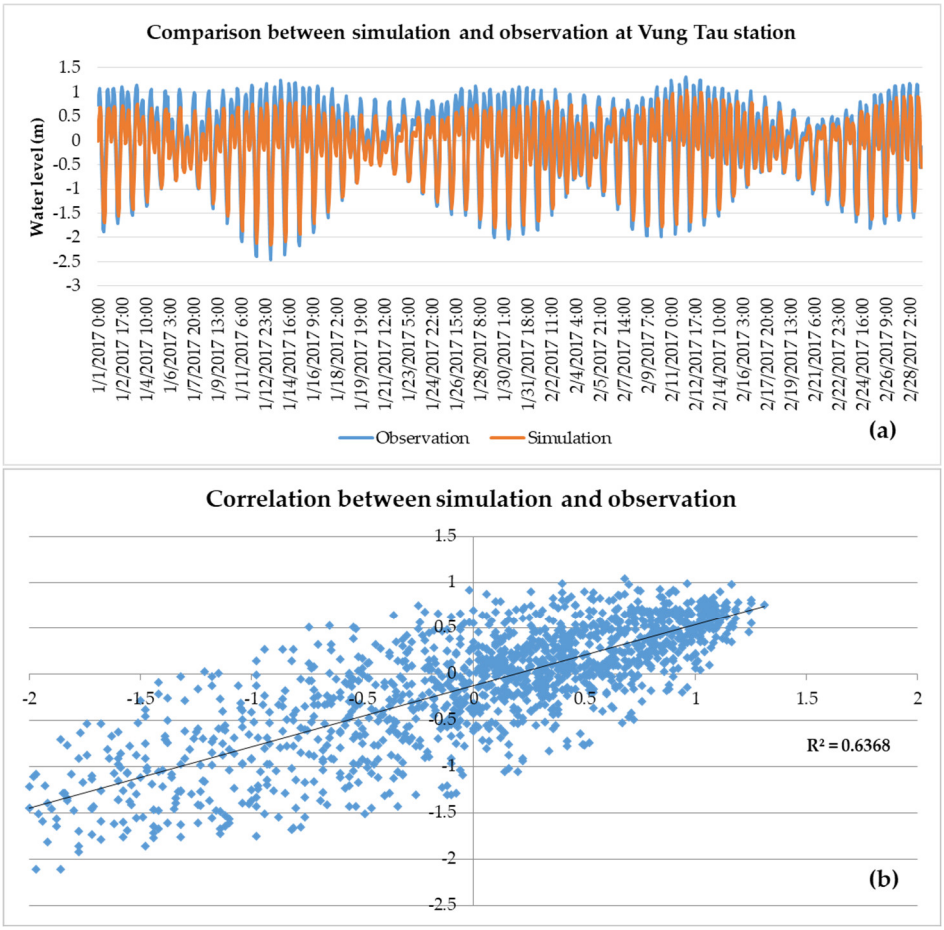

Figure 6. (a) Comparison between simulation and observation at Vung Tau station; (b) correlation between simulation and observation.

3.2. Tidal constituents' energy

The results showed that the energy variation (E: Total energy, P: Potential energy, K: Kinetic energy) of the semi–diurnal constituent M_2 are the most important, followed by the tidal constituents K_1, O_1 and S_2. As the coast of Hau Estuary is influenced by the mixed regime of semi–diurnal tides, the greatest tidal energy is M_2, followed by the tidal constituents K_1, O_1 and S_2.

The highest total energy of constituent M_2 values about 6.6 x 10^{10} KJ (in which, the value of the potential energy is 4.3 x 10^{10} KJ while that of kinetic energy is lower, at about 4 x 10^{10} KJ) (Figure 7). For the tidal constituents S_2, the highest values of total energy E, the potential energy P and the kinetic energy are 0.82 x 10^{10} KJ, 0.58 x 10^{10} KJ and 0.42 x 10^{10} KJ, respectively (Figure 7).

The results of energy balance are described by the results of variation in energy in the domain (Et), total energy across the liquid boundary (W), loss of energy caused by bottom friction (D_1) and energy balance ((W+D)–Et). The obtained results are extracted within the period 9th of all four tidal constituents M_2, S_2, K_1 and O_1 in Figure 8.

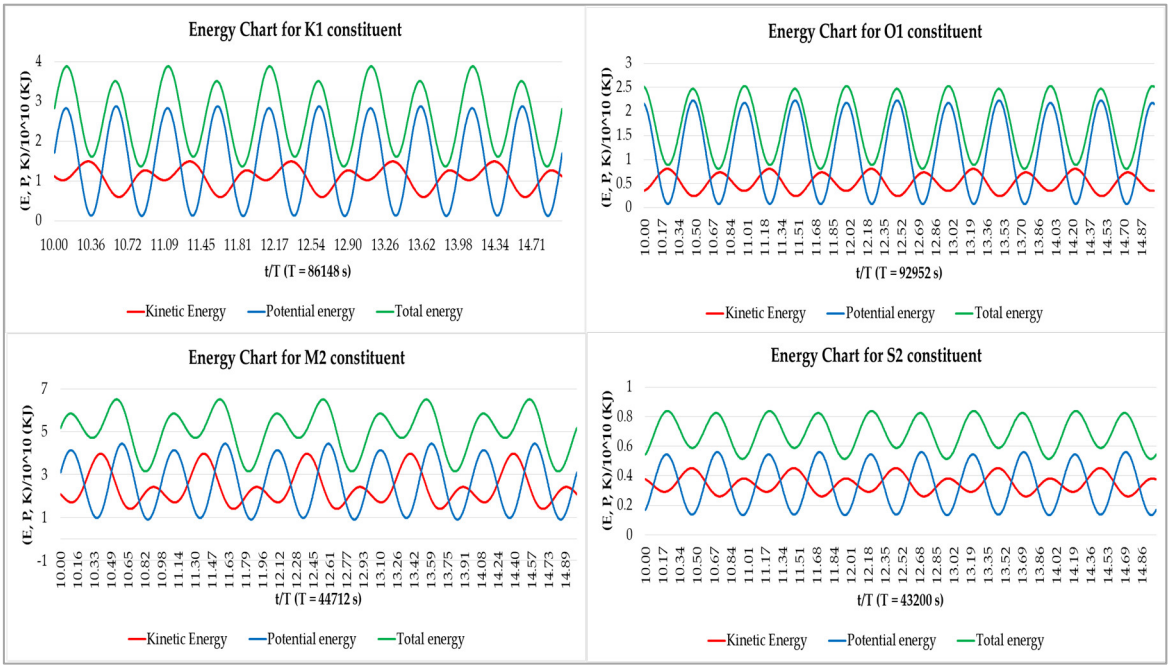

Figure 7. The simulation results of the energy of the constituents K_1, O_1, M_2 and S_2.

In general, the oscillations of the lines are sequences of sinusoidal. The oscillation of the total energy (W) and loss of energy caused by bottom friction (D_1) has an opposite phase while the total energy oscillates in phase with variation in energy in the domain (E_t). The energy balance oscillation in the variable region around axis "0" represents the energy balance in the region. The homogeneity of the oscillation of the energy inflow in the region and the energy variation is substantial for all four constituents, and the energy loss because friction is virtually small.

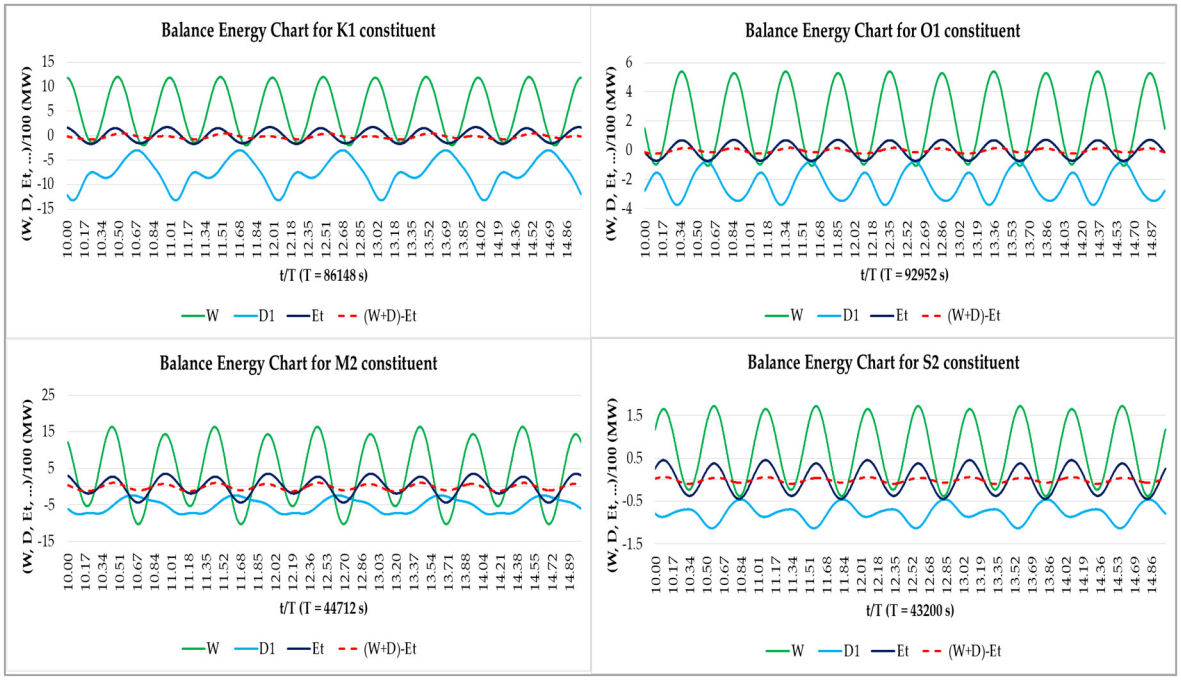

Figure 8. The simulation results of the tidal constituents energy balance: K_1, O_1, M_2 and S_2 (The orange line represents the results of variation in energy in the domain (E_t), the green line is total energy across the liquid boundary (W), the blue line represents loss of energy caused by bottom friction (D_1) and the red color is energy balance ($(W+D)–E_t$).

3.3. The tidal ellipse maps

The residual tidal ellipse maps were constructed from the results of the amplitude and phase simulation of the four main tidal constituents: K_1, O_1, M_2 and S_2 (from 5th period onwards). At the beginning of the periods (1th – 5th), the harmonic constituent oscillations are unstable. The ellipses of the diurnal constituent K_1 are quite small in size and the constituent has the most ellipses which are clockwise rotation in the 4 main constituents K_1, O_1, M_2 and S_2. From Vung Tau to Bac Lieu, these tidal ellipses change in both direction and magnitude, particularly in Tra Vinh coast. From Ba Ria–Vung Tau to Ben Tre, the tidal ellipses rotate clockwise direction with small sizes. However, in the Vung Tau coast, some tidal ellipses change direction but the tidal ellipse magnitude is unchanged. When reaching Tra Vinh coast, the ellipses change simultaneously direction (counterclockwise rotation) and the magnitude of the tidal ellipses increase. The ellipses rotate counter–clockwise from the coast of Tra Vinh to Bac Lieu (Figure 9). In particular, the coast of Soc Trang is a region full of tidal ellipses that rotate counterclockwise with a relatively large size (Figure 10).

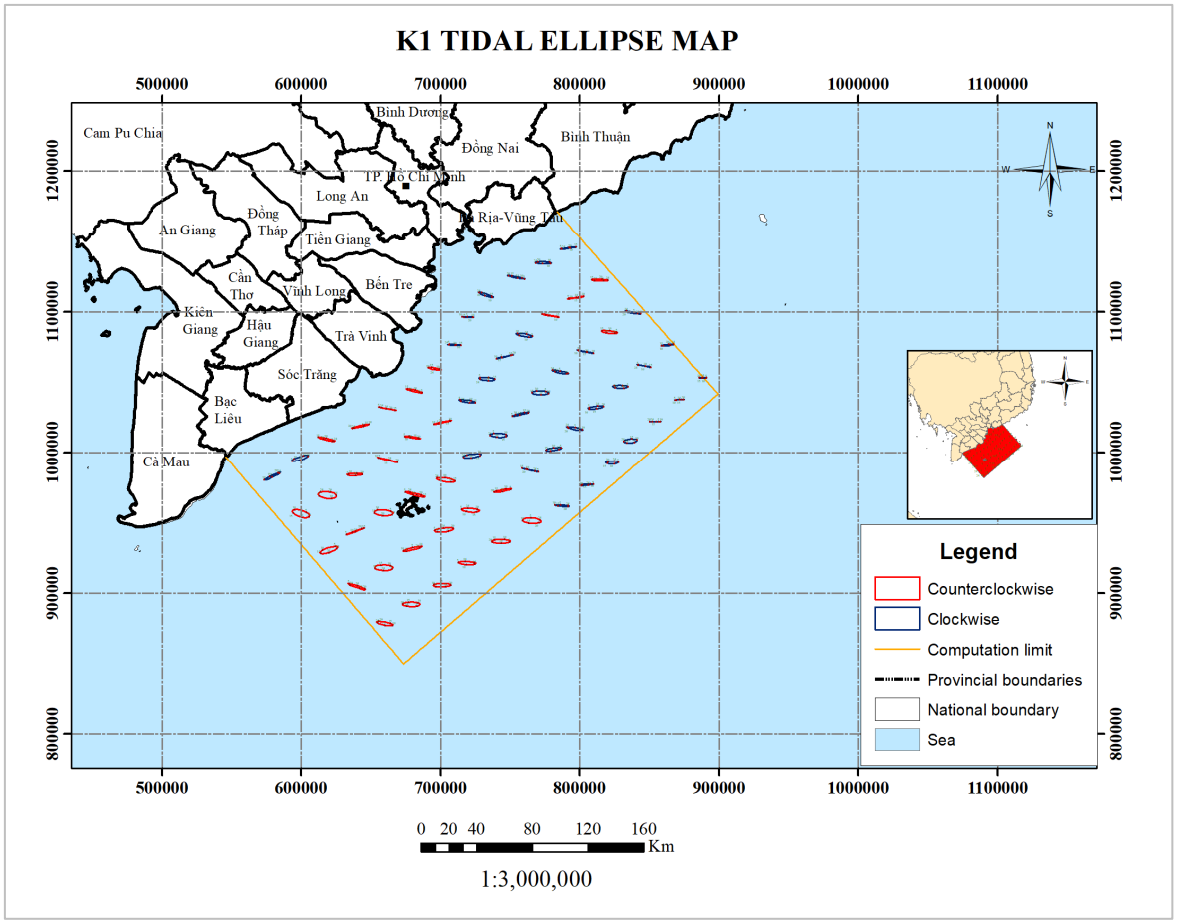

Figure 9. K_1 tidal ellipse map.

Similar to the K_1 diurnal constituent, the O_1 diurnal constituent has tidal ellipses that vary in both direction and magnitude from Vung Tau to Bac Lieu and it has the smallest ellipses size in 4 main tidal constituents. The tidal ellipses from Vung Tau to Tra Vinh rotate mainly clockwise direction with small sizes. However, in the coastal area, only a few ellipses change their direction. From the coast of Tra Vinh to Bac Lieu, the tidal ellipses change simultaneously in both direction and magnitude. The tidal ellipses turn counterclockwise rotation and the magnitudes also increase significantly (Figure 11). In the

coast of Soc Trang, ellipses rotate mainly in a counter–clockwise direction. But in the coast near the Hau estuary and a part of Vinh Chau, there are tidal ellipses that are opposite to the whole coast of Soc Trang but their size are small (Figure 12).

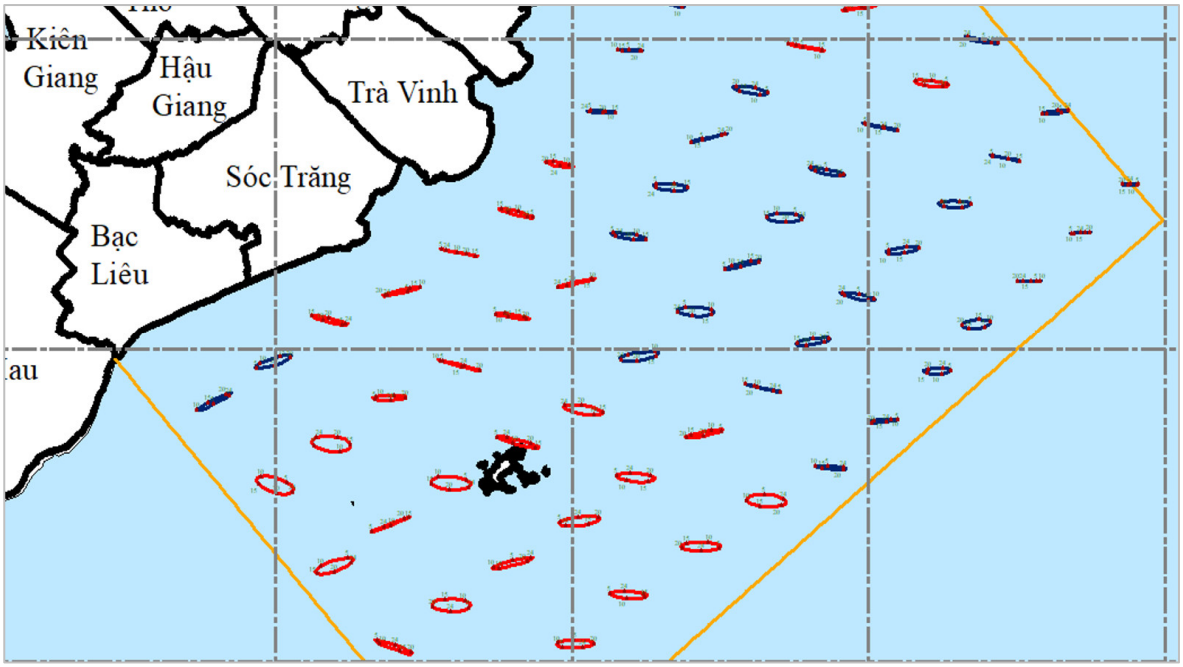

Figure 10. The tidal ellipse of K_1 constituent in Soc Trang.

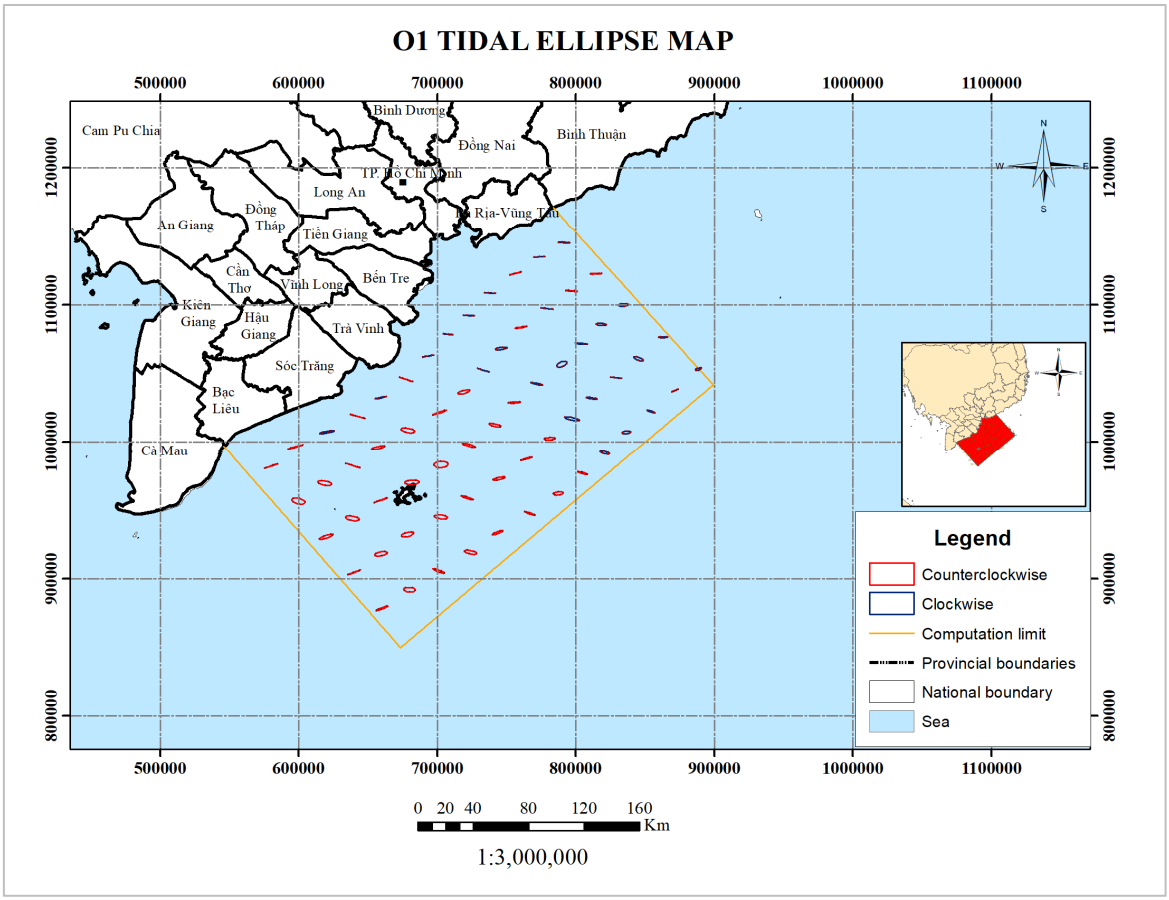

Figure 11. O_1 tidal ellipse map.

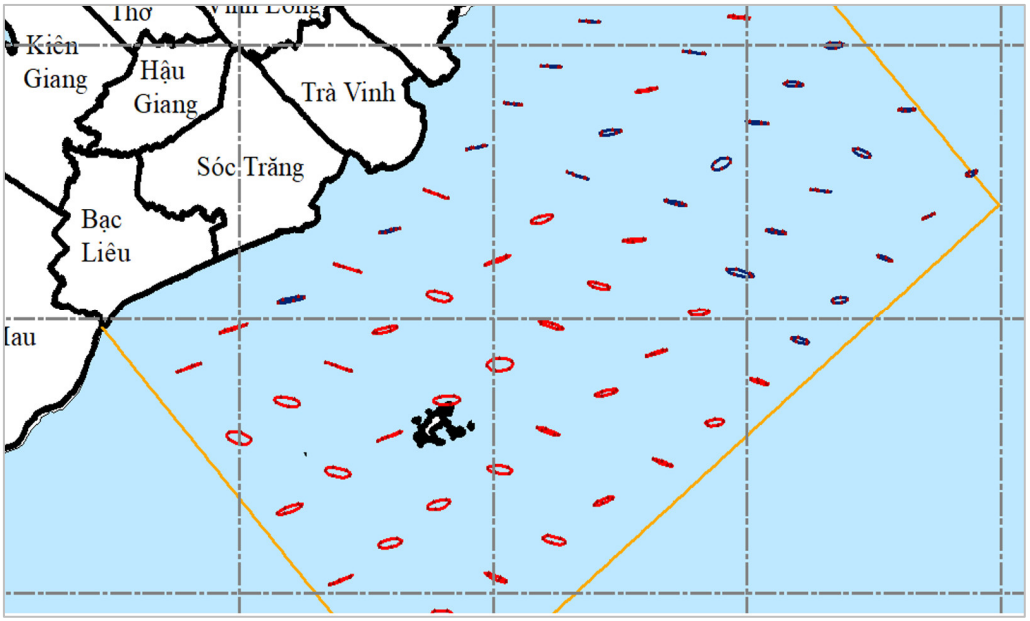

Figure 12. The tidal ellipse of O_1 constituent in Soc Trang.

The M_2 semi–diurnal constituent in the sea from Vung Tau to Bac Lieu is mainly ellipses rotating counterclockwise and it has the largest elliptical size in 4 main constituents. From Vung Tau to Ben Tre, the tidal ellipses change continuously direction with the tidal ellipses rotating clockwise (in the offshore zone) and counter–clockwise rotating ellipses (distributed mainly in the coastal area). From Tra Vinh to Bac Lieu, there are only counterclockwise tidal ellipses with large size (Figure 13). Similarly, Soc Trang coast is full of counterclockwise tidal ellipses with ellipse magnitude increasing as they are offshore, this is the area which has the largest tidal ellipse magnitude in whole calculation area (Figure 14).

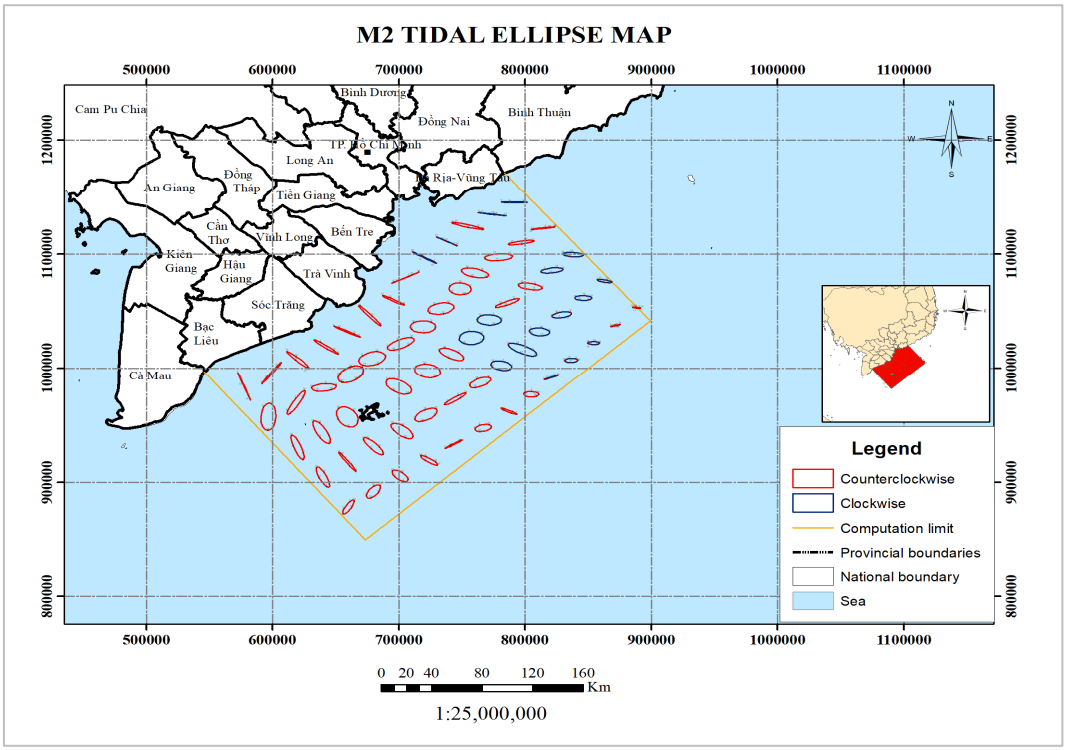

Figure 13. M_2 tidal ellipse map.

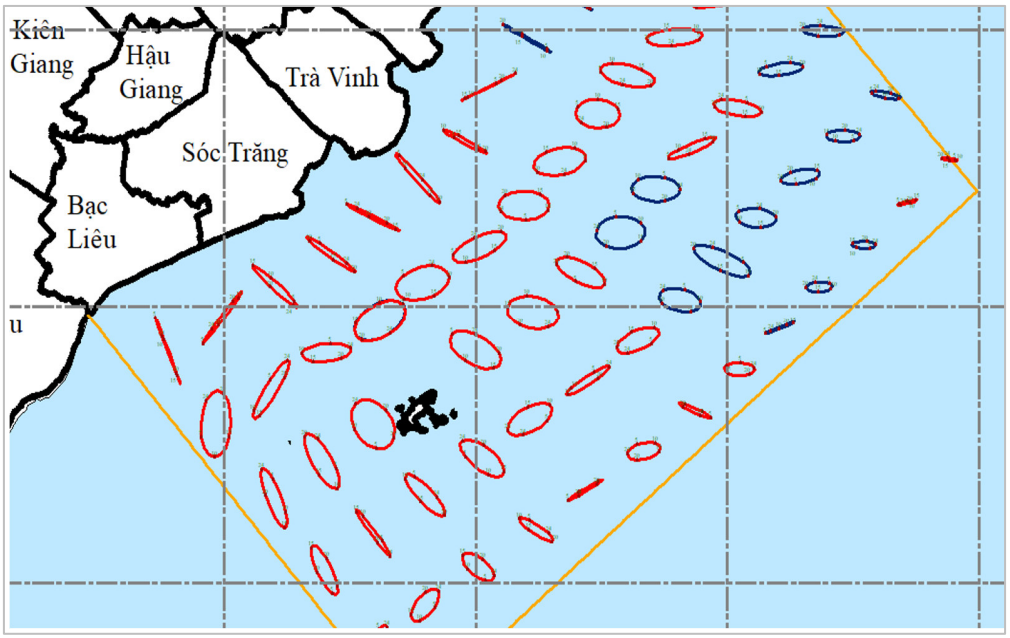

Figure 14. The tidal ellipse of M_2 constituent in Soc Trang.

The S_2 semi–diurnal constituent has some tidal ellipses that rotate counterclockwise and the ellipses are large in size, just smaller than the ellipse of M_2 constituent. The tidal ellipses have large size at the center of the study area, at the East Sea boundaries, these ellipses are very small. This is the constituent that has the least quantity of ellipses rotating clockwise with a few tidal ellipses in the coast of Vung Tau, Ho Chi Minh City and Hau estuary (Figure 15). In the coast of Soc Trang, ellipses rotate mainly counterclockwise direction, but at the Hau estuary, the tidal ellipse changes in direction but does not change in magnitude (Figure 16).

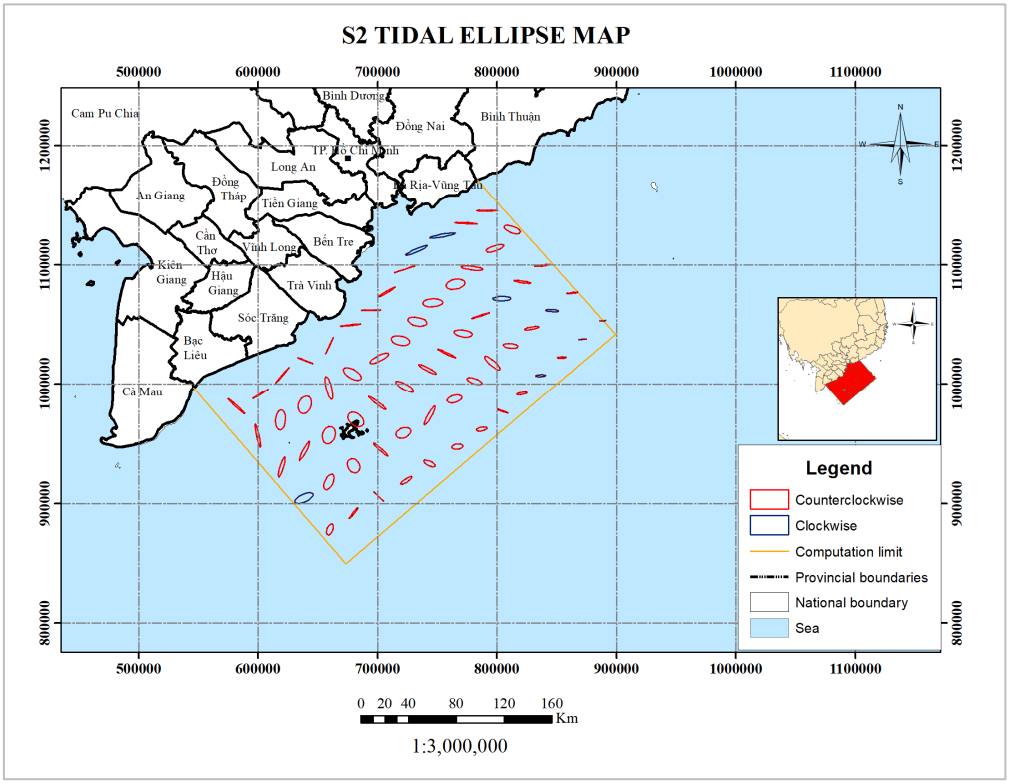

Figure 15. S_2 tidal ellipse map.

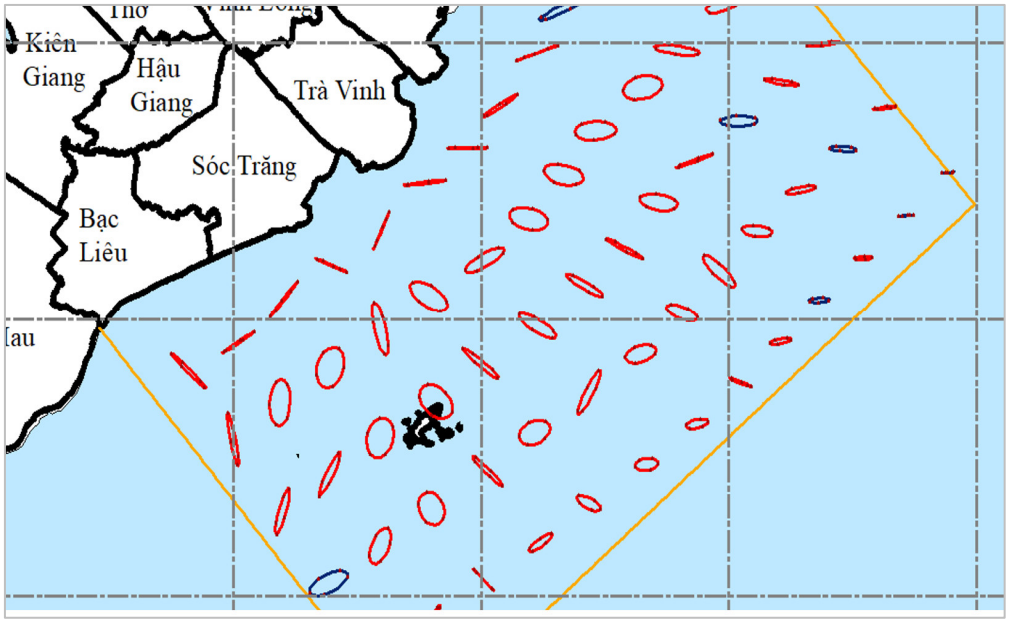

Figure 16. The tidal ellipse of S_2 constituent in Soc Trang.

4. Conclusions

In this paper, a hydraulic model in curvilinear coordinates was applied to build tidal ellipses for 4 main tidal constituents, namely K_1, O_1, M_2 and S_2 in a region from Vung Tau–Bac Lieu, Viet Nam. The numerical method of this model derives from the solution of the Reynolds system of equations averaged over depths in the curvilinear coordinate systems. The model verification is implemented based on the equilibrium of the tidal currents of energy. The model is set up with the friction bed coefficients for four tidal constituents changing the water depth with the range of 0.026 to 0.058. Generally, for coastal area from Vung Tau to Bac Lieu, the highest total energy of constituent M_2 values about 6.6 x 10^{10} KJ (in which, the value of the potential energy is 4.3 x 10^{10} KJ while that of kinetic energy is lower, at about 4 x 10^{10} KJ). For the tidal constituents S_2, the highest values of total energy E, the potential energy P and the kinetic energy are 0.82 x 10^{10} KJ, 0.58 x 10^{10} KJ and 0.42 x 10^{10} KJ, respectively. The oscillation of the total energy and loss of energy caused by bottom friction has an opposite phase while the total energy oscillates in phase with variation in energy in the domain. The homogeneity of the oscillation of the energy inflow in the region and the energy variation is substantial for all four constituents, and the energy loss because friction is virtually small.

The results recorded that the residual tidal ellipse M_2 from Vung Tau–Bac Lieu, the greatest ellipses are M_2, followed by the tidal constituents K_1, O_1 and S_2. This rotation of the ellipse is almost the same with clockwise. The S_2 semi–diurnal constituent has some tidal ellipses that rotate counterclockwise and the ellipses are large in size, just smaller than the ellipse of M_2 constituent while these of the diurnal constituent K_1 and O_1 are quite small in size. In particular, the coast of Soc Trang is a region full of tidal ellipses that rotate counterclockwise with a relatively large size for of the diurnal constituent K_1 and O_1.

Author Contributions: Conceptualization, T.T.K., N.T.B.; Methodology, T.T.K., N.K.P., N.T.B.; Software, T.T.K., N.K.T.L.; Validation, N.T.T.H., N.K.T.L.; Formal analysis, T.T.K., N.K.T.L.; Investigation, P.T.M.D.; Resources, T.T.K., N.T.B.; Data curation, N.T.B., N.K.T.L.; Writing–original draft preparation, T.T.K., N.K.T.L.; Writing–review and editing, T.T.K., N.T.T.H., N.K.T.L; Visualization, T.T.K., N.K.T.L.; Supervision, N.K.P., N.T.B.; Project administration, N.K.P.; Funding acquisition, N.K.P.

Funding: Tran Thi Kim was funded by Vingroup Joint Stock Company and supported by the Domestic Master/ PhD Scholarship Programme of Vingroup Innovation Foundation (VINIF), Vingroup Big Data Institute (VINBIGDATA).

Conflicts of Interest: The authors declare no conflict of interest.

References

1. Parker, B.B. Tidal analysis and prediction. Silver Spring, Maryland **2007**, pp. 388.
2. Xu, Z. Ellipse parameters conversion and vertical velocity profiles for tidal currents. Bedford Institute of Oceanography, Dartmouth, Nova Scotia, Canada. **2000**, pp. 20.
3. Stanton, B.R.; Goring, D.G.; Bell, R.G. Observed and modelled tidal currents in the New Zealand region. *N. Z. J. Mar. Freshw. Res.* **2001**, *35(2)*, 397–415.
4. Dias, J.M.; Valentim, J.M. Numerical modeling of Tagus estuary tidal dynamics. *J. Coast. Res.* **2011**, *64*, 1495–1499.
5. Jung, K.Y.; Ro, Y.J.; Kim, B.J. Characteristics of tidal current and tidal residual current in the Chunsu Bay, Yellow Sea, Korea based on numerical modeling experiments. *J. Korean Soc. Coast. Ocean Eng.* **2013**, *25(4)*, 207–218.
6 Mandal, S.; Sil, S.; Gangopadhyay, A.; Murty, T.; Swain, D. On extracting high–frequency tidal variability from HF radar data in the northwestern Bay of Bengal. *J. Oper. Oceanogr.* **2018**, *11(2)*, 65–81.
7. Ahmed, S.N.; Siddiqa, T. The study of tidal current dynamics and impact of bathymetry in training the currents along the Coast of Karachi, Pakistan. *Int. J. Marine Sci. Ocean Technol.* **2019**, *6(1)*, 110–116.
8. Long, B.H.; Chung, T.V. Caculations of tidal currents in the North Danger reef using finite element method. Proceedings of National Conference "Bien Dong – 2007", **2007**.
9. Phan, H.M.; Ye, Q.; Reniers, A.J.H.M.; Stive, M.J.F. Tidal wave propagation along The Mekong deltaic coast. *Estuarine Coast. Shelf Sci.* **2019**, *220*, 73–98.
10. Kim, T.T.; Long, N.K.T.; Phuoc, N.V.; Phung, N.K.; Bay, N.T. A coupled hydraulic and sediment transport model in the curvilinear coordinate. *VN J. Hydrometeorol.* **2021**, *728*, 14–30.
11. Androsov, A.A.; Klevanny, K.A.; Salusti, E.S.; Voltzinger, N.E. Open boundary conditions for horizontal 2–D curvilinear–grid long–wave dynamics of a strait. *Adv. Water Resour.* **1995**, *18(5)*, 267–276.
12. Massel, S.R. Hydrodynamics of coastal zones. Amsterdam: Elsevier **1989**, *48*, 336.
13. Fletcher, C.A.J. Computational Techniques for Fluid Dynamics. Mir, Moscow **1991**, 2. (Russian translation)
14. Thompson, J.F.; Warsi, Z.U.A.; Mastin, C.W. Numerical grid generation: Foundations and Applications. North–holland Amsterdam: Elsevier, 1985.
15. Bay, N.T.; Phung, N.K. Some study results for the tide in Tonkin gulf. Proceedings of the fourth National Conference of Marine science and technology. 1998.
16. Androsov, A.A.; Kagan, B.A.; Romanenkov, D.A.; Voltzinger, N.E. Numerical modelling of barotropic tidal dynamics in the strait of Messina. *Adv. Water Resour.* **2002**, *25(4)*, 401–415.

VIETNAM JOURNAL OF HYDROMETEOROLOGY

Research paper

The necessity of water resources inventory in Vietnam

Nguyen Thi Minh Hang[1*], Nguyen Cao Don[2]

[1] Thuyloi University, No. 175 Tay Son Street, Dong Da, Hanoi, Vietnam; hangntm@tlu.edu.vn
[2] Water Resource Institute, Ministry of Natural Resources and Environment, No.8 Phao Dai Lang Street, Dong Da, Hanoi; ncaodonwri@gmail.com

*****Corresponding author: hangntm@tlu.edu.vn; Tel.: +84–354607643

Received: 05 June 2021; Accepted: 03 August 2021; Published: 25 August 2021

Abstract: Water resources inventory has become one of the important issues in many countries including Vietnam in order to build a database on the quantity of water sources, of water amount, water quality, current status of exploitation and polluted discharge into the water sources, economic value of water, so as to serve national water resource reports and information needs on water resources for socio-economic activities, national defense, security, science, education, training and other needs, etc., and serve as a basis for formulating and adjusting master plans and plans on water resources, as a basis for adjusting policies and laws on water resources. Till now, a number of countries have carried out activities for water resources inventory, but the inventory of water resources in Vietnam has not been officially implemented due to lacks of scientific basis in developing the inventory indicators and limitation of other resources. This article presents the contents related to water resource inventory in some countries and the current status of national water resource inventory activities in order to provide a system inventory criteria and methodology to be used in the inventory of water resources in future development.

Keywords: Water resources; Water resources statistics; Water resources inventory; Sets of inventory indices; Water planning.

1. Introduction

Over the past few decades, the inventory of water resources has become one of the important issues in many countries around the world, because it is the basis for proposing and building water resource planning, socio-economic activities, national defense and security. A series of inventory criteria on the quantity and quality of water resources, exploitation and use of water resources as well as statistical indicators to assess the sustainability of water resource have been developed. According to the availability of documents and the needs for information provision, the system of statistical indicators, methods of calculation, synthesis and inventory, statistics of water resources in research as well as in international organizations and countries are different. The statistics of international organizations often focus on basic indicators of water resource including the total amount of water inside and outside the country, the total amount of rainwater and annual evapotranspiration in countries [1]. The Food and Agriculture Organization (FAO) has issued a guidance on statistics, inventory and audit of water resources [2]. This is a comprehensive document that introduces the steps, methods and tools used in water balance analysis, providing information and quantification of flows and the distribution of water reserves over space and time. Four groups of indicators are related to statistics, inventory and assessment of the water sector, including the group of characteristics of water resources, the process of and use, the efficiency of water exploitation and water policies [3]. The United Nations

Statistic Division has also developed a technical report [4] to update and strengthen its water resource information systems for integrated management of water resources and introduce selected criteria for national measurements, including indicators related to water storage capacity; indicators on the potential of water sources, indicators on water exchange between surface water and ground water, surface water and surface water, groundwater and groundwater; indicators on water exploitation; indicators on water sources between economic fields; and indicators of water return.

In the US, the statistics of the physical characteristics of a river basin, its area, the proportion of each type of land, the type of landuse, the area and the ratio of the reservoir area; surface water flows, underground flows, targets on exploitation and use of water, indicators on flow quality, and environmental quality have been implemented [5], while in Australia, water surface is inventoried according to the average annual water volume, water distribution, average salinity, average current flow, scientific and technical level [6]. The countries in West Asia have based their inventory on factors: river basin characteristics, rainfall changes, annual fluctuations and trends in surface water sources, flow regimes, and water reserves on basins and in dams, water quality and environmental impacts, linkage of groundwater with surface water, water management in countries in the region [7]. In China, water resource statistics have also been carried out. The indicators of water resource inventory include: quantity of water, movement, quantity of water supplied, used, drained and discharged, exploitation and use of water resources, quality of water resources, natural disaster situation. It can be seen that international organizations (FAO), developed countries (the UK, USA, Australia, etc.) have all made statistics and provided information on the country's water resources for scientific research and socio-economic development. The information includes runoff, precipitation, monthly/ yearly evaporation, changes in groundwater and surface runoff during the year, floods, droughts, temperature, and annual precipitation. Most of them are published on the websites of professional organizations and are not restricted to different users. However, statistical and inventory information on water resources is quite limited. Particularly, there is very little information about research, inventory methods or indicators used for water resource inventory.

In Vietnam, water resources are considered as a kind of public property, possessed by the people, and managed by the Government as the only management unit [1]. Therefore, water resources are managed, exploited, protected, and fully assessed in terms of quantity and use value. According to the Article 38 of the Law on Management and Use of Public Property [8]: "Public property must be assessed timely and adequately in terms of the values according to the the law on statistics, accounting and related laws. State agencies assigned to manage and use public assets are responsible for inventorying assets at the end of the annual accounting period and making inventories according to the Prime Minister's decision on inventory and re-evaluation of public assets". Another study [9] has built a system of statistical indicators of water resources, which includes 06 statistical indicators of rain water resources, 11 statistical indicators of surface water resources, 14 statistical indicators of groundwater, 07 statistical indicators of water exploitation and use; and 04 groups of statistical indicators related to water quality and discharge into water sources. The document "Vietnam Water Resources and Management" [10] also provides information and knowledge on water resource management, and refers to the system of water resource management indicators such as socio-economic, water resource, ecological environment and synthetic criteria. Some indicators such as total surface runoff, total reservoir capacity and water stress index in 16 major river basins in our country were also evaluated [11].

2. Water inventory activities in Vietnam

The water resource inventory is guided in Article 7 of Decree 201/2013/ND-CP dated November 27, 2013 of the Government guidance on the the Law on Water Resources [12],

whereby the water resource statistics shall be made uniformly nationwide, once every five (05) years, in accordance with the national socio-economic development plan and the responsibility on the inventory of water resources [12]. At present, Vietnam has carried out several projects on measuring and drawing hydrogeological maps, maps of surface water and underground water at various scales and other water resources investigation and assessment projects. However, the projects on inventory of surface water and groundwater resources have not yet been implemented [1]. The Department of Water Resources Management (Ministry of Natural Resources and Environment) has proposed to expand the system of statistical indicators on groundwater resources to better serve the state management of water resources [13] with specific contents as shown in Table 1.

Table 1. Inventory of groundwater resources

No.	Inventory Indicator	Scope	Term	Methodology
1	**Group 1** Investigation, evaluation and development of maps for groundwater resource with the ratio is 1:200.000, in km^2, value 10^6đ	Nationwide	5 years	Cummulative, chart
2	Investigation, evaluation and development of maps for groundwater resource with the ratio of 1:100.000, in km^2, value 10^6đ	Nationwide, large river basin	5 years	Cummulative, chart
3	Investigation, evaluation and development of maps for groundwater resource with the ratio of 1:50.000, in km^2, value 10^6đ	Nationwide, river basin, locally	5 years	Cummulative, chart
4	Investigation, detail evaluation of groundwater resource, km^2, value 10^6đ	Nationwide, river basin, locally	5 years	Cummulative, chart
5	**Group 2** Underground natural dynamic reserve, static reserve, m^3/day	Nationwide, river basin, locally	5 years	Cummulative
6	Exploitable underground water reserves (potential reserves), m^3/day	Nationwide, river basin, locally	5 years	Cummulative
7	Exploited underground water reserves investigated and evaluated, m^3/day	Nationwide, river basin, locally	5 years	Cummulative
8	**Group 3**			
	Hydrogeological units	Area investigated	1 time	Chart
9	Physical data of hydrogeological units, thickness: m; permeability coefficient: m/ng; water release coefficient: %...	Area investigated	1 time	Arithmetic average, median
10	Characteristics of underground water quantity: pressure column, m; flow rate, l/s; flow rate, l/s.m; water depth, m…	Area investigated	1 time	Arithmetic average, median
11	Characteristics of underground water quality: TDS, g/l; primary ions; PH; EH, mv; Mn, Fe, As… annual and multi-year average, mg/l.	Area investigated	1 time	Arithmetic average, median
12	**Group 4** Report on the construction of monitoring networks, buildings and stations	Aquifers in regions (networks), the whole country	5 years	Cummulative
13	The quantitative dynamics include the maximum and minimum water level (or flow) of groundwater, the average daily, monthly, yearly and multi-year;	Monitoring works, aquifers in the region (network)/province	1 year and 5 years	Arithmetic average
	The minimum volume of monthly average water level (flow) with frequency of 85, 90 and 95%.	Typical monitoring works		Calculated variation

No.	Inventory Indicator	Scope	Term	Methodology
14	The qualitative dynamic features include the annual average data of water quality monitoring factors, the seasonal average of many years.	Monitoring works, aquifers in the region (network)/province	1 year and 5 years	Average value

According to studies and projects, those have been carried out at local and international levels, it can be seen that the methodology of statistics and inventory of water resources is diverse by province/city, river basin, and country, transnational and territorial areas. In the field of water resources, the subject of inventory is often separated from surface water and groundwater because the relevant characteristics of these two types of water resources are different. That leads to the inventory indicators of these two categories are also different [1].

In general, the study of water resources including rainwater, surface water and groundwater for the socio-economic development, basin management, and sustainable management of water resources has been conducted in Vietnam. In which, the assessment of natural resources and conditions in terms of hydrometeorology, demand for water use and the ability to exploit water supply, statistics of water resources and so on have been discussed and mentioned in many studies with varying degrees and details. These results make an important contribution to the management of water resources. However, the establishment of statistical and inventory methods, especially the development of criteria for the inventory of water resources, applied to river basins with different features are not covered in the reviewed studies. Therefore, the study and development of criteria for the inventory of water resources for different river basins to show the change of water resources compared to the base year is important for the state management of water resources. Accordingly, it is applied to a specific basin to clearly see the change of water resources in the context of rapid socio-economic development as well as the change in hydrological regime due to the impacts of upstream exploitation (most of the main river basins in Vietnam are transboundary basins), internal changes in the supply and demand for water use in the basin.

From the above analysis, it can be seen that each country has a different inventory approach, most of the water resource assessment methods usually focus only on individual water source, or many resources from different regional or national scales. Many findings have raised questions about the potential of water resources, changes in water resources over time, water quality, and the exploitability of water sources. Through the research objectives, it is clear to see that these studies only focus on looking at statistics on water resources, assessing the influence of these data on water resources and water balance calculation. In addition, in Vietnam, current studies only focus on the statistics on water resources, methodology and criteria for statistics on water resources. Therefore, finding a comprehensive approach to the assessment of water resources that considers the effects of many factors at different regional scales and stages will be better for water resources management [1].

Currently, the inventory of water resources has not been officially implemented in Vietnam. Particularly, in Decision No. 81/2006 QD-TTg on National Strategy on Water Resources vision to 2020 [14] emphasized the implementation of “periodic inventory; periodic assessment on the exploitation and use of water resources, discharge of waste into water sources…”. Decision No. 305/2005/QD-TTg [15] on the promulgation of the National Statistical Indicator System, which contains a number of indicators related to water resources and environment. On the basis of Decision No. 305/2005/QD-TTg, on November 5, 2007 the Minister of Natural Resources and Environment (MONRE) issued Decision No. 18/2007/QD-BTNMT [16] on the System Statistical indicators of the natural resources and environment sector, with 231 indicators related to land, environment, measurement and cartography, hydrometeorology, water resources, geology and minerals, of which there are 09 statistical criteria on water resources, including: (1) natural reserves of underground water;

(2) underground water reserves have been investigated and assessed; (3) the natural area that has been mapped of underground water resources; hydrogeological map; (4) total amount of rainwater; (5) total amount of surface water; (6) numbers of large reservoirs (with design capacity greater than 1 million m^3), total capacity of large reservoirs; (7) total amount of wastewater; (8) ratio of extracted surface water to total surface water; (9) the ratio of exploitable groundwater to total exploitable reserves (Table 2).

Table 2. Governing documents related to statistical indicators of water resources

Decision 18/2007/QD-BTNMT Promulgating a system of statistical indicators for the natural resources sector		**Circular No. 29/2013/TT-BTNMT Promulgating the system of statistical indicators for the natural resources sector** [20]		**Circular No. 02/2014/TT-BTNMT Regulation on reporting regime for statistics of natural resources industry**		**Circular No. 73/2017/TT-BTNMT Promulgating the system of statistical indicators for the natural resources sector** [21]		**Circular No. 20/2018/TT-BTNMT Statistical reporting regime for natural resources and environment sector**	
Code	**Group, target name**	**Code**	**Group, target name**	**Code**	**Group, target name**	**Code**	**Group, target name**	**Code**	**Group, target name**
N198	Natural dynamic reserve of underground water	201	Area to be investigated and assessed for ground water	0201/BTNMT	Area to be investigated and assessed for ground water	0201/BTNMT	Area to be investigated and assessed for ground water	0201/BTNMT	Area to be investigated and assessed for ground water
N199	The underground water reserve has been investigated and evaluated	202	Water level, temperature, physical properties and chemical composition of underground water	0202.1/BTNMT	Ground water level	0202.1/BTNMT	Ground water level	0202.1/BTNMT	Ground water level
N200	The natural area has been mapped of underground water resources; hydrogeological map			0202.2/BTNMT	Ground water temperature	0202.2/BTNMT	Ground water temperature	0202.2/BTNMT	Ground water temperature
N201	Total amount of rain water	203	Total surface water volume of some main river basins	0202.3/BTNMT	Physical properties and chemical composition of groundwater	0202.3/BTNMT	Physical properties and chemical composition of groundwater	0202.3/BTNMT	Physical properties and chemical composition of groundwater
N202	Total amount of surface water	204	Change of ground water level	0203/BTNMT	Total surface water volume of major river basins	0203/BTNMT	Total surface water volume of major river basins	0203/BTNMT	Total surface water volume of major river basins
N203	Large number of reservoirs (with design capacity greater than 1 million m3), total capacity of large reservoirs	205	Change of total surface water in some main river basins	0204/BTNMT	Change of ground water level	0204/BTNMT	Change of ground water level	0204/BTNMT	Change of ground water level
N204	Total amount of wastewater	206	Total volume of exploitation, use of water resources, discharge of wastewater into water sources of some main river basins	0205/BTNMT	Change of total surface water in major river basins	0205/BTNMT	Change of total surface water in major river basins	0205/BTNMT	Change of total surface water in major river basins
N205	Ratio of exploited surface water to total surface water			0206/BTNMT	Total amount of exploitation, use of water resources, discharge of wastewater into licensed water sources in the main river basins	0206/BTNMT	Total amount of exploitation, use of water resources, discharge of wastewater into licensed water sources in the main river basins	0206/BTNMT	Total amount of exploitation, use of water resources, discharge of wastewater into licensed water sources in the main river basins
N206	Ratio of exploitable groundwater to total exploitable reserves								

From 2007 to 2018, MONRE has three times issued the system of statistical indicators for the natural resources and environment sector including water resources (in 2007, 2013, 2017) and twice issued the system of statistical natural resources and environment sector (in 2014, 2018). Recently, Circular No. 20/2018/TT-BTNMT [17] on Statistical reporting regime of natural resources and environment sector was issued to replace the Circular No. 02/2014/TT-BTNMT [18].

The statistics and inventory of water resources of the Ministry of Natural Resources and Environment have not been implemented synchronously at all levels. The main reason is that the concepts, contents and methods for statistical indicators and inventory of water resources have not been unified and standardized in calculation, moreover, the indicators do not reflect the relationship between water resources and exploitation process, etc. Especially, in the context of climate change, most of Vietnam's rivers have had construction projects to exploit and regulate water, therefore the regularity and natural law of hydrometeorology and water resources have also changed. Statistical criteria of water resources (Table 2) of the natural resources sector in Circular 20/2018/TT-BTNMT [17] are the major and necessary criteria for the management at the national scale. However, they are not detailed, do not fully reflect the natural feature of water resources, including quantity and quality, and reflect the water

resources of a basin/ region in terms of its development over time, space, extremes, exploitation effects, environmental factors and water quality, etc.

There have been no legal guidance or studies on how to calculate and produce the most accurate data that fully reflects water resources at all levels of river basin, region, nation, etc. However, to do statistics of the required indicators in the appendix tables attached to the instructions, it is necessary to synthesize statistics from the reports of the Department of Natural Resources and Environment and the data from the hydrological stations at the estuary. This is a difficult task because collecting all data is impractical and if there is no agreed method, the results will be very different between localities and watersheds. Currently, the guidelines on the content or inventory forms, and reports on the results of water resource inventory are not adequate, leading to difficulties for agencies in the inventory of water resources.

3. Future indicators for water resource inventory in Vietnam

In the study of water resources inventory, the selection of criteria related to water quality and quantity of the basin is necessary. Besides, human exploitation activities in river basins, especially water tranfering from the reservoirs to other basins have a significant impact on the reserve and distribution of water reserves in the nature of the river, so these indicators show the extent of affected water resources, the remaining resources can be exploited without seriously affecting the inventory and quality of the water over a period of 5 years based on the national socio-economic development plan period. In addition, selecting some specific criteria for rivers (or river basins) whose typically specific characteristics and actual exploitation and use of water is also a necessary task.

The guidance of river basin water resource planning in the Law on Water Resources 2012 [19] of the Government clearly stipulates that the first step of river basin planning is: "Assessment of natural, economic, societal and environmental characteristics of water sources, the current status, exploitation, usage and water resource protection and prevention, from the harmful consequences". According to the Law on Water Resources 2012 [19], water resources include surface water, underground water, rain water and sea water in the territory of the Socialist Republic of Vietnam. However, the inventory of water resources focuses on surface water, underground water, and rain water. For sea water, the inventory will focus on the exploitation and the use of seawater, discharging waste into seawater sources belonging to the territory of Vietnam.

"Indicators" mean (1) the required levels to be achieved; or (2) the expression levels of a feature, a function. In the inventory of water resources, an "indicator" is understood in the second term, the latter. Thus, the water resource indicator system is a collection of indicators on various types of water resources, including rainwater, surface water, groundwater resources, and seawater resources (if any). They are expressed in terms of (i) numbers of water sources, numbers of monitoring stations; (ii) amounts of water; (iii) water quality; (iv) fluctuations and trends (variations in space and time between years and within the year; changes due to human impacts, including socio-economic activities, pollution, depletion, etc); (v) capacity and current status of exploitation and use; and (vi) economic value of the water.

An indicator must include (i) a name code and name of that indicator; (ii) quantitative value; (iii) reflection space; (iv) subjects of reflection; and (v) measurement/ calculation time. Quantitative data can be expressed as absolute numbers or ratios. Thus, indicators are always associated with certain numbers and a certain time frame. An indicator can be measured by many indices. Sometimes there are indicators that are not quantifiable. It should be noted that in order to manage by results, the number of indicators should not be too many, and more attention should be paid to indicators for specific goals. It is recommended to gradually move from single indicators to integrated indicators that combine many variables [1].

Table 3. Proposed water resource inventory indicator system.

No.	Water inventory indicators	Water resources		
		Rainwater	**Surface water**	**Groundwater**
1	Quantity	×	×	×
2	Quality	×	×	×
3	Variation	×	×	×
4	Use and exploitation	×	×	×
5	Economic value	×	×	×

Note: × = Yes, to be characterized by indicators.

Therefore, through international experience and the actual situation in Vietnam, we have introduced a systematic indicator for the inventory of water resources including rainwater, surface water and groundwater resources with a set of indicators representing quantity, quality, variation, use and exploitation as well as econominc value of water resources as described in Table 3. Specific contents and methods to determine inventory indices will be presented in another paper.

4. Conclusion

The article presents the water resource inventory in some countries and the current status of water resource inventory activities at national levels to provide a system of criteria and methods. The results show that each country has different statistical approaches, most of the statistical methods and assessments usually focus only on separate water source, or several resources in regional or national scale or on the basis of an annual inventory, the article determines the potential of water sources, changes in water sources over time, water quality, and the exploitation capacity of water sources. In addition, in Vietnam, practical studies and topics only focus on the statistics of water resources, giving methods and criteria for statistics on water resources in Vietnam. In order to manage the water resource planning in the river basin and a plan for the exploitation and use of sustainable water resources, the inventory and assessment of water resources is very necessary. Through international experience and the actual situation in Vietnam, the authors have systematized and proposed a system of standards/ indicators for water resource inventory and the inventory of rainwater, surface and underground water resources include the quantity, quality, fluctuations, exploitation, use and value of water resources, thereby serving the development of relevant circulars and guidelines.

Author contribution: The author authorizes to develop the ideas methods and write the article by themselves.

Acknowledgments: The content in this paper is part of the outcomes from the "*Scientific basis for establishing a system of indicators for water resource inventory. Application to the Ba River basin* (Nghiên cứu cơ sở khoa học xây dựng hệ thống chỉ tiêu kiểm kê tài nguyên nước. Áp dụng thử nghiệm cho lưu vực sông Ba)" of the Ministry of Natural Resources and Environment (MONRE), coded TNMT.2019.02.01 (in Vietnamese). Principal researcher: Assoc.Prof. Dr. Nguyen Cao Don.

Conflicts of Interest: The authors declare no conflict of interest.

Reference

1. Don, N.C. Research proposal on "Scientific basis for establishing a system of indicators for water resource inventory. Application to the Ba River basin". Coded TNMT.2019.02.01, 2019 (in Vietnamese).
2. Charles, B.; Jippe, H.; Jean-Marc, F.; Livia, P. Water accounting and auditing: A sourcebook. FAO Water Report 43, **2016**, pp. 232.
3. UN-Water "UN-Water Task Force on Indicators, Monitoring and Reporting: Final report", **2006**, pp. 44.
4. United Nation. International Recommendation for Water Statitics. Statistical papers Series M, No.91. ST/ESA/STAT/SER.M/91, 2012.
5. USGS and ERSI. An online geographic information system that provides information on watersheds in the United States. Online available: https://streamstats.usgs.gov/ss/. Assessed 15/06/2021.
6. Bureau of Meteorology. Information on Water Resources, at Website http://www.bom.gov.au/water/, Assessed **15/06/2021**.
7. United Nations Economic and Social Commisssion for Western Asia (UN-ESCWA) và German Federal Institute for Geosciences and Natural Resources (BGR). Inventory of Shared Water Resources in Western Asia. Online available: https://waterinventory.org/.
8. Law on Management and Use of Public Property. No. 15/2017/QH14, dated 21 June, 2017, **2017** (in Vietnamese).
9. Dung, N.K. Project "Research on scientific and practical basis to determine content, methods of calculation, synthesis and statistics of water resource indicators", MONRE, **2010** (in Vietnamese).
10. Xuan, T.T. và Tuyen H.M. "Vietnam's water resources and management". **2012** (in Vietnamese).
11. ADB. Project on technical support for water sector assessment for Vietnam, 2005-2009.
12. Decree 201/2013/ND-CP dated November 27, 2013 of the Government guiding the implementation of a number of articles of the Law on Water Resources, 2013 (in Vietnamese).
13. Water Resources Management Department, MONRE. Research and propose to expand the system of statistical indicators of underground water resources to better serve the state management of water resources, 2012 (in Vietnamese).
14. Decision No. 81/2006/QD-TTg dated April 14, 2006 of the Prime Minister approving the National Strategy on water resources until 2020, 2006 (in Vietnamese).
15. Decision No. 305/2005/QD-TTg on the promulgation of the National Statistical Indicator System, 2005 (in Vietnamese).
16. Decision No. 18/2007/QD-BTNMT promulgating the System of Statistical Indicators of the Natural Resources and Environment Sector, 2007 (in Vietnamese).
17. Circular No. 20/2018/TT-BTNMT on Statistical reporting regime of natural resources and environment industry, 2018 (in Vietnamese).
18. Circular No. 02/2014/TT-BTNMT stipulating the regime of statistical reporting of the natural resources and environment sector, 2014 (in Vietnamese).

19. Law on Water Resources 2012, No. 17/2012/QH13, 2012 (in Vietnamese).
20. Circular No. 29/2013/TT-BTNMT Promulgating the system of statistical indicators for the natural resources sector, 2013 (in Vietnamese).
21. Circular No. 73/2017/TT-BTNMT Promulgating the system of statistical indicators for the natural resources sector, 2017 (in Vietnamese).

Table of content